USAAMRDL-TR-77-14

(12)

# HELICOPTER TRANSMISSION VIBRATION AND NOISE REDUCTION PROGRAM

Kaman Aerospace Corporation
Old Windsor Road
Bloomfield, Conn. 06002



June 1977

Final Report for Period May 1974 - February 1977

Approved for public release;
distribution unlimited.



Prepared for

EUSTIS DIRECTORATE
U. S. ARMY AIR MOBILITY RESEARCH AND DEVELOPMENT LABORATORY
Fort Eustis, Va. 23604

# DISCLAIMER NOTICE

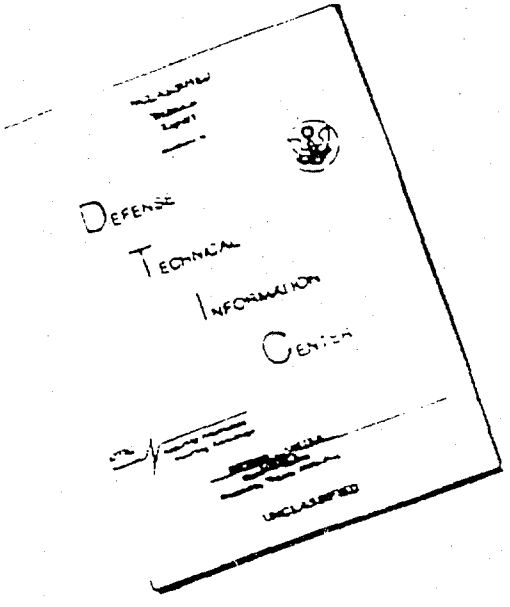


THIS DOCUMENT IS BEST QUALITY AVAILABLE. THE COPY FURNISHED TO DTIC CONTAINED A SIGNIFICANT NUMBER OF PAGES WHICH DO NOT REPRODUCE LEGIBLY.

## EUSTIS DIRECTORATE POSITION STATEMENT

This report provides the details of a program which has developed an analytical procedure for determining the vibration and noise characteristics of a helicopter transmission. This program included the testing of a baseline transmission, transmission design changes, and analysis of the modified transmission to verify the validity of the technical approach. The program was not extended beyond the analysis of the modified transmission. A recommendation to correlate operational testing data with the anaiytical data is presented; however, no effort is planned to achieve this objective at this time.

Mr. Allen C. Royal, Propuision Technical Area, Technology Applications Division, served as Project Engineer for this effort.

UNCLASSIFIED

SECURITY CLASSIFICATION OF THIS PAGE (When Data Entered)

## REPORT DOCUMENTATION PAGE

READ INSTRUCTIONS BEFORE COMPLETING FORM

1. REPORT NUMBER: USAAMRDL-TR-77-14
2. GOVT ACCESSION NO.
3. RECIPIENT'S CATALOG NUMBER

4. TITLE (and Subtitle): HELICOPTER TRANSMISSION VIBRATION AND NOISE REDUCTION PROGRAM
5. TYPE OF REPORT & PERIOD COVERED: Final Report. May 1974 — Feb 1977
6. PERFORMING ORG. REPORT NUMBER: R-1495

7. AUTHOR(s): Michael A. Bowes, Nicholas Giansante, Robert B. Bossler, Jr. and Alex Berman
8. CONTRACT OR GRANT NUMBER(s): Contract DAAJ02-74-C-0039

9. PERFORMING ORGANIZATION NAME AND ADDRESS: Kaman Aerospace Corporation, Old Windsor Road, Bloomfield, CT 06002
10. PROGRAM ELEMENT, PROJECT, TASK AREA & WORK UNIT NUMBERS: 62207A 1G262207AH89, 02 003 EK

11. CONTROLLING OFFICE NAME AND ADDRESS: Eustis Directorate, U. S. Army Air Mobility R&D Laboratory, Fort Eustis, VA 23604
12. REPORT DATE: June 1977
13. NUMBER OF PAGES: 155

14. MONITORING AGENCY NAME & ADDRESS (if different from Controlling Office)
15. SECURITY CLASS. (of this report): Unclassified
15a. DECLASSIFICATION/DOWNGRADING SCHEDULE

16. DISTRIBUTION STATEMENT (of this Report)

Approved for public release; distribution unlimited.

17. DISTRIBUTION STATEMENT (of the abstract entered in Block 20, if different from Report)



18. SUPPLEMENTARY NOTES

19. KEY WORDS (Continue on reverse side if necessary and identify by block number)

Helicopter
Vibration
Noise
Transmission
Dynamic Modeling
Component Synthesis

20. ABSTRACT (Continue on reverse side if necessary and identify by block number)

A combined analytical and test program has been performed to develop a method for analytically determining the vibration and noise characteristics of a helicopter transmission. This effort included formulation of the necessary analytical method, validation of this method through direct comparison with test data, and use of the method to predict the effects of various transmission design changes.

DD FORM 1 JAN 73 1473 EDITION OF 1 NOV 65 IS OBSOLETE

UNCLASSIFIED

SECURITY CLASSIFICATION OF THIS PAGE (When Data Entered)

404

20. Abstract (Continued)

The analytical method formulated in this program makes use of available techniques for predicting gear-mesh-induced excitations. These techniques have been expanded to include a more rigorous treatment of spiral bevel and helical gear induced mesh excitations. Response of the dynamic system is predicted using a coupled torsion and bending analysis of the gearshafts, and includes the effects of bearing and case dynamics. Predicted case surface response is used directly to calculate radiated sound power.

The analytical method makes use of component synthesis techniques which permit dynamic modeling of transmission components on an individual basis. Each shaft is modeled separately using physical shaft/gear data including shaft geometry, mass distribution, and mechanical properties. Bearings are similarly modeled, as orthogonal spring/dampers. The transmission case, because of its inherent complexity, is modeled from dynamic response test data. These individual models are then joined, using component synthesis techniques, resulting in a system dynamic model.

The analytical method was used to predict the dynamic responses of an actual helicopter gearbox, which were compared to measured responses obtained from operational testing of this transmission. The test article used was the Navy/Kaman SH-2D main transmission; it was subjected to a simulated operational test, over a range of realistic torque and rpm conditions, using a regenerative test stand. Response parameters measured included shaft bending and torsion strain, lateral shaft deflection, housing acceleration, and radiated sound pressure level. Comparisons of model predictions with measured data showed good agreement, thus verifying the validity of the technical approach.

The analytical method was used to predict the effects of a variety of transmission design changes including: shaft mass and stiffness redistribution, bearing stiffness reduction and relocation, planetary carrier stiffness reduction, and case mass redistribution and increased damping. All of the design changes evaluated produced some changes in transmission response, although several appear more promising than others, and were recommended for further study. Those recommended include planetary carrier stiffness reduction, case mass redistribution, and increased case damping. It is further recommended that the analytical method be extended through development of a generalized transmission case dynamic model.

# PREFACE

The Helicopter Transmission Vibration and Noise Reduction Program was performed under Contract DAAJ02-74-C-0039 with the Eustis Directorate, U. S. Army Air Mobility Research and Development Laboratory (USAAMRDL), Fort Eustis, Virginia. The program was performed under the technical cognizance of Mr. A. Royal of the Propulsion Group, Technology Applications Division, USAAMRDL. This program resulted in the development and validation of a method for predicting the dynamic response characteristics of helicopter transmissions. This method will be a useful tool, enabling the design of helicopter transmissions having reduced noise and vibration qualities.

The program was conducted by Kaman Aerospace Corporation, Bloomfield, Connecticut, with the subcontracted assistance of Shaker Research, Ballston Lake, New York. Overall project management was provided by Mr. R. B. Bossler, Jr. of Kaman with significant technical contributions from Mr. N. Giansante and Mr. A. Berman, also of Kaman, and Mr. J. Frarey and Mr. C. Pan of Shaker Research.

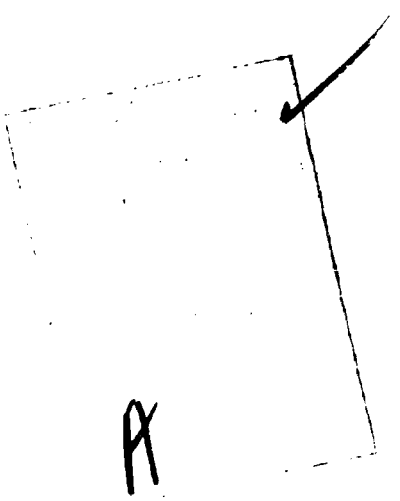

TABLE OF CONTENTS

TABLE OF CONTENTS (Continued)

## LIST OF ILLUSTRATIONS

LIST OF ILLUSTRATIONS (Continued)

LIST OF ILLUSTRATIONS (Continued)

LIST OF ILLUSTRATIONS (Continued)

## LIST OF TABLES

# INTRODUCTION

## BACKGROUND

Large vibratory forces are produced at the gear meshes of helicopter transmissions. These forces are the sources of high-frequency vibratory loads which reduce transmission component lives, impair gearbox performance, and reduce reliability. These forces also cause high cabin noise levels which degrade the efficiency, health, and comfort of both crew and passengers. In recognition of this problem, Eustis Directorate, USAAMRDL, has undertaken a comprehensive program to gain an understanding of the physical mechanisms involved in the generation, propagation, radiation, and control of helicopter transmission vibration and noise. This effort has concentrated on the development of analytical methods enabling the prediction of transmission vibration and noise, coupled with the use of these analytical tools to formulate means of control and reduction.

Research in the area of helicopter transmission vibration and noise began in the early 1960's, with the efforts described in References 1 and 2. These studies, which dealt with all sources of helicopter noise, both internal and external, concluded that internal noise is dominated by contributions from the drive system and more specifically, by discrete frequency components associated with the gear-meshing process. Having defined the problem, work began to develop a more complete analytical understanding which, it was hoped, would eventually lead to discovery of cost-effective means for reducing transmission noise and vibration at the source, obviating the necessity for heavy cabin soundproofing treatments.

The first preliminary analytical efforts along these lines are described in Reference 3. The fundamental gear-mesh excitations were found to result from the nonuniform transmittal of torque across the gear meshes.

---

[1] Sternfeld, H., Jr., Spencer, R. H., and Schaeffer, E. G., STUDY TO ESTABLISH REALISTIC ACOUSTIC DESIGN CRITERIA FOR FUTURE ARMY AIRCRAFT, TREC Technical Report 61-72, U. S. Army Transportation Research Command, Fort Eustis, Virginia, June 1961.

[2] Cox, C. R., et al, A STUDY OF THE ORIGIN AND MEANS OF REDUCING HELICOPTER NOISE, Bell Helicopter Company; TREC Technical Report 62-73, U. S. Army Transportation Research Command, Fort Eustis, Virginia, November 1962.

[3] Laskin, I., Orcutt, F. K., and Shipley, E. E., ANALYSIS OF NOISE GENERATED BY UH-1 HELICOPTER TRANSMISSION, Mechanical Technology, Inc.; USAAVLABS Technical Report 68-41, U. S. Army Aviation Materiel Laboratories, Fort Eustis, Virginia, June 1968, AD 675457.

This nonuniformity was related to a lack of constant tooth deflection under torque loading, due to both variation in effective tooth bending stiffness and time-variant tooth loading during the mesh cycle. These effects were combined in an analysis which enabled the calculation of mesh deflection as a function of time, based on tooth geometry and material properties, gear geometry, and operating torque. The resulting deflection time history was Fourier analyzed to obtain the amplitudes of the frequency components of the mesh excitation.

The work of Reference 3 also includes an analysis of the torsional response of the transmission dynamic system, based on the torsional stiffness and inertia distributions of all shafts in the system. This torsional response model was used, in conjunction with the mesh deflection predictions, to calculate mesh-induced dynamic forces. The calculated dynamic forces were related to transmission-radiated noise, using a simplified analytical and empirical method based on available energy at the gear mesh. Available energy was converted to noise, using empirically derived proportionality factors. This method seemed to result in good correlation with measured UH-1D noise levels, also obtained under the Reference 3 program.

The study of Reference 4 applied the analytical methods developed in Reference 3 to a CH-47 transmission. This effort also included an experimental evaluation of the effect of transmission-case response on the ratio of available mechanical energy to radiated acoustic energy. This experiment was undertaken to investigate the validity of the assumption that the effect of casing response can be considered through the use of a proportionality factor in the noise-vs.-mechanical-energy equation used in Reference 3. In addition, calculation of gear-mesh dynamic deflections was extended to include spiral bevel gearing as well as spur gearing, although Reference 4 points out that the method used for approximating spiral bevel gearing was considered to be preliminary and subject to considerable improvement. The Reference 4 effort also included comparison of calculated and measured CH-47 transmission noise, using measured data obtained within the study, and correlation was again shown to be good.

---

[4] Badgley, R. H., and Laskin, I., PROGRAM FOR HELICOPTER GEARBOX NOISE PREDICTION AND REDUCTION, Mechanical Technology, Inc.; USAAVLABS Technical Report 70-12, U. S. Army Aviation Materiel Laboratories, Fort Eustis, Virginia, March 1970, AD 869822.

The studies of References 3 and 4 predict noise based on gear-mesh forces and deflections, considering only torsional vibration of the transmission shaft system. This approach assumes that only the torsional response affects the magnitude of forces generated at the gear meshes and that, more importantly, noise radiated from the case is simply related to the forces and deflections at the meshes. The work reported in Reference 5 attempts, at least partially, to remove the second of these assumptions, by considering the mechanism through which mechanical energy generated at the gear mesh is transmitted to the gearbox casing. To accomplish this, an analysis of the lateral (bending) vibration response of several of the UH-1D and CH-47 gearshafts studied previously is undertaken. This analysis, which includes the effects of bearing stiffness as well as shaft inertias, masses, and bending stiffnesses, is used to calculate the dynamic forces which are induced in the shaft support bearings as a result of the gear-mesh deflections and forces calculated previously. Noise radiated from the case is assumed to be proportional to the induced bearing forces, and changes in noise level are predicated on changes in the bearing forces.

The study of Reference 5 carries the calculation of radiated noise from gear meshes in the planet system one step further. For the case of the planet system, at least a part of the noise is assumed to be due to induced motion of the planet system ring gear, which can be approximately calculated by considering the ring gear as a free body, subject to planet/ring gear-mesh forces. Within the Reference 5 study, ring-gear noise is calculated based on the assumption that the ring gear may be considered as composed of several point sources of sound, which radiate independently of each other, due to cyclically induced motion of the fluid medium (air) surrounding the ring gear.

The extensions of the analytical methods made in the study of Reference 5, and described above, represent the most recent improvements made prior to the present effort. In the interim, these analyses have been used to specify modifications of the CH-47 transmission for reduced noise. Reference 6 describes these recommended modifications, estimates their expected effect in terms of noise reduction, and includes a comparison

---

[5] Badgley, R. H., and Chiang, T., INVESTIGATION OF GEARBOX DESIGN MODIFICATIONS FOR REDUCING HELICOPTER GEARBOX NOISE, Mechanical Technology, Inc.; USAAMRDL Technical Report 72-6, Eustis Directorate, U. S. Army Air Mobility Research and Development Laboratory, Fort Eustis, Virginia, March 1972, AD 742735.

[6] Badgley, R. H., RECOMMENDED DESIGN MODIFICATIONS TO THE CH-47 FORWARD ROTOR-DRIVE GEARBOX FOR REDUCTION OF HIGH-FREQUENCY VIBRATION AND NOISE, Mechanical Technology, Inc.; USAAMRDL Technical Report 73-33, Eustis Directorate, U. S. Army Air Mobility Research and Development Laboratory, Fort Eustis, Virginia, June 1973, AD 769062.

of the weight penalty associated with each. Several of these modifications were experimentally evaluated, with results given in Reference 7. In general, the results of this experimental effort were inconclusive, neither verifying nor denying the validity of the analytical methods used. This study recommended that a more comprehensive evaluation of the analytical method should be undertaken prior to acceptance of the method for general use. The present effort is a direct response to this recommendation.

## PURPOSE AND SCOPE

The purpose of the present study is threefold: First, existing elements of the helicopter transmission vibration and noise prediction method embodied in References 3-7 are to be reviewed and, where necessary, revised or expanded to eliminate known deficiencies. Second, the resulting method elements are to be incorporated into a consistent comprehensive analytical tool capable of generating predictions of transmission noise and vibration from available design data, and suitable for use as a part of the helicopter transmission design process. Finally, the validity of this design tool is to be concretely established through direct comparison of analytical predictions with experimental data. Attainment of these objectives has resulted from the performance of a combined analytical and experimental program, all details of which are discussed in subsequent sections of this report.

Based on a review of existing analytical methods, it was concluded that deficiencies existed in several critical areas. First, in the area of gear-mesh deflection calculation, the method used to approximate spiral bevel and helical gearing was felt to require improvements. Consequently, this method has been revised for use in the present program. The method used to generate gear-mesh forces was similarly found to be deficient, in that only torsional system response was included. For the present program, a coupled torsion/bending response has been derived and used to generate gear-mesh forces.

The most serious deficiency of the existing analytical method was felt to be the lack of consideration of the response of the transmission case. Failure to consider the case impacts the validity of the method in several fundamental areas. First, the response of the case directly

---

[7] Sternfeld, H., Schairer, J., and Spencer, R., AN INVESTIGATION OF HELICOPTER TRANSMISSION NOISE REDUCTION BY VIBRATION ABSORBERS AND DAMPING, Vertol Division, The Boeing Company; USAAMRDL Technical Report 72-34, Eustis Directorate, U. S. Army Air Mobility Research and Development Laboratory, Fort Eustis, Virginia, August 1972, AD 752579.

influences induced gear-mesh forces by affecting the shaft bearing support responses and consequently the coupled, bending/torsion responses of the shafts. Second, and perhaps most important, vibration of the case is the major means by which noise is radiated, and failure to include case response makes direct calculation of radiated noise impossible. Within the present program, this deficiency has been corrected by incorporation of a dynamic model representing the transmission case.

The analytical methods developed through the studies of References 3-7 are research oriented and, as such, not directly suitable for use by the helicopter transmission designer. The underlying theme of the present effort has been to incorporate these methods, with necessary improvements, into a useful design tool. To accomplish this, emphasis has consistently been placed on the development of self-contained analytical models which would be directly usable by transmission designers, and which, wherever possible, would require only input data readily available during the transmission design or development process. Furthermore, consideration has been given to the costs of performing the required analyses, since excessive cost would most certainly limit, if not completely negate, its ultimate utility. Given these considerations, a building block approach to system modeling has been adopted. This approach relies heavily on dynamic component synthesis techniques, partially developed under government sponsorship, and reported in References 8 and 9.

Use of component synthesis permits dynamic modeling of transmission components on an individual basis. Each shaft is modeled separately, in as much detail as desired, using physical shaft/gear data including shaft geometry, mass distribution, and mechanical properties. Bearings are similarly modeled, as orthogonal spring/dampers, using bearing geometry and transmission operating data. The transmission case, because of its inherent complexity, is modeled from dynamic response test data. These individual models are then joined, using component synthesis techniques, resulting in a system dynamic model, which is fully representative of the entire dynamic system.

---

[8] Berman, A., VIBRATION ANALYSIS OF STRUCTURAL SYSTEMS USING VIRTUAL SUBSTRUCTURES, The Shock and Vibration Bulletin, Volume 5, No. 6, The Shock and Vibration Information Center, Naval Research Laboratories, Washington, D. C., June 1973, pp 13-22.

[9] Flannelly, W. G., Berman, A., and Barnsby, R. M., THEORY OF STRUCTURAL DYNAMIC TESTING USING IMPEDANCE TECHNIQUES, VOLUME I - THEORETICAL DEVELOPMENT, Kaman Aerospace Corporation; USAAVLABS Technical Report 70-6A, U. S. Army Aviation Materiel Laboratories, Fort Eustis, Virginia, June 1970, AD 874509.

The advantages of this approach are threefold: First, since components are modeled separately, analytical changes in these components can also be made separately, permitting rapid and efficient evaluation of the effects of physical changes on system response. Second, although each component may be modeled in great detail, with many degrees of freedom, only those degrees of freedom needed to join the individual components together must be retained in the system model, even though system responses will reflect all the complexities included in the individual components. This drastically reduces the computational effort required to evaluate the effects of changes in the individual components, and consequently reduces the cost to use the analysis. Third, and perhaps most important, lack of excessive complexity in the system model promotes physical understanding of model results, making the analysis more amenable to use by the transmission designer.

All of the analytical methods used to generate component and system dynamic models have been programmed for machine computation. Descriptions of these computer programs and instructions for their use are given in the users guide (Reference 10). Within the present study, these programs have been used to generate dynamic models of the SH-2 helicopter main transmission, shown schematically in Figure 1. These models have been used to calculate system dynamic responses to gear-mesh-induced excitations, and the resulting calculated responses have been compared to measured data obtained from testing of the SH-2 transmission. In this manner, the validity of the analytical approach has been evaluated, and its practicality established.

The SH-2 helicopter main transmission was selected for study primarily because it contains essentially all of the various types of mechanical components which are presently used, and will continue to be used, in helicopter drive systems. Referring to Figure 1, the first speed reduction is obtained through a spiral bevel gear/pinion set. The shafts involved with this mesh are supported with both axial thrust and radial load-carrying bearings. The second speed reduction takes place through a spur gear/pinion mesh using a large-diameter spur gear. The spur gear shaft is supported by radial load-carrying bearings only. The final stage of speed reduction consists of a fixed ring-gear-type planetary system with six planet gears. The planet carrier drives the output (main rotor) shaft, which is supported with both thrust and radial load-carrying bearings. A total speed reduction of 21.3/1 is achieved with this transmission, which has a rated input torque capacity of 15,000 in.-lb at an input shaft speed of 6120 rpm.

---

[10] Giansante, N., HELICOPTER TRANSMISSION VIBRATION/NOISE REDUCTION PROGRAM ANALYTICAL PREDICTION COMPUTER PROGRAM - USERS GUIDE, Kaman Aerospace Corporation; USAAMRDL Technical Report (To be published).

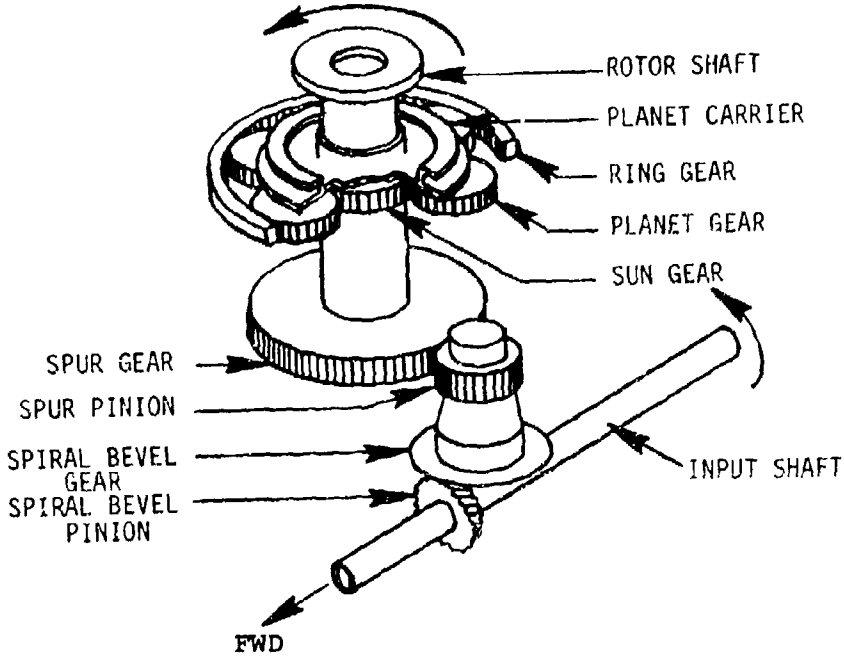


Figure 1. SH-2 Helicopter Main Transmission

The SH-2 main transmission was tested using a regenetative test stand capable of applying variable torque and rotor-lift loads, over a significant range of transmission speed. Testing was performed at two conditions of torque loading and at two speeds. Measurements included dynamic bending and torsion strain and lateral displacement of the input and output shafts. Accelerations at 14 points on the case surface were also measured, along with radiated noise at 10 locations surrounding the transmission. In order to separate the effects of the test gearbox, an acoustic enclosure was installed, completely enclosing the transmission, and a vibration isolating coupling was used on the test transmission output shaft.

All test data were analyzed, using a real-time spectrum analyzer, to extract the amplitudes of the various gear-mesh-related frequency components. These data provided the means for evaluating the validity of analytical model predictions. Having validated the analytical methods in this manner, potentially beneficial modifications of the basic transmission were selected and analytically evaluated.

Design changes which have been analyzed in the present study include reduced shaft support bearing stiffnesses, increased shaft stiffness and increased shaft and case mass. Also evaluated were stiffness reduction of the planet system carrier, increased case damping and relocation of shaft support bearings. In all cases, the impact of changes on case-radiated noise was determined for all sources of gear mesh-induced excitation.

## PROGRAM RESULTS

Performance of this program has resulted in the establishment of an analytical method for predicting the noise and vibration characteristics of helicopter transmissions. The form of this analytical method is such that it is readily usable by helicopter transmission designers as a part of the transmission design process. This method has been fully evaluated and validated through direct comparison of analytical predictions with test data.

The utility of the analytical method has been demonstrated through the evaluation of several transmission design changes having the potential for reduced noise and vibration. In addition to demonstrating the utility of the analytical method, this evaluation has revealed several promising means for obtaining immediate improvements in helicopter transmission noise and vibration characteristics. Recommendations for pursuing development of these noise-reduction methods are presented in a subsequent section of this report.

## REPORT FORMAT

This report consists of seven major sections, four of which deal specifically with the technical tasks performed.

The ANALYTICAL METHODS section discusses, in detail, each of the elements which together comprise the helicopter transmission vibration and noise prediction analytical method. Included in this section are descriptions of the methods used to obtain gear-mesh excitations, individual shaft dynamic models, bearing dynamic models and t e transmission case model. As part of the discussion of case modeling, a review of the case response test method used in the program is presented, along with the means used to convert the resulting test data into an analytical model of the case. This section also includes a discussion of the case-radiated noise prediction method. Finally, the component synthesis technique, used to construct a system dynamic model from the various elemental models, is discussed.

The test program conducted with the SH-2 main transmission is discussed in the TRANSMISSION TESTING section. This section includes descriptions of the test article, instrumentation, and test procedures used. The data obtained from this testing is also presented and discussed.

The METHOD CORRELATION section compares analytical predictions of transmission responses with test data, and evaluates the analytical method in light of this comparison.

In the METHOD APPLICATION section, the analytical method is used to evaluate a number of potentially beneficial transmission design changes. The predicted effects of each change are presented in terms of anticipated reduction in case-radiated sound power level.

## ANALYTICAL METHODS

A helicopter transmission is a complex dynamic system comprised of many interconnected mechanical elements. This system responds, under the influence of periodic forces produced at the various gear meshes, causing vibration of all of the individual elements and noise radiation from the transmission housing. The mechanical elements involved in this response include all of the gears/gearshafts, their support bearings, and the transmission housing. Analytical prediction of the transmission response, and consequently its vibration and noise-generation characteristics, requires knowledge of the dynamics of each mechanical element, the nature and extent of coupling between these elements, and the characteristics of the gear-mesh-induced forcing functions.

In general, knowledge of the three facets of transmission response prediction - element dynamics, system coupling, and mesh forces - cannot be obtained independently. While the individual mechanical elements can be modeled separately, and their responses calculated on that basis, these "free-free" responses are not directly indicative of the responses which occur if these elements are considered part of the total dynamic system. The same is true when considering the degree of coupling between the mechanical elements. This coupling occurs because the various elements are physically in contact with each other at points of gear meshing and at shaft support bearings, and while the nature of this coupling is a function of system geometry, the degree of coupling is highly influenced by the elemental and system dynamic response characteristics. Similarly, although the dynamic deflections which bring about gear-meshing forces are related to only local gear-tooth and steady loading conditions, prediction of the forces themselves requires consideration of the reaction of the total dynamic system.

The problem of transmission response prediction is further compounded by the fact that the gear meshing forces involved occur at high frequency, typically in the hundreds and thousands of hertz. Since the frequency for which accurate response prediction can be made is a direct function of the degree of detail in which the individual mechanical elements are modeled, very detailed elemental models are required. If the direct approach is taken and the total system is modeled as a whole, such as with finite-element modeling methods, the requirement to model in great detail quickly results in an excessively large, complex model which is not amenable to ease of manipulation and use. Fortunately, however, an alternative to this approach exists, which greatly reduces the difficulty of dynamic modeling and the complexity of the ultimate system model. This alternate approach, which relies on the concept of component synthesis developed through previous government-sponsored

research (References 8 and 9), has been used in the present effort.

## STRUCTURAL DYNAMICS CONCEPTS

The transmission dynamic system modeling methods employed in the present program rely on structural dynamics concepts which, while commonly used by structural dynamicists, may be unfamiliar to the transmission designer. Familiarization with these concepts, while not essential to the use of the transmission vibration and noise prediction method, is needed to understand the technical basis for the modeling methods used. For this reason, a review of these concepts is presented.

The steady-state equations of motion of a structurally damped linear dynamic system having n degrees of freedom may be expressed as

$$((1 + jg)[K] - \omega^2[m])\{y\} = \{f\} \tag{1}$$

where $[K]$ = stiffness matrix, of order n x n

$[m]$ = mass matrix, of order n x n

$\{y\}$ = system deflection vector, of order n

$\{f\}$ = system force vector, of order n

$\omega$ = forcing frequency

$g$ = structural dynamic coefficient

$j$ = $\sqrt{-1}$

At any forcing frequency, $\omega$, the deflection and force vectors are related by the system mechanical impedance matrix $[z]$, with

$$[z]\{y\} = \{f\} \tag{2}$$

where

$$[z] = (1 + jg)[K] - \omega^2[m] \tag{3}$$

The objective of dynamic modeling is to identify the elements of the stiffness and mass matrices, and consequently, the impedance. Given the impedance matrix, system response may be calculated, either in terms of forces due to applied displacements as in Equation (1), or, more commonly, in terms of displacements due to applied forces. This second characteristic response is obtained using the mechanical mobility matrix [Y], which is the inverse of the impedance matrix. System dynamic displacements are then given by

$$\{y\} = [Y]\{f\} \tag{4}$$

where

$$[Y] = [z]^{-1} \tag{5}$$

The impedance and mobility representations are fundamentally different. Each element in the impedance matrix represents the internal force at some system coordinate due to a unit displacement applied at that, or some other coordinate, when all remaining system coordinates are restrained to have no motion. This condition of restraint, in general, precludes the possibility of directly measuring the values of the individual elements of the impedance matrix. Although these values cannot be directly obtained from test, they are directly obtainable from analytical modeling of the structure, if this is feasible. Once obtained in this manner, the impedance matrix may be inverted to obtain the system mobility matrix, which can then be used to calculate system displacements due to applied forces. It is important to note that the system mobility matrix obtained in this manner will be a valid representation of the structure, as modeled, limited in exactness only by the nature and extent of approximations made in deriving the impedance matrix.

Each element of the mobility matrix relates the displacement at one system coordinate due to the force applied at that or some other coordinate, under the actual physical boundary conditions of the structure. The elements of the mobility matrix are directly measurable quantities, which can be obtained through shake-testing of the structure. In general, however, the values of the elements of the mobility matrix cannot be determined directly through modeling of the structure, since they do not explicitly relate to the physical stiffness, mass, and damping characteristics of the structure. The mobility matrix, therefore, can only be obtained through testing or through inversion of an appropriate impedance matrix.

While it is always possible to obtain a valid mobility matrix by inversion of a valid impedance matrix, the opposite is not true. Both the mobility and impedance matrices relate displacements to forces. The total displacement at any point on a structure due to force excitation at a given frequency is equal to the sum of the displacements in the structure's response modes. In general, the higher the natural frequency of a given mode, the less it contributes to the total displacement produced,* with the modal influence inversely proportional to the square of the modal natural frequency.

Similarly, the force at a point on a structure due to displacement excitation is equal to the sum of the forces induced by the structure's various response modes. In this case, however, the force due to each mode of response is directly proportional to the square of the modal natural frequency. In summary, the forces in a structure are influenced most by the highest frequency response modes, while the displacements are influenced most by the lowest frequency modes. These factors are directly related to the difficulty of obtaining a valid structural impedance matrix from a measured mobility matrix.

The mobility of a structure is determined by measuring the displacement, or more commonly the acceleration, at a number of points on the structure, and ratioing these measured displacements to the applied force. Total displacement is measured, and the influence of all structural response modes will be reflected in the measured mobility only to the extent that each modal response influences the total displacement. For a real structure, having many response modes extending over a wide frequency range, limitations on measurement accuracy cause the displacements due to higher modes to be effectively ignored. In short, the resulting mobility matrix is not a complete representation of the actual structure, since information about the higher response modes is missing. This missing information is not a significant consideration if the mobility is used directly to calculate system responses, since the higher modes do not contribute greatly to the total response. These modes do, however, contribute most significantly to the generation of forces from applied displacements, and consequently, information about the high frequency modes is essential in defining a valid impedance matrix. Since this information is missing in the truncated mobility matrix, inversion of this matrix results in an invalid impedance matrix, which cannot legitimately be used for further manipulations.

---

* This argument is strictly true only when considering the influence of modal responses on the zero frequency or static displacement. The general significance of the argument is, however, pertinent to the response at any frequency.

In the present program, determination of valid impedance matrices for the various transmission dynamic system elements is essential for three reasons. First, impedance representations are needed to perform the component synthesis operation used to join the elemental models to form the total system model. An impedance representation is also needed to calculate the gear-mesh forces which result from the applied gear tooth deflections. Finally, elemental mass and stiffness matrices are required in order to analytically simulate changes in the mechanical elements and calculate their effects, and these matrices can only be obtained from an impedance representation. A system mobility representation is also needed, to calculate total system responses to the induced gear mesh forces.

## COMPONENT SYNTHESIS

The component synthesis concept, fully described in References 8 and 9, relies on the fact that dynamic models of individual mechanical elements may be combined to form a total system dynamic model, provided that the individual models may be represented in terms of appropriate mechanical impedance matrices having one or more common points of response. The mathematical procedure involved in obtaining this system model is illustrated as follows.

The impedance matrix of a complex system containing more than one mechanical element may be obtained by summing the terms in the elemental impedance matrices which correspond to the same physical point. To illustrate this procedure, consider a system comprised of two meshing gearshafts, with impedance matrices given by

$$z_A = \begin{bmatrix} A_{1,1} & A_{1,2} & A_{1,3} \\ A_{2,2} & A_{2,2} & A_{2,3} \\ A_{3,1} & A_{3,2} & A_{3,3} \end{bmatrix} \qquad (6)$$

and

$$z_B = \begin{bmatrix} B_{1,1} & B_{1,2} & B_{1,3} \\ B_{2,1} & B_{2,2} & B_{2,3} \\ B_{3,1} & B_{3,2} & B_{3,3} \end{bmatrix} \tag{7}$$

where $z_A$ = impedance matrix of shaft A

$z_B$ = impedance matrix of shaft B

$A_{1,1}$, $A_{1,2}$, etc. = the terms of the impedance matrix of shaft A

$B_{1,1}$, $B_{1,2}$, etc. = the terms of the impedance matrix of shaft B

The diagonal terms of these matrices ($A_{1,1}$, $A_{2,2}$, $A_{3,3}$, and $B_{1,1}$, $B_{2,2}$, $B_{3,3}$) relate the force produced at a point on the shaft due to a displacement at that point. If the two shafts are in mesh, the displacements of the two shafts at this meshing point will be equal, and the total force produced at this point will be equal to the product of this displacement and the sum of the individual shaft impedances at this point. For example, if point (3) on Shaft A and point (1) on Shaft B correspond to a gear mesh point, then their displacements are equal, and the total impedance at this point is equal to the sum of the impedances at these points, on the two shafts. The combined system impedance is then given by

$$z_{AB} = \begin{bmatrix} A_{1,1} & A_{1,2} & A_{1,3} & 0 & 0 \\ A_{2,1} & A_{2,2} & A_{2,3} & 0 & 0 \\ A_{3,1} & A_{3,2} & (A_{3,3} + B_{1,1}) & B_{1,2} & B_{1,3} \\ 0 & 0 & B_{2,1} & B_{2,2} & B_{2,3} \\ 0 & 0 & B_{3,1} & B_{3,2} & B_{3,3} \end{bmatrix} \tag{8}$$

In the simple case shown, only one pair of terms are added. The resulting matrix has a number of terms equal to the sum of the terms in the elemental matrices, minus one, and terms in the combined matrix which are undefined in either elemental matrix are equal to zero. This same procedure may be applied to combine any number of elements.

As indicated in Equation (8), the system impedance matrix will grow in size almost directly with the sizes of the individual elemental matrices which are combined. Proceeding in this manner, the ultimate system impedance matrix will contain almost as many terms as the sum of the terms in the elemental matrices. An impedance matrix constructed in this manner will retain all of the detail response prediction capability of the individual matrices, enabling calculation of responses at any point considered in the formulation of the elemental models. This matrix will, however, be too large to permit easy and efficient manipulation if great detail is required in the elemental models, as in the present problem. Fortunately, the size of the system impedance matrix may be substantially reduced, through elimination of unnecessary response points, while retaining a complete representation of the dynamic system.

The size of the individual element impedance matrices is dictated by the need to make accurate calculations of element response at the highest forcing frequency of interest. For the high frequencies associated with transmission gear-meshing forces, a large number of shaft and case degrees of freedom must be considered and the impedance matrices for these elements contain many terms. However, if only the responses at the case surface to one exciting force are ultimately required, the system impedance matrix need only contain terms relating that force to the desired surface responses. This reduced system impedance matrix may be produced as follows.

First, detailed elemental models are derived and impedance matrices representing these models are generated for each forcing frequency. The impedance matrices are then inverted to obtain elemental mobility matrices. Since the terms of these mobility matrices are independent of one another, terms which relate displacements and forces not of interest in the final system model may be eliminated. For example, the mobility matrix of a gearshaft will contain terms relating displacements and forces at many points on the shaft. If shaft response need not be calculated, as in the case where only transmission case surface response is required, many of these terms may be eliminated. Only points which will interface with other physical components, such as points where bearings are located or where gear meshing takes place, must be retained.

Having eliminated the extraneous terms from the elemental mobility matrices, they are inverted to form new reduced elemental impedance matrices. These reduced impedance matrices implicitly contain all of the degrees of freedom included in the original impedance matrices. They may now be combined, using the method of Equation (8), resulting in an impedance matrix of the total system for each forcing frequency.

A system impedance matrix derived in this manner may still include excessive detail, resulting from the retention of system interconnection points needed only to combine the individual reduced impedance matrices. This system impedance matrix may be further reduced by inverting it to form a mobility matrix, removing those terms not directly involved in obtaining the desired responses, and reinverting to obtain the final reduced system impedance matrix. In the example discussed previously, only those terms in the mobility matrix which directly relate the gear-mesh force of interest to the case surface responses need be retained.

Application of the preceding methods in the present program resulted in substantial reduction in the size of the impedance matrix ultimately used to represent the SH-2 transmission system. The SH-2 transmission system consists of four gearshafts and a planetary system. The total number of degrees of freedom used to model these shafts was 445. The case was modeled with 44 degrees of freedom, for a total of 489 individual element degrees of freedom. The synthesized system impedance model for these combined elements would have been a 473 x 473 term matrix, considering elimination of duplicated interconnection points for the gear meshes and bearings. Reduction of many extraneous degrees of freedom from this impedance model reduced it to a 48 x 48 matrix. Although further reduction could have been achieved, this matrix size was compatible with the available computer capability, and no additional reduction was performed. It is interesting to note, however, that the most commonly performed response calculation, prediction of case surface response to a single gear clash force, could have been accomplished with a 14 x 14 impedance matrix, which represents a 34/1 reduction in size from the unreduced system impedance matrix.

## TRANSMISSION CASE MODELING

Previous efforts in the dynamic modeling of helicopter transmissions (References 3, 4, 5, and 6) have not included development of explicit dynamic models of the transmission case. While the importance of case dynamics has been recognized, modeling has not been attempted because of the difficulty of the task, and because of a lack of confidence that a case model developed by purely analytical means would adequately reflect actual case responses. In the present program, the importance of the transmission case is similarly recognized, and concern for the ability of analytical means to handle the task of case modeling is shared. However, it is believed that inclusion of an appropriate representation of the case is so fundamental to the prediction of transmission vibration and

noise that case dynamics cannot reasonably be ignored. As a consequence of these conclusions and concerns, an explicit model of the transmission case has been derived from actual test data, using incomplete modeling methods, described in Reference 11. The application of these methods in the present program is described in the following paragraphs.

Derivation of the Modeling Method

As stated in the report section dealing with structural dynamics concepts, modeling of a mechanical structure in terms of its impedance or mass and stiffness characteristics cannot proceed directly from measurement of the structure's mechanical mobility. There exists, however, a method which can be used to derive these necessary characteristics from measured data. This method, which has been used successfully in previous efforts (Reference 11), makes use of the measured normal modes of the case, in conjunction with an analytically determined case mass matrix.

The dynamic model required to represent the transmission case consists of a mass matrix [m], a stiffness matrix [K], and a structural damping matrix, jg[K], where g is the structural damping coefficient and $j = \sqrt{-1}$. It is possible to express these matrices in terms of the normal modes of the system, as can be seen below. However, it is not physically possible to accurately measure as many modes as there are degrees of freedom in the system and thus these matrices can not be completely derived from test data alone. The method of incomplete models makes use of the necessary orthogonality conditions among the modes of the system. This is expressed as

$$\{\phi_i\}^T[m]\{\phi_j\} = 0, \quad i \neq j \tag{9}$$

where $\{\phi_i\}^T$ = the transpose of the normal mode vector of mode i

$[m]$ = the mass matrix

$\{\phi_j\}$ = the normal mode vector of mode j

[11] Berman, A., Flannelly, W. G., THEORY OF INCOMPLETE MODELS OF DYNAMIC STRUCTURES, AIAA Journal, Volume 9, No. 8, August 1971, pp 1481-1487.

Since there are an infinite number of solutions to this equation, physical validity is obtained by first deriving a mass matrix through normal analytical methods. Mathematical validity of this intuitively derived mass matrix is obtained by adjusting the terms of the matrix to satisfy the orthogonality relationships of Equation (9). In performing this operation, a relatively small number of measured structural modes are used, resulting in fewer equations than there are unknown masses. Retention of physical validity is further promoted by prescribing sensitivities to change for each term of the matrix. Those terms believed to have the highest physical validity, generally the diagonal terms, are permitted to change the least in response to the requirements of the orthogonality relationships, while those felt to be most approximate are allowed to change more. Since no unique solution exists for a set of equations having more unknowns than equations, the solution which produces the smallest change in the intuitively derived mass matrix is determined. To achieve this, the sum of the squares of the changes in the terms of the mass matrix is minimized, considering the prescribed sensitivities to change. The mathematical procedure for obtaining this least-squares solution is described in Reference 11.

Given the identified mass matrix and the incomplete set of measured modes, an impedance representation of the structure can be derived. In these terms, the modal expansion of the impedance of the structure is

$$[z]_{inc} = [m] \left\{ \sum_{i=1}^{N} \frac{1}{m_i} [(\omega_i^2 - \omega^2) + j\, \omega_i^2 g_i] \psi_i \phi_i^T \right\} [m] \qquad (10)$$

where $[z]_{inc}$ = incomplete structural impedance matrix

$[m]$ = identified mass matrix of the structure

$\omega$ = forcing frequency

$N$ = number of measured modes

The effects of structural damping are included in Equation (10). The complex incomplete stiffness matrix including damping may be written:

$$[\bar{K}]_{inc} = [m]\left(\sum_{i=1}^{N} \frac{\Omega_i^2}{m_i}(1 + jg_i)\phi_i\phi_i^T\right)[m] \tag{11}$$

where $\Omega_i$ = natural frequency of the i-th mode

$g_i$ = modal damping coefficient of the i-th mode

$j$ = $\sqrt{-1}$

$\phi_i$ = modal response of the i-th mode

$m_i$ = modal mass of the i-th mode

The modal mass, $m_i$, and modal damping may be obtained directly from the measured modes and mechanical mobility test data, and the identified mass matrix, as follows:

$$m_i = \phi_i[m]\phi_i^T \tag{12}$$

$$g_i = (Y_i)_{imag} \cdot m_i \cdot \Omega_i \tag{13}$$

where $(Y_i)_{imag}$ = imaginary driving point mobility measured for the i-th response mode

Equation (12) is exact and Equation (13) is a good approximation for lightly damped structures.

Since the method of component synthesis used in this analysis requires that the impedance matrices be inverted, the form of Equation (10) is not suitable, since it is singular. However, a small deviation in form, which uses the complete identified mass matrix, may be written

$$[z]_H = -\omega^2[m] + \bar{K}_{inc} \tag{14}$$

where $[z]_H$ = hybrid impedance matrix

The hybrid impedance is nonsingular and is valid for all frequencies within the range of the natural frequencies of the modes used in the analysis. This method is more completely described in Reference 12. The mobility of the system at any frequency is given by

$$[Y]_H = [z]_H^{-1} \tag{15}$$

Equations (14) and (15) have been used in the present program to generate impedance and mobility matrices for the transmission case, using measured case mechanical mobility data.

Transmission Case Mechanical Mobility Testing

The SH-2 helicopter main transmission case that was tested is shown in Figure 2. This is a typical case structure weighing approximately 100 pounds. Testing was performed under free-free boundary conditions, by suspending the case from soft rubber springs. All internal components, including all shafts and bearings, were removed prior to testing, with the exception of the steel bearing liners, which were left in place.

A total of 44 case degrees of freedom were assumed in the analytical model and, consequently, case responses at 44 locations were measured, each location corresponding to one coordinate of the analytical model. Radial responses in two orthogonal directions were measured at each of eight shaft support locations, and six radial responses were measured on the outside circumference of the ring gear. These data were needed to define case dynamic characteristics at the case-gear/gearshaft interface points. An additional eight response measurements were made at the transmission-to-airframe mounting points, to provide the data needed to evaluate the effects of transmission support dynamics. The remaining fourteen response measurements were made at locations distributed over the case external surface. These data were needed to enable the calculation of case surface response and radiated noise.

[12] Berman, A., SYSTEM IDENTIFICATION OF A COMPLEX STRUCTURE, AIAA Paper No. 75-809, Presented at the AIAA/ASME/SAE 16th SDC Meeting, Denver, Colorado, May 1975.

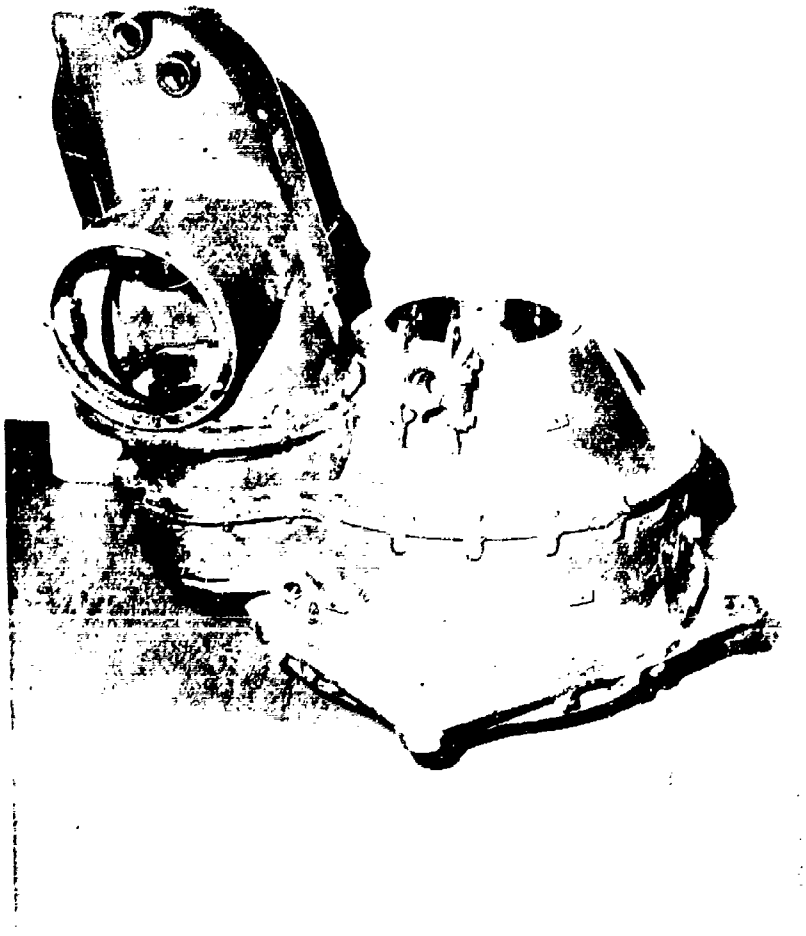

Figure 2. SH-2 Transmission Case

Case response testing was performed using the test setup shown in Figure 3. The case was elastically supported with a low-rate suspension system to simulate a free-free boundary condition. Dynamic force was applied, through an impedance head, with an electromagnetic shaker, and case responses were measured with a piezoelectric accelerometer. Accelerometer mounting blocks, machined to conform with the local case contour, were used to provide attachment of the impedance head and accelerometer. These mounting blocks were permanently attached to the case surface with a rigid epoxy bonding agent, and the accelerometer was connected to the mounting block with a threaded fastener. This approach permitted using a single accelerometer to make all 44 response measurements, greatly reducing calibration requirements.

The instrumentation network used is shown schematically in Figure 4. The detail characteristics of this instrumentation are given in Table 1. The key element of the instrumentation network is the mechanical impedance co/quad analysis system. This system provides an oscillator signal which controls the frequency of excitation which is applied to the case through the power amplifier and shaker. The system also conditions the measured response signals, filtering out all extraneous responses not occurring at the excitation frequency. Finally, the conditioned response signals, which are analogous to the applied force and induced acceleration, are analyzed to produce the coincident (Co) and quadrature (Quad) components of mechanical mobility.* These Co and Quad, or real and imaginary, mobility signals are directed to an x-y plotter.

* The coincident or real component is in phase with the applied force, while the quadrature, or imaginary component, is 90° out of phase with the applied force.

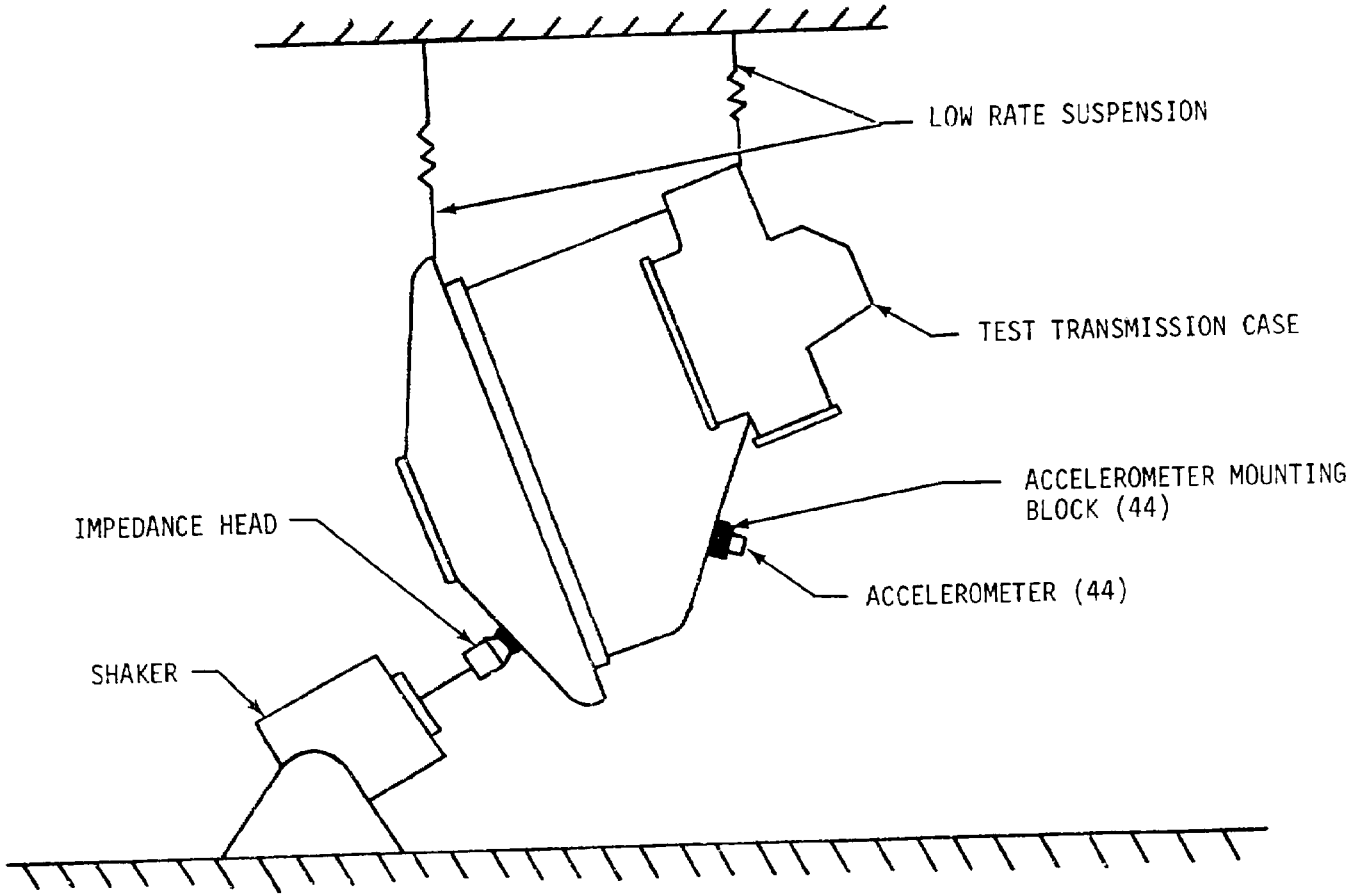


Figure 3. Transmission Case Shake Test Setup

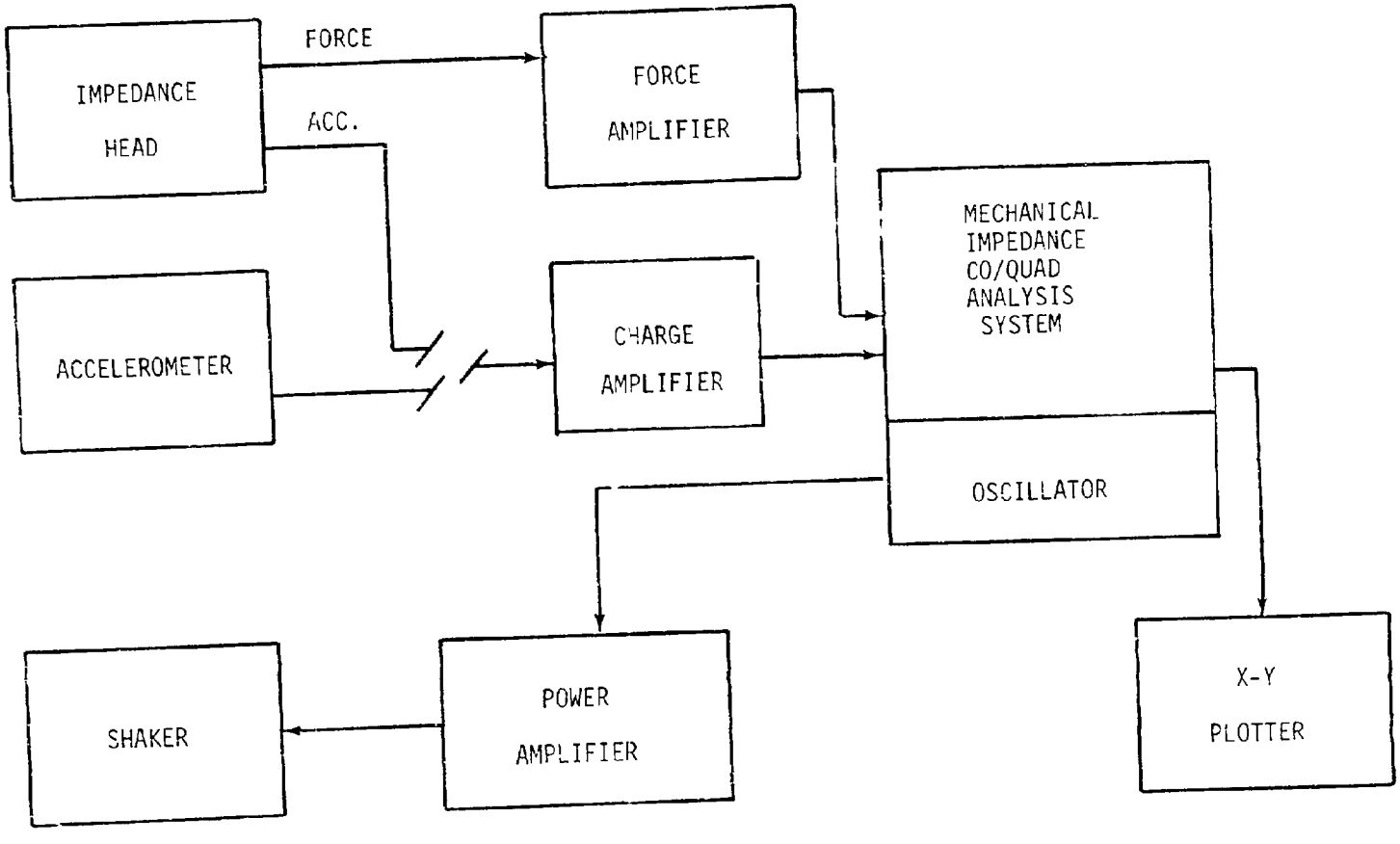


Figure 4. Case Mobility Test Instrumentation Network

TABLE 1. CASE MOBILITY TEST INSTRUMENTATION

| Description | Manufacturer | Model No. |
|---|---|---|
| Impedance Head | Wilcoxon | Z602 |
| Accelerometer | B & K | 4332 |
| Charge Amplifier (2) | Kistler | 504A |
| Analysis System | Spectral Dynamics | SD1002E |
| Shaker | Ling | 411 |
| Shaker Amplifier | MB | - |

Two transducers were used, an impedance head and an accelerometer. The impedance head, which includes both force and acceleration sensing elements, was used to measure applied dynamic force and dynamic acceleration induced at the point of excitation (driving point). The accelerometer was used to measure induced dynamic acceleration at all other points on the case. Both the impedance head and accelerometer are piezoelectric devices, which generate very low-level signals. These signals were amplified, prior to being applied to the analysis system, through the use of separate charge amplifiers.

The instrumentation network was physically calibrated prior to performance of the case mobility test. The calibration procedure involved measurement of the real mobility of a known 1-pound mass, using the impedance head alone, and the impedance head force transducer with the separate accelerometer. Real mobility of the known mass was measured over the test frequency range of 500 Hz to 5500 Hz, for a 10/1 range of measurement system gain. Data from these calibrations, which correspond to a mobility of 1 g/lb, were used to establish the magnitude of actual measured case mobility.

The test procedure used to obtain the case mobility data is as follows: Excitation was applied and the frequency of excitation was slowly swept over the range of interest. Initially, this frequency range extended from 100 Hz to 5500 Hz, but the lower limit was raised to 500 Hz when no significant case responses were found between 100 Hz and 500 Hz. The sweep rate, which is controllable through the analyzer, was kept low enough to accurately define peak mobility at the case resonant frequencies. System gain was adjusted for each response point to contain the generated mobility curve within the plotter limits. Real and imaginary mobilities were measured through separate excitation sweeps, and excitation amplitude was kept constant for all measurements through the use of the analyzer's servo control capability. To maximize accuracy of the generated mobility curves, the total frequency range of interest was covered in two separate sweeps, the first extending from 500 Hz to 3000 Hz and the second from 3000 Hz to 5500 Hz.

The data which resulted from this testing is typified by the driving point mobility curves of Figure 5. Similar curves were obtained for the transfer mobilities relative to each of the remaining 43 case response positions.

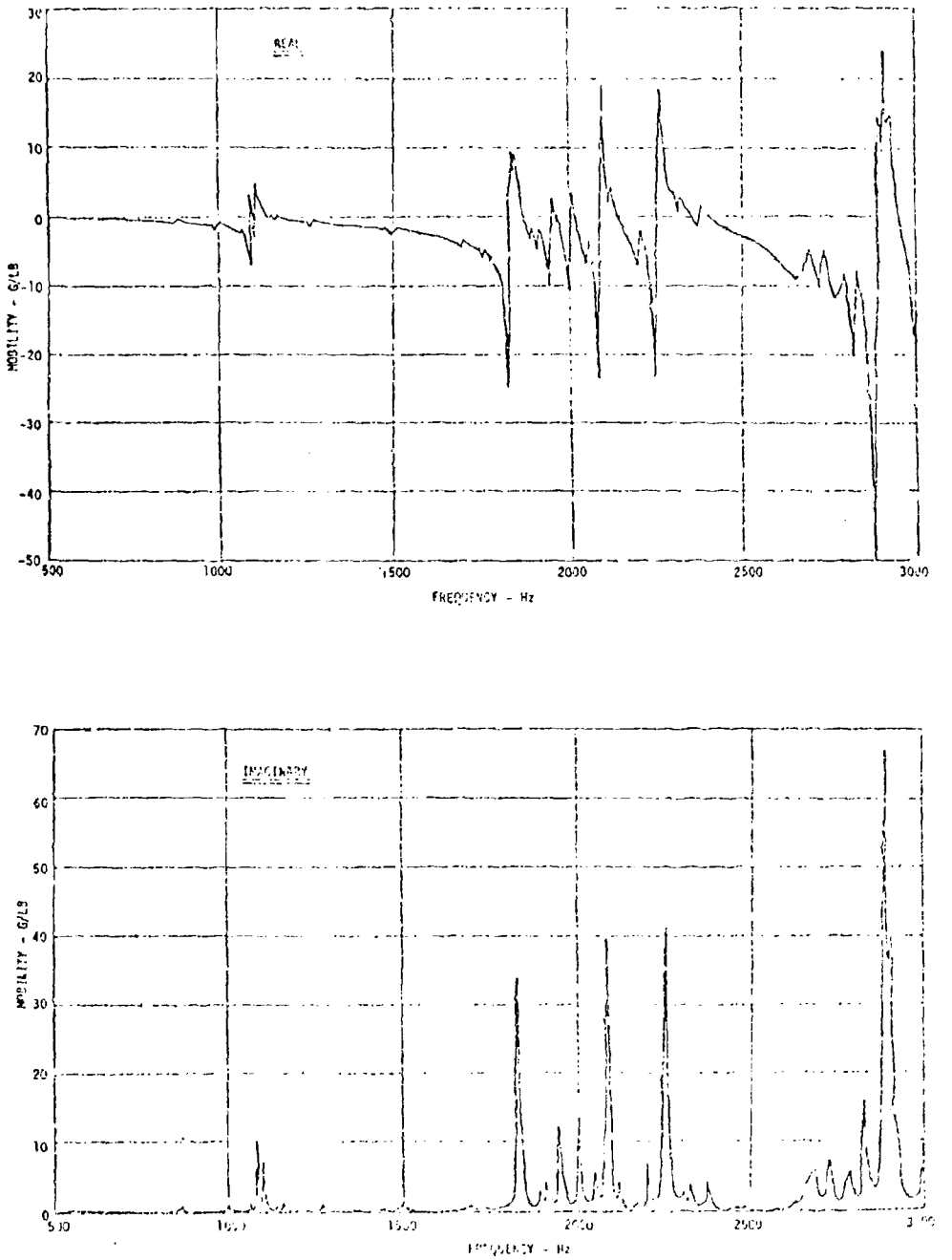


Figure 5. Measured Case Driving Point Mobility

Development of the Case Model From the Test Data

The approximate mass matrix of the transmission case was obtained in a simple intuitive manner. First, the case was divided into 44 regions, corresponding to the 44 established case coordinates, with the center of each region one of the response measurement locations. The weights of each region were estimated and adjusted so that the resulting diagonal mass matrix would satisfy the rigid body equations of motion, for the three translational rigid body degrees of freedom. This procedure resulted in the definition of the diagonal elements of the required 44 x 44 mass matrix. Each element was assigned a weighting factor indicative of the confidence placed on the estimated value. These weighting factors were needed to apply the incomplete modeling method described previously.

Off-diagonal elements of the mass matrix were similarly defined, but in this case, only the existence of significant off-diagonal terms was specified and not their actual values. The existence of these terms was predicated on geometrical reasoning, with elements specified only where two physically adjacent case coordinates, or response positions, were geometrically far apart. For this condition, the off-diagonal element connecting these two coordinates was specified to have a non-zero but otherwise unknown value. Weighting factors for these elements were also assigned.

The mass matrix resulting from the preceding intuitive analysis is approximate in that the necessary conditions of orthogonality, expressed in Equation (9), have not been considered. As discussed previously, these relationships must be satisfied in order to obtain mathematical validity of the mass matrix, and application of these relationships requires knowledge of the normal modes of the structure. Given certain assumptions, the normal modes of the transmission case are obtainable directly from the mobility test data.

For a lightly damped structure, such as the transmission case, the normal modes are approximately equal to the normalized imaginary responses at the resonant frequencies. Since the mobility data obtained in the case mobility testing are normalized responses (normalized to applied force) the imaginary mobilities were used directly as the required normal modes.

Use of the measured imaginary mobilities as the normal modes is based on an additional criterion, independent of the assumption of low case damping. These data can only be interpreted in this manner if the modes are well separated with respect to frequency for the transmission case. This condition is approximately satisfied, as indicated in Figure 5, only up to a frequency of 3000 Hz. Above this frequency, the response modes are not well separated, and this condition is not met. For this reason it was decided to use the mobility data only up to 3000 Hz. Consequently, the case dynamic models developed from these data are only applicable for this frequency range.

The transmission case exhibited more than 20 normal modes within the range of 500 Hz to 3000 Hz. Since the impedance is required at discrete frequencies only, there is no necessity for the same analytical model to be used throughout the entire frequency range. All that is required is that, at each frequency used, the inverse of the impedance matrix is representative of the dynamic response of the structure. It was found to be convenient and effective to develop several models, each using up to 10 normal modes in the frequency range of interest.

The validity of this approach can be demonstrated through interpretation of Equation (15), which is an expression of the case mobility as derived from incomplete modeling methods. This equation can be rewritten as (Reference 12)

$$[Y]_H = \frac{1}{\omega^2} \sum_{i=1}^{P} \frac{1}{m_i} \left\{ \frac{[(\frac{\Omega_i}{\omega})^2 - 1] - j(\frac{\Omega_i}{\omega})^2 g_i}{[(\frac{\Omega_i}{\omega})^2 - 1]^2 + (\frac{\Omega_i}{\omega})^4 g_i^2} \right\} \phi_i \phi_i^T \qquad (16)$$

with $\Omega_i = 0$ for $i = (N+1)---P$

In this equation the modes which contribute most to the mobility are those whose natural frequencies ($\Omega_i$) are closest to the forcing frequency ($\omega$). Consequently, the dynamic model, represented by the mobility matrix, will be valid if all significant modes close to the forcing frequency are included in defining the impedance matrix and its constituent mass and stiffness matrices. Conversely, those modes sufficiently removed in frequency from the forcing frequency can be ignored. This approach could be applied in the present program because the system dynamic model was to be used to predict responses only at discrete frequencies. Consequently, several case models could be developed, and the appropriate model used for any given discrete frequency excitation.

Three distinct case mass matrices were developed. A mass matrix appropriate for the frequency range of 500 Hz to 1900 Hz was developed using the lowest seven significant modes with natural frequencies of 1080 Hz to 2250 Hz. Eight modes with natural frequencies of 1827 Hz to 2370 Hz were used to identify a mass matrix suitable for the 1900 Hz to 2300 Hz range. The mass matrix required to predict responses in the 2300 Hz to 3000 Hz range was identified using 10 modes, extending from 1827 Hz to 2890 Hz.

Each of the three frequency-limited case mass matrices was identified from the same intuitively derived approximate mass matrix. Because different modal data were used, however, the three identified mass matrices differed slightly from each other, as well as from the approximate matrix. The magnitude of change from the approximate matrix is an indication of the physical validity of the identified matrices, with large changes indicating decreased physical validity. For the three case mass matrices identified in the present program, only small changes occurred. Thirty-four percent of the diagonal elements changed less than 1 percent, and 63 percent changed less than 5 percent. All elements remained positive and all were considered to have reasonable values. The mean absolute value of the diagonal terms of a typical identified case mass matrix was .019 pound-sec$^2$/inch, while the mean of the non-zero off-diagonal elements was .012 pound-sec$^2$/inch.

Having identified suitable case mass matrices, the stiffness matrices and case impedance matrices were determined using Equations (11) and (14). This completed the development of the case dynamic model.

Evaluation of the Case Dynamic Model

Once the case mass matrices were identified, the modal masses ($m_i$) and modal damping coefficients ($g_i$) were calculated. The modal mass for each measured response mode was calculated, using Equation (12). These were used in conjunction with the measured imaginary mobilities ($Y_i$), and natural frequencies ($\Omega_i$), in Equation (13), to calculate the modal damping. This calculation was performed in order to evaluate the assumption of low case damping used to perform the analysis. Modal damping coefficients calculated in this manner ranged from .0015 to .03, which are well within the range of damping coefficients normally considered for lightly damped structures. This confirmed the assumption that the transmission case was a lightly damped structure.

Only the measured imaginary mobilities were used to develop the case dynamic model; however, the resulting model has the capability of calculating real as well as imaginary mobility. In order to verify the accuracy of the model, calculations of real case mobility were made and compared to measured real mobility. This comparison is illustrated in Figure 6, which shows measured and calculated real mobilities for response at the driving point and at one other point on the case.

The high degree of correlation evident in Figure 6 was obtained, in the low- and mid-frequency ranges, with the directly derived mobility matrices. However, the initial correlation obtained with the high-frequency model, applicable over the range of 2300 Hz to 3700 Hz, was not considered adequate, and this model was subsequently changed.

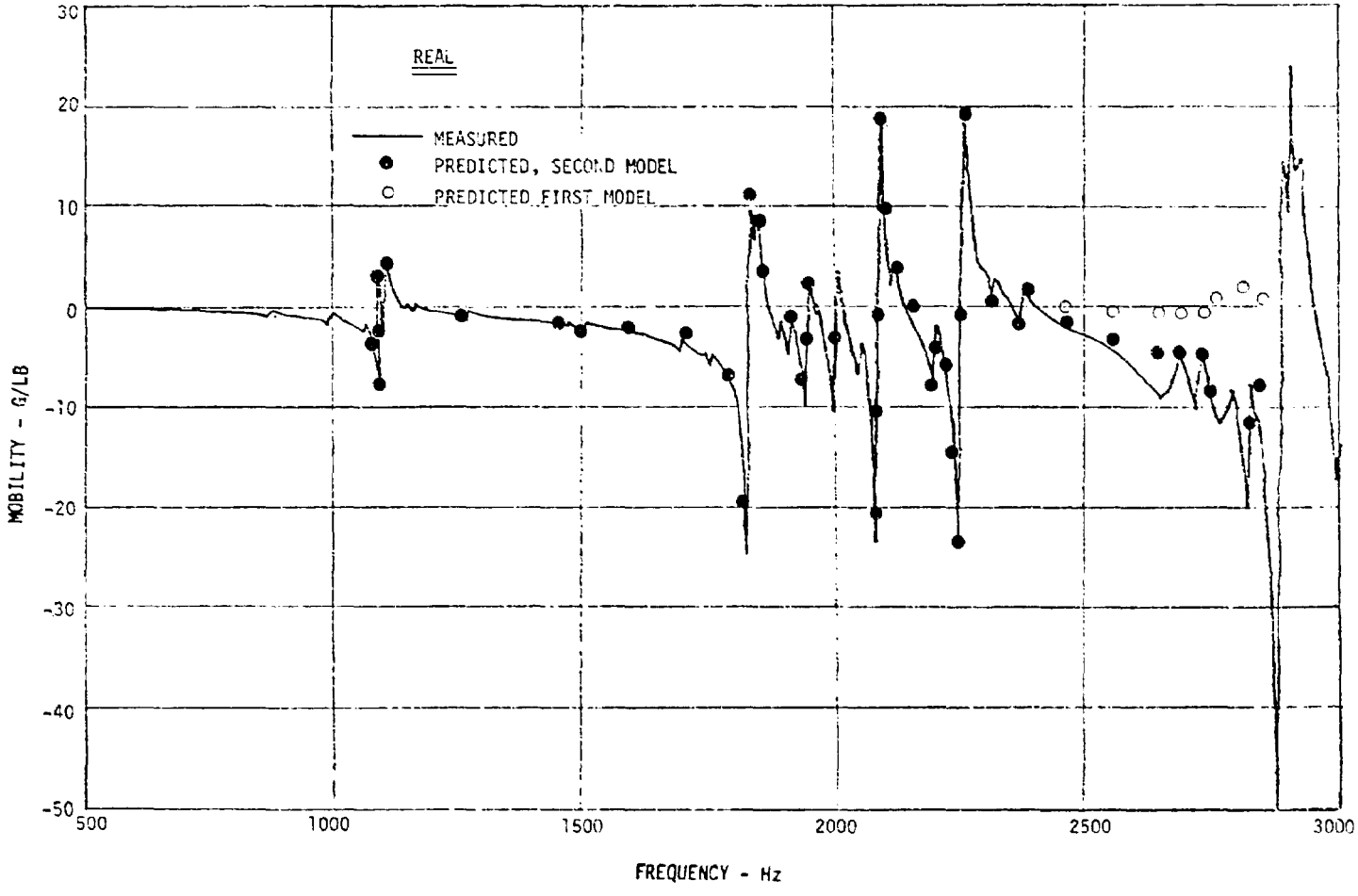


Figure 6. Real Mobility Correlation

Good correlation was then obtained, as shown in Figure 6, by changing the values of modal mass ($m_i$) and modal damping ($g_i$) while keeping their product constant. This causes variations in the calculated real mobility, but does not change the imaginary mobility. The physical significance of the initial model deficiency relates to the fact that the actual number of degrees of freedom inherent in the transmission case is much greater than the 44 degrees of freedom assumed in the analysis.

It should be pointed out that the changes in the analytical model which were introduced to improve correlation did not reduce either the physical or mathematical validity of the resulting model. Ultimately, the most important criterion in judging the validity of the model is how well it predicts actual case responses. In this regard, the validity of the transmission case model developed in the present program is adequately demonstrated by the correlation data of Figure 6.

## SHAFT MODELING

The objective of gearshaft modeling is to obtain valid mechanical impedance representations of each shaft. These shaft impedance matrices can then be joined with the case impedance matrix, using component synthesis methods, to form a dynamic response model of the total transmission system. In contrast to the previously described case modeling approach, which is based on physical test data, gearshaft modeling is accomplished by purely analytical methods. The Holzer-Myklested technique for dynamic modeling of slender shafts is used, with local nonslender shaft elements, such as the gears themselves, treated as lumped masses and inertias. Both shaft flexure (bending) and torsion are considered.

### Theoretical Background

In the mathematical analysis of the vibrations of a slender rotating shaft, the shaft is described by a succession of (N) shaft segments, which are interspersed between (N+1) stations. Each segment is treated as a uniform torsion-flexure element with distributed inertia. At each station, there may be assigned an attached rigid-body inertia and/or an external excitation. A typical shaft model is illustrated in Figure 7.

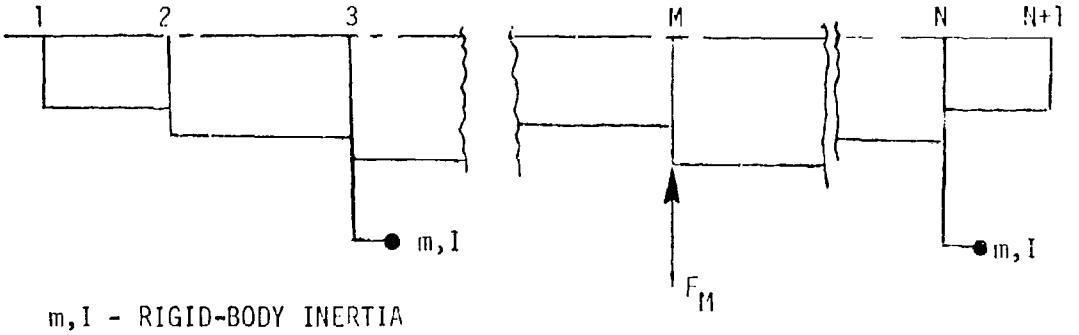


m,I - RIGID-BODY INERTIA

$F_M$ - EXCITATION

Figure 7. Gearshaft Representation

In matrix notation, the generalized external excitation $\underline{F}_M$ is a column vector, consisting of five elements:

- Lateral force in the major or vertical plane,
- Lateral moment in the major or vertical plane,
- Lateral force in the minor or horizontal plane,
- Lateral moment in the minor or horizontal plane, and
- Torsional moment.

Corresponding to the generalized excitation $\underline{F}_M$, there is a generalized displacement $\underline{X}_M$, also consisting of five elements, which repsectively designate the five degrees of freedom:

- Lateral displacement in the major or vertical plane,
- Lateral slope in the major or vertical plane,
- Lateral displacement in the minor or horizontal plane,
- Lateral slope in the minor or horizontal plane, and
- Angle of twist.

If there are m stations at which external excitations act, then the overall excitation vector $\underline{f}$ and the overall displacement $\underline{x}$ each have 5 x m elements. The objective of shaft modeling is to establish an impedance matrix, $\underline{z}$, such that

$$\underline{f} = \underline{\underline{Z}} \cdot \underline{x} \tag{17}$$

If the ordering of the matrix elements is

Lateral displacement and slope in the major or vertical plane,

Lateral displacement and slope in the minor or horizontal plane,

Twist,

then the structure of the impedance matrix is

$$\underline{\underline{Z}} = \begin{bmatrix} \underline{\underline{Z}}_{11} & \underline{\underline{Z}}_{12} & \underline{0} \\ \underline{\underline{Z}}_{21} & \underline{\underline{Z}}_{22} & \underline{0} \\ \underline{0}^T & \underline{0}^T & \underline{\underline{Z}}_{33} \end{bmatrix} \tag{18}$$

where $\underline{\underline{Z}}$ = shaft impedance matrix

$\underline{\underline{Z}}_{11}$ = impedance submatrix relating responses in major (vertical) plane to excitations in major (vertical) plane

$\underline{\underline{Z}}_{22}$ = impedance submatrix relating responses in minor (horizontal) plane to excitations in minor (horizontal) plane

$\underline{\underline{Z}}_{12}$ = impedance submatrix relating responses in major (vertical) plane to excitations in minor (horizontal) plane

$\underline{\underline{Z}}_{21}$ = impedance submatrix relating responses in minor (horizontal) plane to excitations in major (vertical) plane

$\underline{\underline{Z}}_{33}$ = impedance submatrix relating torsional response (twist) to torsional excitation

$\underline{0}, \underline{0}^T$ = null submatrices

Similarly, the force and displacement vectors may be partitioned as

$$\underline{f} = \begin{bmatrix} \underline{f}_1 \\ \underline{f}_2 \\ \underline{f}_3 \end{bmatrix} \tag{19}$$

and

$$\underline{x} = \begin{bmatrix} \underline{x}_1 \\ \underline{x}_2 \\ \underline{x}_3 \end{bmatrix} \tag{20}$$

where $\underline{f}_1$, $\underline{x}_1$ = excitation and response submatrices in major (vertical) plane

$\underline{f}_2$, $\underline{x}_2$ = excitation and response submatrices in minor (horizontal) plane

$\underline{f}_3$, $\underline{x}_3$ = excitation and response vectors in the torsional plane

Partitioning of the shaft impedance matrix in the form of Equation (18) reveals the characteristics and significance of the various matrix elements. The lateral (bending) responses are reflected in the submatrices $\underline{Z}_{11}$, $\underline{Z}_{22}$, $\underline{Z}_{21}$, and $\underline{Z}_{12}$. Each of these submatrices contains two elements for each shaft station, one element for responses due to lateral force excitation and one for responses due to bending moment excitation. The order of each of these submatrices is then Z x m, where m is the number of shaft stations. The diagonal submatrices, $\underline{Z}_{11}$ and $\underline{Z}_{12}$, are driving point impedances while the off-diagonal submatrices, $\underline{Z}_{21}$ and $\underline{Z}_{12}$, are transfer matrices. The off-diagonal submatrices are, in general, nonzero because of coupling between the major (vertical) and minor (horizontal) lateral bending responses. This coupling is due to shaft rotation and, because of shaft symmetry, the off-diagonal submatrices $\underline{Z}_{21}$ and $\underline{Z}_{12}$ are negative reflections of each other.

Shaft torsional responses are reflected in the submatrix $\underline{\underline{Z}}_{33}$. Since only one source of excitation is considered in torsion, this submatrix is of rank m. Since linear slender-shaft vibration theory states that lateral (bending) and torsional response degrees of freedom are uncoupled, the remaining submatrices of Equation (18) are null matrices. All terms of the Q and $\underline{\underline{Q}}^T$ submatrices are zero. The $\underline{\underline{Q}}$ matrix is of order 2m x m, while the $Q^T$ matrix, which is the transpose of the $\underline{\underline{Q}}$ matrix, is of rank m x 2m.

Matrix Transfer Method

The characteristics of the shaft impedance matrix, $\underline{\underline{Z}}$, of Equation (18) are calculated using a procedure known as the "matrix transfer method". This approach considers each shaft segment (Figure 7) independently, with coupling between individual shaft segments treated as boundary conditions. The presence of applied excitations and/or lumped mass/inertia elements at segment connection points is dealt with by considering the impact of these factors on the local boundary conditions. Application of this method proceeds from one shaft segment to the next, until all individual segments are coupled and the full shaft impedance matrix is defined.

Application of the "matrix transfer method" to one generalized shaft segment may be illustrated by considering the diagram of Figure 8. In this diagram the shaft segment m is considered. Also considered are the presence of a local excitation vector, $\underline{F}_m$, and a lumped mass/inertia element, $m_m$, $I_m$. The segment under study is considered to consist of four junctions: $m_a$, $m_b$, $m_c$, and $(m+1)_a$. The local excitation vector, $\underline{F}_m$, is defined as acting between junctions $m_a$ and $m_b$, while the lumped mass/inertia element, $m_m$, $I_m$, is defined as located between junctions $m_b$ and $m_c$. Flexure and torsion of the shaft segment itself is defined as occurring between junctions $m_c$ and $(m+1)_a$. Using these conventions, the shaft segment is placed in force and moment equilibrium, by separately considering the external and internal forces and moments which act between the defined junctions.

At each junction a primitive vector, $\underline{Q}_\alpha$, is defined, where $\alpha$ denotes the junction location. Each of these primitive vectors is a set of 10 local shaft characteristics, including four flexure variables for each orthogonal response direction, and two torsion variables. Flexure variables included in $\underline{Q}_\alpha$ are:

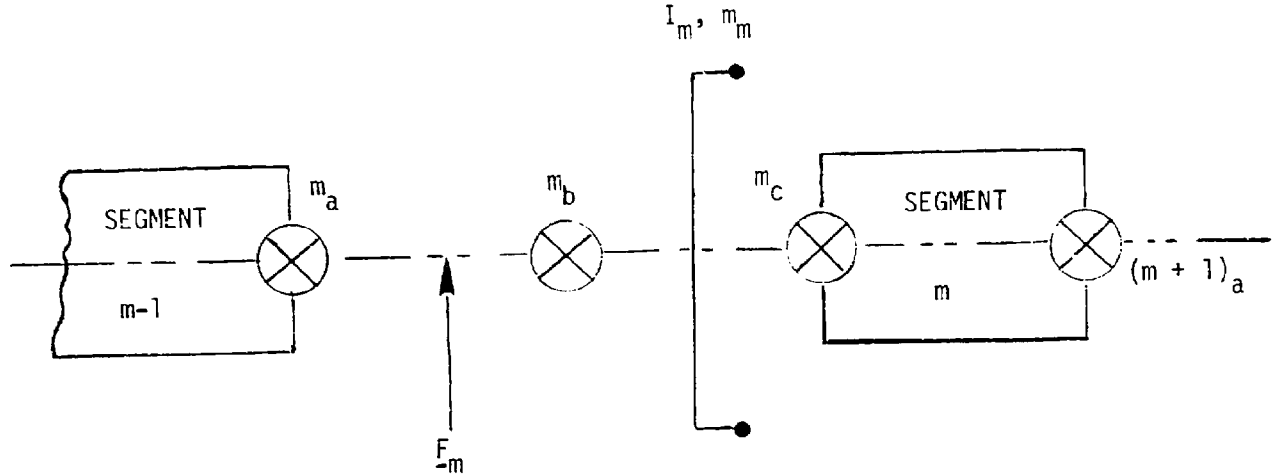


Figure 8. Matrix Transfer Method

- Shear force.
- Bending moment.
- Slope.
- Transverse Displacement.

Torsion variables considered are:

- Torsion moment.
- Twist (torsion) angle.

In vector notation, the primitive vector, $\underline{Q}_\alpha$, is given by

$$\underline{Q}_\alpha = \begin{bmatrix} (P_1)_1 \\ (P_2)_2 \\ (U_1)_1 \\ (U_2)_1 \\ (P_1)_2 \\ (P_2)_2 \\ (U_1)_2 \\ (U_2)_2 \\ P_3 \\ U_3 \end{bmatrix} \tag{21}$$

where $(P_1)_1$, $(P_2)_1$ = shear force and bending moment in major (vertical) plane

$(U_1)_1$, $(U_2)_1$ = lateral deflection and slope in major (vertical) plane

$(P_2)_2$, $(P_2)_2$ = shear force and bending moment in minor (horizontal) plane

$(U_1)_2$, $(U_2)_2$ = lateral displacement and slope in minor (horizontal) plane

where $P_3$ = torsional moment

$U_3$ = twist (torsion) angle

In Figure 8, the presence of the external force vector, $\underline{F}_m$, results in a change in shear force, bending moment and torsional moment between junctions $m_a$ and $m_b$. Therefore, the primitive vectors for these two junctions are different, with $(\underline{Q}_m)_b$ related to $(\underline{Q}_m)_a$ according to:

$$(\underline{Q}_m)_b = (\underline{Q}_m)_a + \Delta Q_m \tag{22}$$

where

$$\Delta \underline{Q}_m = \begin{bmatrix} (F_1)_1 \\ (F_2)_1 \\ 0 \\ 0 \\ (F_1)_2 \\ (F_2)_2 \\ 0 \\ 0 \\ F_3 \\ 0 \end{bmatrix} \tag{23}$$

with $(F_1)_1$, $(F_2)_1$ = externally applied shear force and bending moment in major (vertical) plane

$(F_1)_2$, $(F_2)_2$ = externally applied shear force and bending moment in minor (horizontal) plane

$F_3$ = externally applied torsional moment

No change in displacement occurs between junctions $m_a$, $m_b$, since these junctions are physically coincident, and this condition is expressed by the zero value elements of Equation (23).

The presence of a lumped mass/inertia element between junctions $m_b$ and $m_c$ is accounted for by considering the d'Alembert force associated with this lumped parameter. The relationship between $(\underline{Q}_m)_c$ and $(\underline{Q}_m)_b$ is then given by

$$(\underline{Q}_m)_c = \underline{D}_m \cdot (\underline{Q}_m)_b \tag{24}$$

where $\underline{D}_m$ = d'Alembert force coefficient matrix

The d'Alembert force coefficient matrix consists of a set of coefficients for the various degrees of freedom and is given by

$$\underline{D}_M = \begin{bmatrix} \underline{1} & \underline{\delta}_{11} & \underline{0} & \underline{\delta}_{12} & \underline{0} \\ \underline{0} & \underline{1} & \underline{0} & \underline{0} & \underline{0} \\ \underline{0} & \underline{\delta}_{21} & \underline{1} & \underline{\delta}_{22} & \underline{0} \\ \underline{0} & \underline{0} & \underline{0} & \underline{1} & \underline{0} \\ 0 & 0 & 0 & 0 & \begin{matrix} 1 & \delta_{33} \\ 0 & 1 \end{matrix} \end{bmatrix}_M \tag{25}$$

where $\delta_{11}$, $\delta_{21}$, etc = d'Alembert force coefficient submatrices

If the lumped mass/inertia properties are expressed as

mass, $m_M$,

center of gravity offset, $y_M$,

transverse mass moment of inertia, $I_M$, and

polar mass moment of inertia, $J_M$,

the d'Alembert coefficients are given by

$$\underline{\underline{\delta}}_{11} = \underline{\underline{\delta}}_{22} = \nu^2 \begin{bmatrix} m_M y_M & m_M \\ -(I_M + m_M y_M^2) & -m_M y_M \end{bmatrix}$$

$$\underline{\underline{\delta}}_{12} = -\underline{\underline{\delta}}_{21} = j\omega J_M \begin{bmatrix} 0 & 0 \\ 1 & 0 \end{bmatrix} \tag{26}$$

$$\underline{\underline{\delta}}_{12} = -\nu^2 J_M$$

with $\nu$ = vibrational frequency

$\omega$ = shaft rotation rate

$j = \sqrt{-1}$

Shaft response characteristics at junction $(m+1)_a$ are related to those at junction $m_c$ through shaft segment flexure and torsion. If segment flexure and torsion are expressed in terms of a transfer coefficient matrix, $\underline{\underline{s}}_m$, the primitive vectors at junctions $(m+1)_a$ and $m_c$ are related by

$$(\underline{Q}_{m+1})_a = \underline{\underline{s}}_m \cdot (\underline{Q}_m)_c \tag{27}$$

with

$$\underline{\underline{s}} = \begin{bmatrix} \underline{\underline{s}}_{11} & \underline{\underline{0}} & \underline{\underline{0}} \\ \underline{\underline{0}} & \underline{\underline{s}}_{22} & 0 \\ \underline{\underline{0}} & \underline{\underline{0}} & \underline{\underline{s}}_{33} \end{bmatrix}_m \tag{28}$$

where $\underline{\underline{S}}_{11}$, $\underline{\underline{S}}_{22}$ = shaft segment flexure transfer coefficients

$\underline{\underline{S}}_{33}$ = shaft segment torsion transfer coefficient

The transfer coefficients of Equation (28) are obtainable from slender-shaft vibration theory, and derivations of these coefficients are given in a subsequent paragraph. It is important to note, however, that since slender-shaft vibration theory neglects rotary inertia for flexure, the off-diagonal elements of Equation (28) are zero. Similarly, since shaft polar symmetry is assumed, the nonzero flexure transfer coefficients, $\underline{\underline{S}}_{11}$ and $\underline{\underline{S}}_{22}$ are equal.

Combination of the preceding successive relationships between $(\underline{Q}_m)_A$ and $(\underline{Q}_m)_B$, $(\underline{Q}_m)_B$ and $(Q_m)_C$, and between $(Q_m)_C$ and $(Q_{m+1})_a$, results in a shaft segment relationship given by

$$(Q_{m+1})_a = \underline{\underline{T}}_m \cdot [(\underline{Q}_m)_a + \Delta\underline{Q}_m] \tag{29}$$

where $\underline{\underline{T}}_m = \underline{\underline{S}}_m \cdot \underline{\underline{D}}_m$

$\underline{\underline{T}}_m$ is defined as the modular transfer matrix, and one such modular transfer matrix is defined for each shaft segment.

For a shaft consisting of m segments, with m greater than one, a succession of modular transfer operations is required. The transfer matrix for this m-segment shaft is then given by

$$\pi_{m,1} = T_m \quad T_{m-1} \cdots\cdots T_1 \tag{30}$$

where $\pi_{m,1}$ = transfer matrix between shaft segment m and shaft segment 1.

$T_m, T_{m-1} \ldots T_1$ = modular transfer matrices

The relationship between the primitive vector for shaft segment m and the initial shaft segment is then given by

$$(\underline{Q}_m)_c = \underline{D}_m \cdot [\underline{\pi}_{m-1,1} \cdot (\underline{Q}_1)_a + \sum_{h-1}^{n} \underline{\pi}_{m-1,m_k} \cdot \underline{\Delta Q}_{m_k}] \tag{31}$$

with $(\underline{Q}_m)_c$ = primitive vector at shaft segment m

$\underline{D}_m$ = d'Alembert force coefficient matrix for lumped mass/inertia element at shaft segment m

$(\underline{Q}_1)_a$ = primitive vector at shaft segment 1

$\underline{\pi}_{m-1,1}$ = shaft transfer matrix

$\underline{\Delta Q}_{m_k}$ = transfer matrix for external force vector applied at segment k

Mobility and Impedance Matrices

At any shaft segment where an external force and/or moment is applied, the primitive vector is given by

$$(\underline{Q}_{m_j})_a = \underline{\pi}_{m_j-1,1} \cdot (\underline{Q}_1)_a + \sum_{k=1}^{j-1} \underline{\pi}_{m_j-1,\, m_k} \cdot \Delta Q_{m_{1c}} \tag{32}$$

If one seeks the values of the displacement elements of $(\underline{Q}_{m_j})_a$, one needs from $\underline{\pi}_{m_j-1,1}$ those elements which are "displacement-rows" and "displacement-columns," and also from $\underline{\pi}_{m_{j-1},m_k}$ those elements which are "displacement-rows" and "force-columns". These latter reduced matrices are designated as $\underline{U}_j$ and $\underline{U}_{j,k}$; then,

$$\begin{bmatrix} \underline{u}_1 \\ \underline{u}_2 \\ \underline{u}_3 \end{bmatrix}_{M_j} = - \underline{U}_j \cdot \underline{V}^{-1} \cdot \sum_{k=1}^{m} (\tilde{\underline{V}}_k \cdot \underline{F}_{m_k}) + \sum_{k=1}^{j-1} \tilde{\underline{U}}_{j,k} \cdot \underline{F}_{m_k} \tag{33}$$

With suitable rearrangement, the "column ensemble" of all $\underline{F}_{m_k}$ is in fact the overall excitation vector $\underline{f}$, and the above expression can be rewritten as

$$\underline{x}_j = \underline{Y}_j \cdot \underline{f} \tag{34}$$

$\underline{Y}_j$ is the "row ensemble" of $-\underline{U}_j \cdot \underline{V}^{-1} \cdot \tilde{\underline{V}}_k$ for all k plus that of $\tilde{\underline{U}}_{j,k}$ for k = 1,2,...(j-1). The "column ensemble" of $\underline{x}_j$, again after suitable rearrangement, is the overall displacement vector; thus,

$$\underline{x} = \underline{Y} \cdot \underline{f} \tag{35}$$

where $\underline{Y}$ is a square matrix and is the rearranged "column ensemble" of $\underline{M}_j$. Finally, inverting

$$\underline{f} = \underline{Y}^{-1} \cdot \underline{x} = \underline{Z} \cdot x; \quad \underline{Z} = \underline{Y}^{-1} \tag{36}$$

The $\underline{Y}$ and $\underline{Z}$ matrices of Equation (36) are, respectively, the required shaft mobility and impedance representations.

Shaft Segment Flexural Analysis

The characteristics of the shaft flexure transfer matrix, $s_{11}$, $s_{22}$, given in general terms in Equation (28), are developed in the following paragraphs. Considering the planar, periodic flexural response of a rotating, uniform shaft with rotational symmetry, let $(m_x, m_y)$, $(V_x, V_y)$, $(\theta_x, \theta_y)$, and $(W_x, W_y)$ be, respectively, the bending moments, shear forces, angular and linear displacements in the two transverse planes. Also, let A be the shaft segment cross-sectional area, which along with the mass density, $\rho$, describes parameters concerning d'Alembert's effects per unit shaft length. These parameters are defined in Figure 9. Dynamic equilibrium, in flexure, of the shaft segment of Figure 9 is established according to

$$\frac{\partial}{\partial z} \begin{bmatrix} m_x \\ m_y \end{bmatrix} = \begin{bmatrix} V_x \\ V_y \end{bmatrix} \tag{37}$$

and

$$\frac{\partial}{\partial z}\begin{bmatrix} V_x \\ V_y \end{bmatrix} = -\rho A \frac{\partial^2}{\partial t^2}\begin{bmatrix} W_x \\ W_y \end{bmatrix} \tag{38}$$

In Equations (37) and (38), rotary inertias are neglected; therefore, the rotational speed of the shaft does not enter into the governing equations. The rotational direction, however, is used to define the lateral coordinates according to the right-hand rule. Thus, if the rigid body motion for a shaft with stubby proportions should be of interest, "half-segment rotary inertias" should be added to both ends of the shaft segment as lumped effects.

Periodic time-dependence can be described by associating each variable with a common factor exp {jνt}. For a homogeneous linear system, this common factor is often omitted while the differentiation operator $\frac{\partial}{\partial t}$ is replaced by the factor jν. Thus, Equations (37) and (38) become

$$\frac{d}{dz}\begin{bmatrix} m_x \\ m_y \end{bmatrix} = \begin{bmatrix} V_x \\ V_y \end{bmatrix} \tag{39}$$

and

$$\frac{d}{dz}\begin{bmatrix} V_x \\ V_y \end{bmatrix} = \rho A \nu^2 \begin{bmatrix} W_x \\ W_y \end{bmatrix} \tag{40}$$

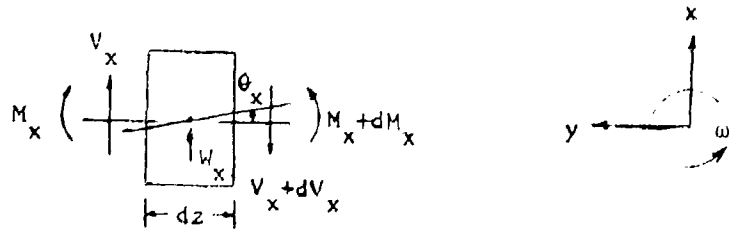


Figure 9. Shaft-Segment Flexure Analysis

In accordance with the first order, slender rod flexure theory,

$$\begin{bmatrix} m_x \\ \\ m_y \end{bmatrix} = EI \frac{d^2}{dz^2} \begin{bmatrix} W_x \\ \\ W_y \end{bmatrix} \tag{41}$$

where E is the modulus of elasticity, and I is the cross-sectional moment of inertia. Since these equations are identical in both directions, the subscripts (x, y) can be dropped, and

$$V = \frac{dm}{dz};\ m = EI \frac{d^2W}{dz^2};\ \theta = \frac{dW}{dz};\ \rho A\nu^2 W = \frac{dV}{dz} \tag{42}$$

Eliminating ($\theta$, m, V), one finds that

$$EI \frac{d^4W}{dz^4} - \rho A\nu^2 W = 0 \tag{43}$$

To simplify notations further, define

$$\bar{z} = z/\ell;\ \alpha^4 = \frac{\rho A\nu^2}{EI\ell^4} \tag{44}$$

with $\ell$ the length of the shaft segment. Then, the differential equation becomes

$$\frac{d^4W}{d\bar{z}^4} - \alpha^4 W = 0 \tag{45}$$

The corresponding general solution is

$$W = \sum_{j=1}^{4} C_j W_j \tag{46}$$

where $W_1 = \cos h\, a\bar{z}$; $W_2 = \sin h\, a\bar{z}$

$W_3 = \cos a\bar{z}$; $W_4 = \sin a\bar{z}$ (47)

Differentiating Equation (46) successively results in

$$\underline{Q}(\bar{z}) = \begin{bmatrix} \frac{\alpha^3 W}{\alpha^3 d\bar{z}^3} \\ \frac{d^2 W}{\alpha^2 d\bar{z}^2} \\ \frac{dW}{\alpha d\bar{z}} \\ W \end{bmatrix} ; \quad \underline{P}(\bar{z}) = \begin{bmatrix} V \\ M \\ \theta \\ W \end{bmatrix} ; \quad \underline{C} = \begin{bmatrix} C_1 \\ C_2 \\ C_3 \\ C_4 \end{bmatrix} \tag{48}$$

Then,

$$\underline{Q}(\bar{z}) = \underline{B} \cdot \underline{P}(\bar{z}) = \underline{K}(\bar{z}) \cdot \underline{C} \tag{49}$$

where

$$\underline{B} = \begin{bmatrix} \frac{\ell^3}{\alpha^3 EI} & 0 & 0 & 0 \\ 0 & \frac{2}{\alpha^2 EI} & 0 & 0 \\ 0 & 0 & \frac{\ell}{\alpha} & 0 \\ 0 & 0 & 0 & 1 \end{bmatrix} \tag{50}$$

$$\underline{K}(\bar{z}) = \begin{bmatrix} \sin h\,\alpha\bar{z} & \cos h\,\alpha\bar{z} & \sin \alpha\bar{z} & -\cos \alpha\bar{z} \\ \cos h\,\alpha\bar{z} & \sin h\,\alpha\bar{z} & -\cos \alpha\bar{z} & -\sin \alpha\bar{z} \\ \sin h\,\alpha\bar{z} & \cos h\,\alpha\bar{z} & -\sin \alpha\bar{z} & \cos \alpha\bar{z} \\ \cos h\,\alpha\bar{z} & \sin h\,\alpha\bar{z} & \cos \alpha\bar{z} & \sin \alpha\bar{z} \end{bmatrix} \quad (51)$$

Equation (49) can be inverted for $\bar{z} = 0$, with

$$\underline{C} = \underline{K}(0)^{-1} \cdot \underline{Q}(0) \quad (52)$$

Setting $\bar{z} = 1$ in Equation (49) and substituting Equation (52) for $\underline{C}$, we find that

$$\underline{Q}(1) = \underline{K}(1) \cdot \underline{K}(0)^{-1} \cdot \underline{Q}(0) \quad (53)$$

Since $\underline{Q} = \underline{B} \cdot \underline{P}$ and $\underline{P} = \underline{B}^{-1} \cdot \underline{Q}$,

$$\underline{P}(z=\ell) = [\underline{B}^{-1} \cdot \underline{K}(1) \cdot \underline{K}(0)^{-1} \cdot \underline{B}] \cdot \underline{P}(z=0) \quad (54)$$

Accordingly, $[\underline{B}^{-1} \cdot \underline{K}(1) \cdot \underline{K}(0)^{-1} \cdot \underline{B}]$ can be regarded as the shaft flexural transfer matrix, which is designated as $\underline{S}_{11} = \underline{S}_{22}$ in Equation (28).

Torsional Analysis of Shaft Segment

The torsional analysis is considerably simpler than the flexural analysis. The shaft segment is characterized by its cross-sectional polar moments of inertia ($I_p$ for the stiffness cross section and $J_p$ for the mass cross section), density $\rho$, shear modulus G, and segment length $\ell$. The physical variables of interest are the angle of twist $\phi$, and the torsional moment T. The angle of twist is assumed to be positive if its sense is the same as that of shaft rotation.

The governing differential equations for a slender torsion beam are the linear law of torsion

$$T = GI_p \frac{\partial \phi}{\partial z} \tag{55}$$

and the dynamic equilibrium equation for rotation is

$$\frac{\partial T}{\partial z} = \rho J_p \frac{\partial^2 \phi}{\partial t^2} \tag{56}$$

where $z$ = axial coordinate

$t$ = time

Periodic time-dependence can be studied with the complex exponential notation and, using the notation, the governing equations become

$$T = GI_p \frac{d\phi}{dz} \; ; \; \frac{dT}{dz} = - \rho J_p \nu^2 \phi \tag{57}$$

Eliminating T and rewriting in dimensionless variables, one obtains

$$\frac{d^2\phi}{d\bar{z}^2} + \beta^2 \phi = 0 \tag{58}$$

where

$$\bar{z} = z/\ell; \; \beta^2 = \frac{(\rho J_p)}{GI_p} \nu^2 \tag{59}$$

The general solution of Equation (58) is

$$\phi = C_1 \cos \beta\bar{z} + C_2 \sin \beta\bar{z} \tag{60}$$

Substituting this solution into Equation (55), we find that

$$T = \frac{\beta GI_p}{\ell} [-C_1 \sin \beta\bar{z} + C_2 \cos \beta\bar{z}] \tag{61}$$

Rewriting in matrix form,

$$\underline{Q} = \begin{bmatrix} T \\ \\ \phi \end{bmatrix} = \underline{\underline{B}} \cdot \begin{bmatrix} \frac{d\phi}{dz} \\ \\ \phi \end{bmatrix}$$

$$= \underline{\underline{B}} \cdot \underline{\underline{K}} \cdot \underline{C} \qquad (62)$$

where

$$\underline{\underline{B}} = \begin{bmatrix} \frac{\ell}{\beta G I_p} & 0 \\ \\ 0 & 1 \end{bmatrix} ; \quad \underline{\underline{K}} = \begin{bmatrix} -\sin \beta\bar{z} & \cos \beta\bar{z} \\ \\ \cos \beta\bar{z} & \sin \beta\bar{z} \end{bmatrix}$$

$$\underline{C} = \begin{bmatrix} C_1 \\ \\ C_2 \end{bmatrix} \qquad (63)$$

Thus,

$$\underline{Q}(z = 0) = \underline{\underline{B}} \cdot \underline{\underline{K}}(0) \cdot \underline{C}$$

$$\underline{Q}(z = \ell) = \underline{\underline{B}} \cdot \underline{\underline{K}}(1) \cdot \underline{C} \qquad (64)$$

Eliminating $\underline{C}$, we find that

$$\underline{Q}(z = \ell) = [\underline{\underline{B}} \quad \underline{\underline{K}}(1) \quad \underline{\underline{K}}(0)^{-1} \quad \underline{\underline{B}}^{-1}] \quad \underline{Q}(z = 0) \qquad (65)$$

Referring to Equation (28),

$$\underline{\underline{S}}_{33} = \underline{\underline{B}} \quad \underline{\underline{K}}(1) \quad \underline{\underline{K}}(0)^{-1} \quad \underline{\underline{B}}^{-1}$$

$$= \begin{bmatrix} \cos\beta & -\frac{1}{\beta G I_p} \cdot \sin\beta \\ \frac{\beta G I_p}{\ell} \sin\beta & \cos\beta \end{bmatrix} \tag{66}$$

where $s_{33}$ is the shaft segment torsional transfer matrix.

## GEAR-MESH EXCITATION ANALYSIS AND SYSTEM RESPONSE CALCULATION

The analytical methods described previously in this report describe the mathematical foundation for modeling helicopter transmissions as dynamic systems. The dynamic model which results from the application of these methods can be used to calculate transmission responses, in terms of shaft strains, bearing loads, and case accelerations, which result from internally generated gear-mesh-induced excitations. This section of the report describes the mechanism whereby these gear-mesh excitations are produced, and reviews the analytical methods which have been developed for calculating their characteristics.

### Excitation Mechanism

The function of gearing in a mechanical power transmission is to transmit essentially steady loads from one gearshaft to another, usually in conjunction with some change in shaft speed and/or orientation. This is accomplished through the meshing of gear teeth, wherein individual gear teeth on the driving gear apply forces to corresponding teeth on the driven gear. As a byproduct of this procedure, deflections occur in the meshing gear teeth and, since the effective stiffness of the meshing tooth pair is not constant throughout the mesh cycle, the resulting tooth deflections vary with time, even under essentially steady loading. These local, time-variant tooth deflections must be compensated by deflection of the gearshafts which support the meshing gear teeth, or the gears would not remain in contact. The local tooth deflections repeat for each successive mesh cycle, which consists of the engagement, loading, and disengagement of a single pair of meshing teeth. Consequently, the local tooth deflections, as well as the induced shaft deflections, are periodic at a rate equal to the tooth engagement rate.

The stiffness, or compliance, of a gear tooth consists of the effects of:

- Tooth bending
- Tooth shear
- Root radiation
- Hertzian (contact) stiffness

Each tooth may be thought of as a trapezoidal cantilever beam. The deflection of such a beam, under a constant load, varies with the point of loading in a nonlinear manner. For loading applied at the free end of such a beam, which corresponds to the tip of the tooth, the deflection is relatively large, and the effective stiffness is, therefore, low. As the loading is moved toward the supported end, the root of the tooth, deflection decreases and, correspondingly, the effective stiffness increases.

In the case of an actual gear mesh, the cycle begins with engagement of the root of the driving gear with the tip of the driven gear. At this point, the driving gear tooth effective stiffness is at its greatest value, the driven gear at its lowest value, and the effective mesh stiffness is equal to the combination of these two stiffnesses acting as series springs. The tooth loading at this point is zero, but increases rapidly as the load is transferred from the previous gear mesh. As the load builds up to its steady value, the two gear teeth deflect, and this deflection is taken up by torsional wind-up and lateral deformation of the supporting gearshafts.

As the mesh cycle proceeds, the point of contact between the meshing teeth moves. On the driving gear tooth, this point moves towards the tip of the tooth, whereas on the driven gear it moves toward the root. This change in contact point changes the effective mesh stiffness, thus changing tooth deflection as well as the magnitude of supporting shaft wind-up and lateral deflection. This change in deflection occurs only as the result of changing mesh stiffness, since the applied load is essentially constant.* Generally, mesh stiffness will increase, and local

* This applies only for the special case where only a pair of teeth at a time is in mesh. In the more usual case, loading will be shared by more than one tooth pair. This load sharing adds complexity to the calculation of tooth deflection, and is considered in the analytical method used in the present program. This effect does not, however, change the basic mechanism of gear-mesh excitation. For simplicity, the effect is not included in the present discussion, which is intended only to describe how the steady torque loads give rise to periodic tooth and system deflections.

and system deflections will decrease, up to the midpoint of the mesh cycle. Mesh stiffness will then decrease, with increasing deflections, until mesh disengagement occurs, at which time the process is repeated for subsequent mesh cycles.

The tooth and shaft deflections described above repeat, in a periodic manner, at a rate equal to the tooth meshing rate. Within each mesh cycle, however, the deflection time function is not sinusoidal, because mesh stiffness does not vary sinusoidally. As a consequence of this, the deflections caused by tooth meshing occur not only at a frequency equal to the mesh rate, but at harmonics of this frequency.

Analytical Method

The basic mechanism for gear-mesh excitation has been incorporated in an analytical calculation technique which permits the determination of local tooth deflections, including fundamental and harmonic components, based on known tooth geometry and loading conditions. This technique was developed through previous Army research efforts, and is described in detail in Reference 3. Within the present effort this method has been improved to the extent of incorporating an equivalent spur-gear approximation technique for representing helical and spiral bevel gearing. This improvement permits calculation of helical and spiral bevel gear-mesh excitations directly from gear data available on gear design drawings. The equivalent spur-gear approximation is that described in Appendix III of Reference 4. Since complete discussions of the gear-mesh excitation analysis methods used in the present program are given in References 3 and 4 they will not be further discussed in the present report.

Application of Gear-Mesh Excitations Within the Dynamic System

The gear-mesh excitation analysis technique discussed in the previous paragraphs is applied on the basis of local gear-mesh characteristics only. Transmission system dynamic responses are not considered within this calculation procedure and, in fact, the resulting dynamic tooth deflections are assumed to be independent of system responses. This assumption is consistent with the fundamental mesh excitation mechanism, which relates induced tooth deflections only to applied loading, tooth geometry and tooth material properties.

Consideration of system dynamic response characteristics would change calculated tooth deflections only to the extent that dynamic reaction forces, which are applied to the meshing gear teeth in response to induced system deflections, modify the instantaneous tooth loading. These induced dynamic reaction forces add to or subtract from the steady-torque loading, and thereby change the magnitude of dynamic tooth deflections relative to values predicated on steady loading only. In practice, however, the effect of these dynamic reaction forces is generally small, since the magnitude of the dynamic force components is usually much lower than the magnitude of the steady-torque loading. On the basis of the above reasoning it can be concluded that the transmission dynamic system is excited by dynamic gear-mesh deflections and not gear-meshing forces. Dynamic forces produced at the gear meshes result from these deflections, but do not cause the deflections to occur. Within the total helicopter transmission system dynamic response calculation method, the mesh excitations are applied in exactly this manner.

Transmission System Response Calculation

Calculation of helicopter transmission system dynamic responses is accomplished in four distinct steps, involving:

- Elemental modeling
- System modeling
- Mesh excitation calculation
- System response calculation

First, dynamic models of each transmission mechanical element are formulated. These models include all gearshafts and the transmission housing. The elemental models are then joined, at points of physical contact. Gearsnafts are joined to each other at points of gear meshing, and to the gearbox housing at shaft support bearing locations. The point of gear meshing for one gear mesh is, however, left unconnected. The unconnected gear mesh is the mesh for which transmission dynamic responses are desired, and it is left unconnected so that dynamic excitation can be applied at this point, in a later stage in the calculation procedure.

Points of gear meshing are connected on the basis of the assumption that these points will have common deflection in response to mesh excitations introduced elsewhere in the system. This is considered to be a valid assumption because, while not mechanically joined, meshing gears are held together by the large steady torque loading which is present throughout the system. The meshing points for the gear mesh under evaluation are not joined because a relative deflection is assumed to occur at this point, between the driving and driven gears. This relative deflection is equal, and opposite, to the local tooth deflections which are calculated for this mesh with the mesh excitation analysis method.

The gearshafts are joined to the gearbox housing, at appropriate support bearing locations, through springs. The stiffness characteristics of these springs are related to the elastic properties of the respective support bearings. These elastic properties are calculated analytically, considering the geometric and mechanical bearing characteristics as well as the shaft speed and steady, torque-induced bearing loading. The analytical method used to generate bearing elasticity is described in Reference 13.

Application of the above procedure results in a transmission system dynamic model. The mesh excitation analysis technique is now used to calculate dynamic tooth deflections for the particular gear mesh under study. This mesh corresponds to the unconnected meshing point defined in the system dynamic model. The calculated mesh deflections are applied to the system model in terms of a relative dynamic displacement at the unconnected meshing point, and system responses to this excitation are calculated.

## SOUND POWER LEVEL ANALYSIS

Gear-mesh-induced excitations within a helicopter gearbox are ultimately transmitted to the gearbox housing, causing vibration of the housing surface. These vibrations couple with the air surrounding the housing, causing pressure fluctuations, which radiate from the housing surface and which are perceived as noise. In order to accurately calculate the characteristics of the noise radiated in this manner, it is necessary to analytically model both the structural response characteristics of the transmission, including the housing, and the noise-radiation mechanism. Previous sections of this report describe structural dynamics models which can be used in the present analysis to calculate housing surface responses. Modeling of the noise-radiation mechanism is discussed in this section.

### Acoustic Source Representation

In the present analysis the transmission case is assumed to consist of a relatively small number of simple, baffled, hemispherical acoustic sources. These sources, which are distributed over the case surface, are assumed to act independently, with the sum of their acoustic outputs equal to the total transmission-radiated noise. The output from each source is computed directly in terms of sound power level. Use of this source representation requires only knowledge of case surface motions, amplitude and frequency, and an estimation of the individual source

[13] Jones, A. B., A GENERAL THEORY FOR ELASTICALLY CONSTRAINED BALL AND RADIAL ROLLER BEARINGS UNDER ARBITRARY LOAD AND SPEED CONDITIONS, Transactions of the American Society of Mechanical Engineers, Series D, Journal of Basic Engineering, Volume 82, June 1960, pp 309-320.

sizes, expressed in terms of hemispherical radiator radius. Within the present program, source size has been estimated as

$$S_i = 2\sqrt{\frac{R_o^2}{n}} \tag{67}$$

where $S_i$ = hemispherical source radius

$R_o$ = radius of sphere enclosing transmission housing

$n$ = number of sources considered

The transmission dynamic response calculation method calculates case surface motion in terms of sinusoidally varying acceleration, with

$$\bar{a}_i = (a_o)_i e^{j(wt + \phi_i)} \quad (i = 1 \text{ to } n) \tag{68}$$

where $\bar{a}_i$ = time dependent acceleration at point i ($in/sec^2$)

$(a_o)_i$ = absolute amplitude of acceleration at point i ($in/sec^2$)

$w$ = frequency (rad/sec)

$\phi_i$ = phase angle of acceleration at point i (rad)

$n_i$ = number of case surface points considered

Acoustic radiation, however, is proportional to source surface velocity, which, in turn, is related to surface acceleration according to

$$\bar{u}_i = \frac{(a_o)_i}{jw} e^{j(wt + \phi_i)} \tag{69}$$

where $\bar{u}_i$ = surface velocity (in/sec)

At the boundary of each hemispherical source the surface velocity ($\bar{u}_i$) must equal the particle velocity in the radiated acoustic wave, $(\bar{U}_w)_i$, given by

$$(\bar{U}_w)_i = \frac{A}{r_i \bar{Z}_i} e^{j(wt - k r_i + \phi_i)} \tag{70}$$

where $A$ = amplitude constant (determined above by boundary condition)

$r_i$ = distance from source to observer

$\bar{Z}_i$ = specific acoustic impedance of a spherical wave

$k$ = wave number (equal to ratio of frequency (rad/sec) to speed of sound in propagating medium)

Use of this boundary condition, namely,

$$(\bar{U}_w)_i = \bar{u}_i \text{ @ } r_i = s_i \text{ (the radius of the hemispherical source)}$$

allows evaluation of the constant, A. Then,

$$\frac{A}{(s)_i (Z_s)_i} e^{j(wt - ks_i + \phi_i)} = \frac{(a_o)_i}{jw} e^{j(wt + \phi_i)} \tag{71}$$

With $(Z_s)_i$, the specific acoustic impedance evaluated at $r_i = s_i$, given by

$$(Z_s)_i = \frac{\rho_o c k s_i (k s_i + j)}{1 + k^2 s_i^2} \tag{72}$$

where $\rho_o$ = density of medium

$c$ = speed of sound in medium

The amplitude constant (A) becomes

$$A = \frac{s_i(a_o)_i}{jw}\left[\frac{\rho_o ck s_i(ks_i + j)}{1 + k^2 s_i^2}\right] e^{j\,ks_i}$$

$$= \frac{s_i^2(a_o)_i \rho_o ck}{w(1 + k^2 s_i^2)}\ \{(1 - js^s i)(\cos ks_i + j \sin ks_i)\} \tag{73}$$

With the acoustic pressure $(P_r)_i$ at a distance $(r_i)$ from the source

$$(P_r)_i = \frac{A}{r_i} e^{j(wt - kr_i)} \tag{74}$$

The intensity at a distance $(r_i)$ from the source is equal to the real part of the product of the complex conjugate of the pressure amplitude and the particle velocity at $r_i$. Since the pressure and velocity are related, by the acoustic impedance, the intensity is simply given as

$$I = \frac{|P|^2}{\rho_o c} \tag{75}$$

and, in this case,

$$I = \frac{s_i^4(a_o)_i^2 \rho_o ck^2}{w^2 r^2(1 + k^2 s_i^2)} \tag{76}$$

The acoustic power radiated through the hemispherical surface enclosing the source is given as the product of intensity, at $r_i$, and hemisphere area, also at $r_i$, with

$$W_i = \frac{s_i^4(a_o)^2{}_i \rho_o ck^2 \pi}{w^2(1 + k^2 s_i^2)} \tag{77}$$

where $W_i$ = acoustic power radiated by a single hemispherical source

## Summation of Single-Source Sound Powers to Yield Total Gearbox Case Radiated Power

With regard to the problem of predicting gearbox case noise radiation, several approximations and/or assumptions must be made before Equation (77) may be used. First the use of Equation (77) implies large separation between individual simple sources, since in general, closely spaced simple sources interact to the extent that the total radiated power is less than that which would be predicted by simply summing the contributions predicted by Equation (77). Part of the generated power is not radiated but is stored in an acoustic nearfield. Selection of appropriate source surface areas (reflected in the variable $s_i$ of Equation (77)) also poses a problem, since case surface response characteristics are not known (nor can they be analytically predicted) in sufficient detail to precisely define areas of constant, or nearly constant, vibratory amplitude and phase.

For the purpose of the present effort, no attempt has been made to estimate interaction effects. Total radiated sound power has been estimated simply by summing the contributions of each assumed source with

$$W_T = \sum_{i=1}^{n} \left[\frac{s_i^4 (a_o)_i^2 \rho_o c_k^2 \pi}{w^2 (1 + k^2 s^2 i)}\right] \qquad (78)$$

where $W_T$ = total case radiated sound power

Effective source radii have been calculated using Equation (67).

## TRANSMISSION TESTING

Testing was performed to determine the actual vibration and noise characteristics of an operating helicopter transmission. These data were needed, for comparison with analytically calculated transmission noise and vibration characteristics, to validate the analytical methods used. The SH-2D helicopter main transmission, shown in Figure 1, was subjected to simulated operational testing, using a regenerative test stand. Within this test program measurements were made of all significant dynamic response characteristics, including:

- Shaft bending strain
- Shaft torsional strain
- Lateral shaft displacement
- Housing surface acceleration
- Radiated sound pressure level

The details of this test effort are discussed in this section.

### TEST ARTICLE

The test article for the present effort is the SH-2 main transmission. The continuous input torque rating of this gearbox is 15,000 in.-lb, at an input speed of 6120 rpm. The speed reduction ratio of the transmission is 21.3/1, which results in an output speed of 287 rpm at the main rotor.

All types of gearing commonly used in helicopter gearboxes are represented in the test article: spiral bevel, spur, and planetary gearing. Shaft speeds, the number of teeth for each gear and gear clashing (excitation) frequencies for the SH-2 transmission at its nominal output speed of 287 rpm, are given in Table 2.

### TEST PARAMETERS

Two types of parameters were monitored during the subject test. The primary test objectives were satisfied through acquisition of the dynamics data, including shaft responses, case accelerations and radiated noise. All dynamics data were recorded on tape during testing and reduced off-line. In addition, operating condition data were obtained, in order to define the conditions under test. In general, operating condition data, including input shaft speed, steady torque, and oil output temperature, were monitored in real time, with only rpm recorded on tape. Specific parameters measured are defined in the following paragraphs.

TABLE 2. SH-2 MAIN GEARBOX IDENTITIES

| Part | No. of Teeth | Speed - rpm | Excitation Frequency - Hertz |
|---|---|---|---|
| Input Shaft | - | 6120 | - |
| Spiral Bevel Pinion | 30 | 6120 | 3060 |
| Spiral Bevel Gear | 47 | 3906 | 3060 |
| Spur Gear Pinion | 23 | 3906 | 1497 |
| Spur Gear | 87 | 1033 | 1497 |
| Sun Gear | 35 | 1033 | - |
| Planet Gear (6) | 28 | - | 435 |
| Ring Gear | 91 | - | - |
| Planet Carrier | - | 287 | - |
| Output Shaft | - | 287 | - |

## Dynamic Data

Dynamic parameters monitored in the subject test are summarized in Table 3. As shown, bending and torsion responses of input and output shafts were measured through strain-indicating transducers attached to the shafts. In addition, bending responses of these two shafts were measured through relative-displacement transducers aligned laterally to the shafts in the fixed system. Each parameter was measured at three points on each shaft. The measurement points used are shown in Figure 10.

Lateral and axial bearing support responses were measured at the upper bearing supporting the spiral bevel gear/spur pinion shaft. Acceleration transducers were used; their locations are illustrated in Figure 11. These measurements were intended to either verify or invalidate one of the major assumptions made in the analytical model development; specifically, that lateral bearing forces greatly exceed axial bearing forces and are, consequently, the major case excitation mechanism.

Axial response of the spur (bull) gear was determined through measurement of relative displacement normal to the gear web. Two measurement locations were used, as shown in Figure 11. These measurements were made in order to reveal the presence of a resonant response of this gear in its diaphragm mode.

Acceleration response of the transmission housing (case) was measured at 14 points on the case surface. Measurement locations used are shown in Figure 12. All measurements were made normal to the case surface, with acceleration transducers attached through mounting blocks bonded to the exterior of the housing.

Gearbox radiated noise was measured with an array of 10 acoustic pressure transducers. The transducers were approximately equally spaced around the transmission, equidistant from the case surface. An acoustic enclosure was installed surrounding the test transmission and microphone array. This enclosure, which is described in a subsequent section, isolated the test transmission from interfering noise sources, and provided a nonreflective (anechoic) termination for simulating free-field test conditions.

## Operating Condition Data

Gearbox operating conditions were monitored in real time through measurement and display of input shaft speed, applied torque, applied flight loads (lift only), and oil output temperature.

TABLE 3. DYNAMICS PARAMETERS MEASURED

| Parameter | Location of Measurement* | Number of Points |
|---|---|---|
| Bending Response (Strain) | Input Shaft (10) | 3 |
| Bending Response (Strain) | Output (Main Rotor) Shaft (10) | 3 |
| Bending Displacement | Input Shaft (10) | 3 |
| Bending Displacement | Output Shaft (10) | 3 |
| Torsion Response (Strain) | Input Shaft (10) | 3 |
| Torsion Response (Strain) | Output Shaft (10) | 3 |
| Bearing Support Acceleration (Lateral) | Spiral Bevel Gear/Spur Pinion Shaft Upper Bearing (11) | 1 |
| Bearing Support Acceleration (Axial) | Spiral Bevel Gear/Spur Pinion Shaft Upper Bearing (11) | 1 |
| Gear Web Axial Displacement | Spur Gear Web (11) | 2 |
| Gearbox Case Surface Acceleration | Case Surface (12) | 14 |
| Radiated Sound Pressure Level | Approx. 2 Ft From Case Surface | 10 |

* Specific locations are illustrated in figure numbers shown in parentheses

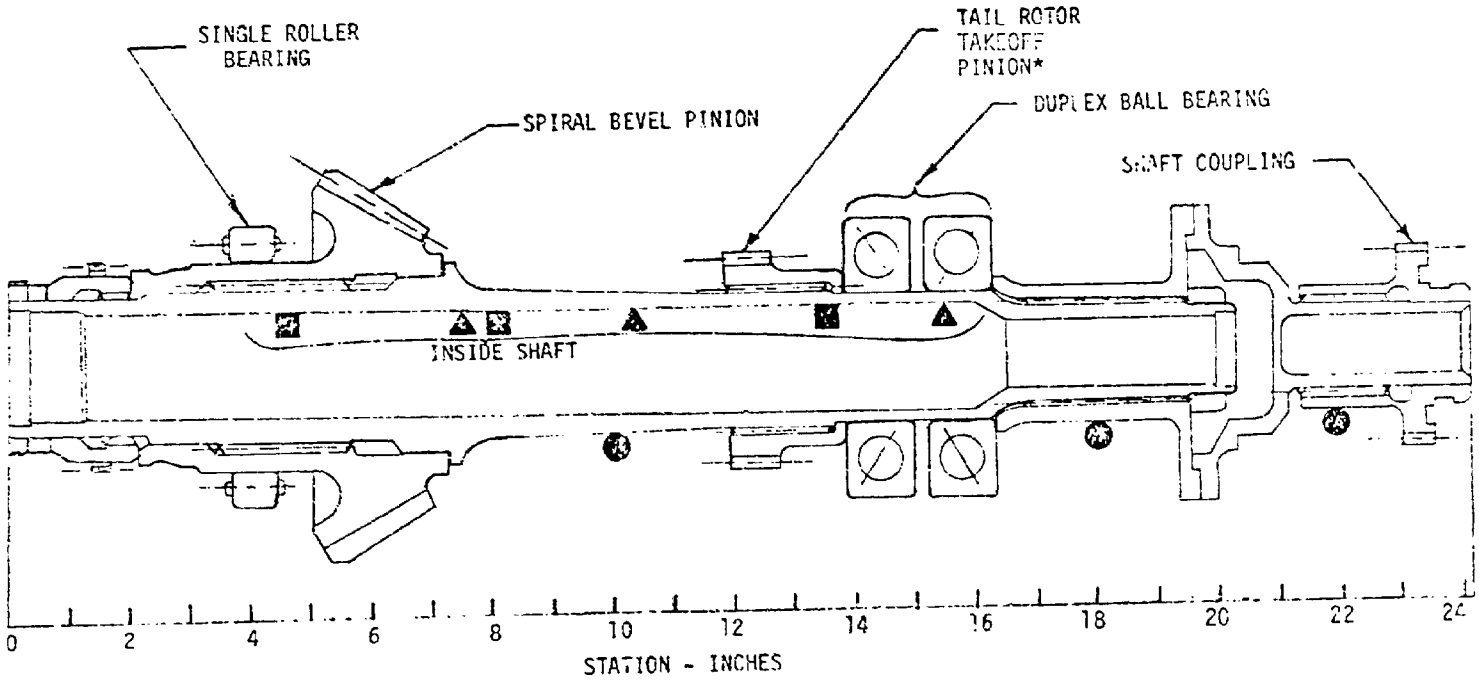


* Tail rotor takeoff pinion installed, but mating gear removed for test

A. Input Shaft

Figure 10. Shaft Response Measurement Locations

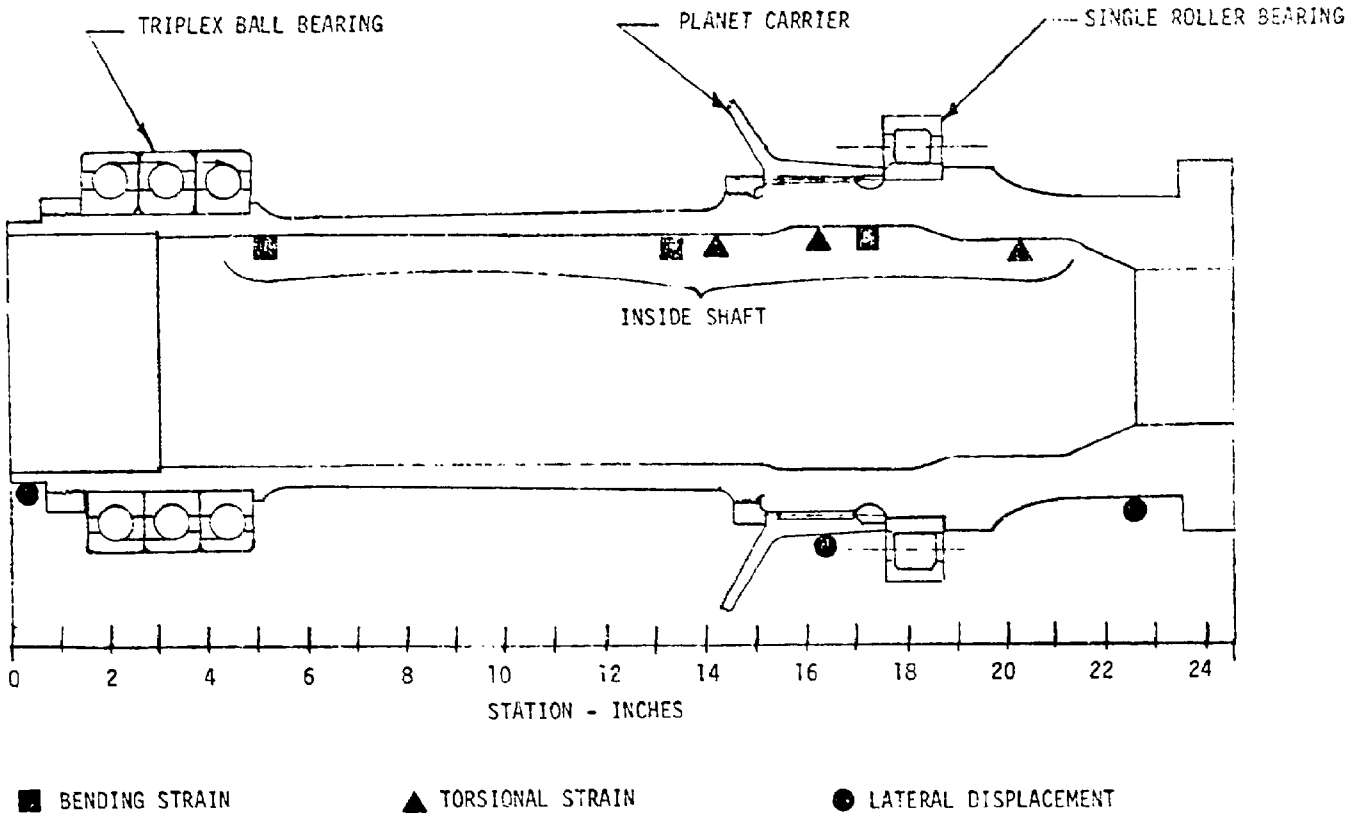


B. Output (Rotor) Shaft

Figure 10 - Continued

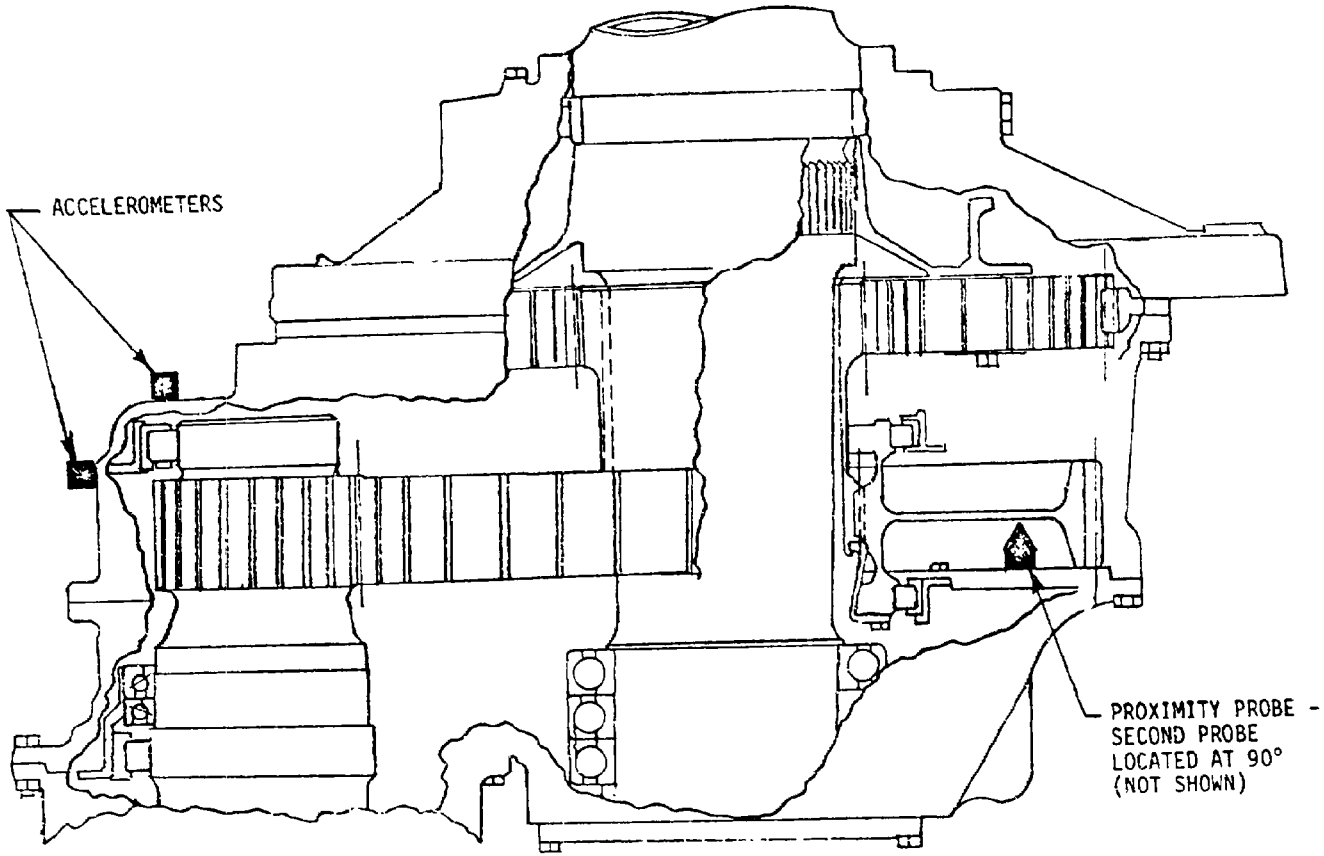


Figure 11. Axial and Lateral Bearing Support Responses and Spur Gear Web, Axial Displacement Measurement Locations


A. View Looking Aft (Case Shown Upside Down) - Locations Numbered

Figure 12. Transmission Case Surface Response Measurement Locations

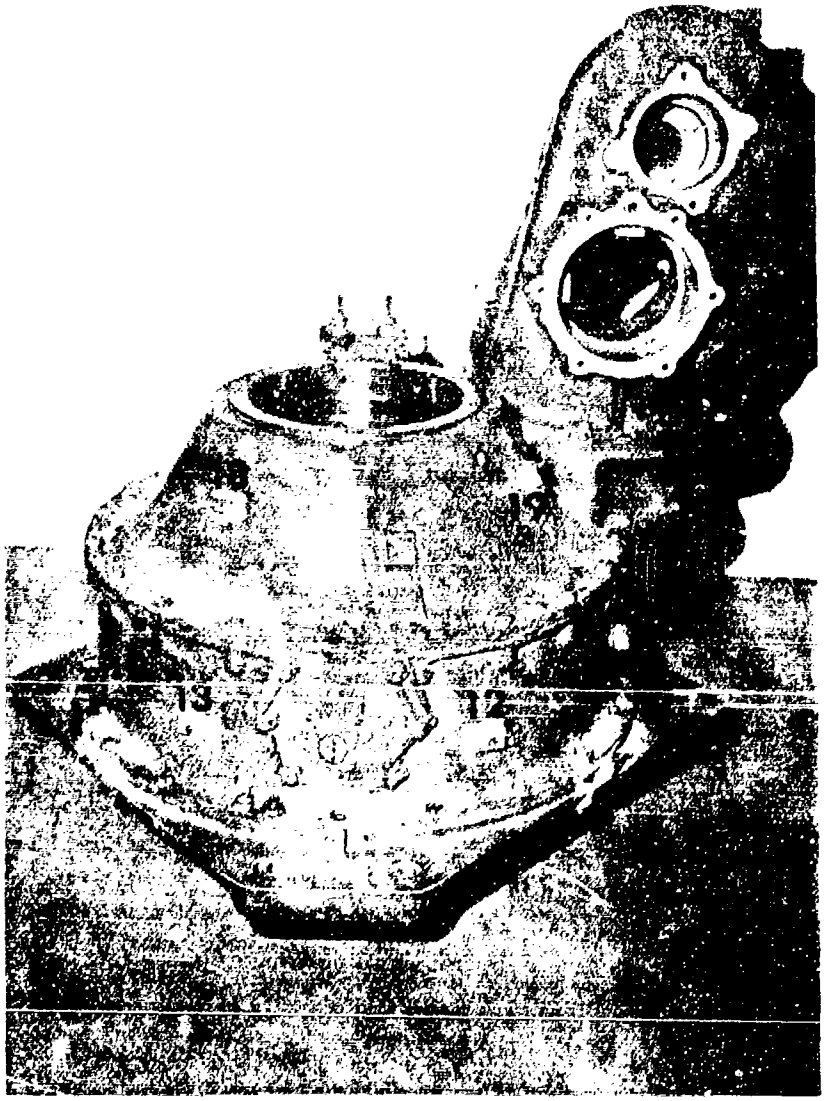


B. View Looking Forward (Case Shown Upside Down) - Locations Numbered

Figure 12 (Continued)

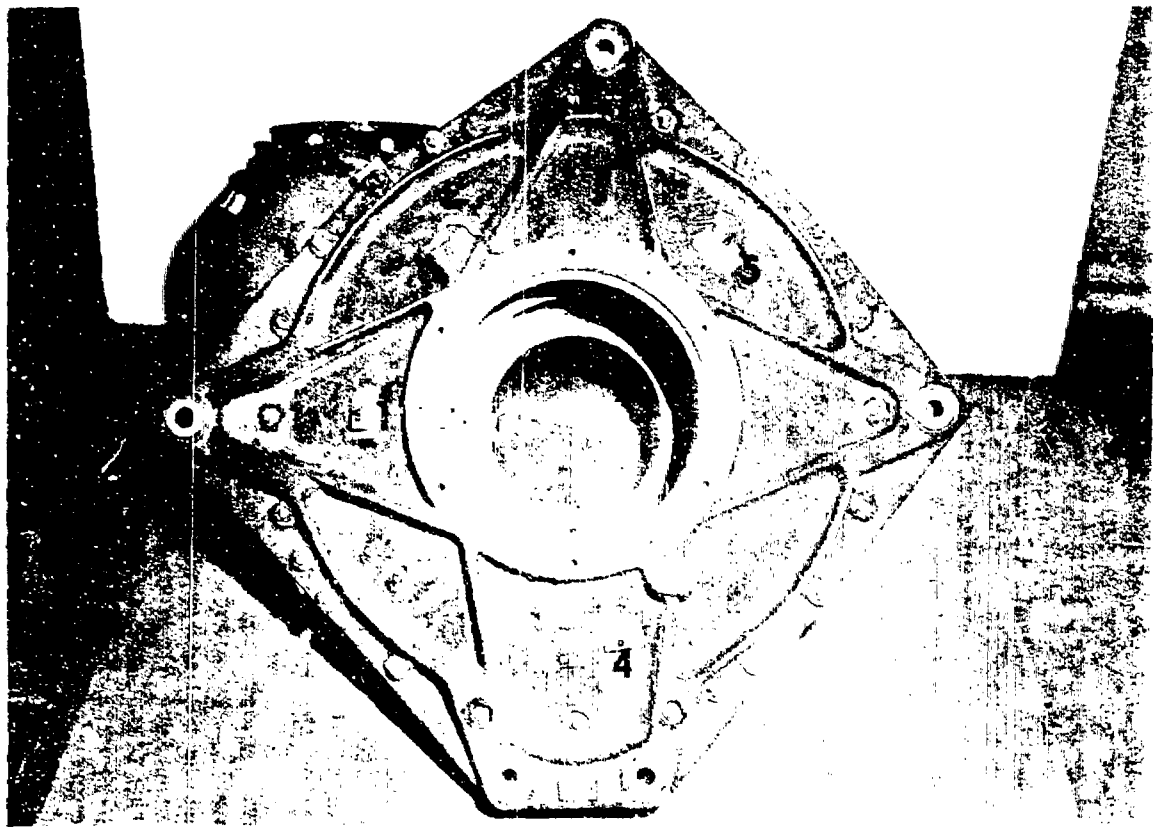


C. View Looking Down (Forward to Top of Picture) - Locations Numbered

Figure 12 (Concluded)

## INSTRUMENTATION

Instrumentation used in the performance of the subject test is listed in Table 4. Schematic diagrams illustrating the use of this instrumentation are presented and discussed in the following paragraphs.

The instrumentation arrangement used in acquiring rotating-shaft strain (bending and/or torque) data is shown, for a single data channel, in Figure 13. All measurement locations were instrumented with full, four-leg strain gage bridges. A slipring assembly (four channels per gage assembly) was used to transmit DC voltage to the bridge as well as to transfer the AC data signals from the rotating to the fixed system. Data signals were applied to a high-pass filter through a switch, which permitted application of a system AC calibration signal. This audio-oscillator-generated calibration signal was delivered to the switch through a voltage-dividing potentiometer, which served to adjust oscillator output voltage to a value appropriate to the gage sensitivity.* Subsequent to filtering, the data signal was amplified and applied to the tape recorder input. FM recording was used.

Acceleration measurements were made using the instrumentation arrangement of Figure 14. Self-generating piezoelectric transducers, rigidly mounted through bonded mounting blocks, were used. The high-impedance, low-level output signal of the transducer was conditioned with a preamplifier/power supply unit, resulting in a high-output, low-impedance signal which was delivered to the tape recorder for FM recording. Each accelerometer was bench calibrated prior to installation on the gearbox. The test accelerometer was mechanically excited, along with a reference accelerometer, and its voltage output (at the power supply signal output) was measured relative to a known "g" input. The audio-oscillator-driven calibration network was then turned on (after removal of the mechanical excitation) and the potentiometer adjusted to match the voltage output for the known acceleration condition. Measuring the calibration voltage (at the calibration resistor) provided a readily repeatable calibration sensitivity, in terms of a calibration-voltage-to-acceleration ratio (mv/g), which was used for system calibration.

The measurement network used in acquiring shaft displacement data is shown in Figure 15. Proximity probes, which sense the varying inductance caused by relative motion between shaft and probe, were rigidly mounted to the fixed structure close to the shaft measurement point. Data signals generated by the transducer system (consisting of probe, demodulator and power supply) were directed, through a switch, to a high-pass filter, where low-frequency components were rejected. The filtered signal was then amplified and applied to the tape recorder input.

* A single oscillator voltage source was used to calibrate all strain-gage data channels.

TABLE 4. INSTRUMENTATION - DATA ACQUISITION

| Item | Manufacturer | Model No. | No. Reqd |
|---|---|---|---|
| Strain Gage (Torque) | Micro-Measurements | CEA-06-187UV-350 (2-Element, 90° Rosette for 1/2-Torque Bridge) | 20 |
| Strain Gage (Bending) | Micro-Measurements | EA-06-125AC-350 (.125" Element, 4 Per Bridge Location) | 40 |
| Proximity Probe | Bently Nevada | 190-FL-36 | 8 |
| Accelerometer | Bruel & Kjaer | 4332 | 14 |
| Microphone Cartridge | Bruel & Kjaer | 4133 | 10 |
| Bridge Power Supply & Balance Unit | Systron-Donner | LVS12-1.4 (±1-15V at 1.4 Amp) | 1 |
| Proximity Probe Demodulator | Bently Nevada | 3115 | 8 |
| Preamplifier(Microphone & Accelerometer) | Bruel & Kjaer | 2619/S | 14 |
| Microphone & Accelerometer Power Supply | Bruel & Kjaer | 2803 | 7 |
| Thermocouple (Oil Temperature) | Thermo-Electric | 2J0111U (Immersion Type) | 2 |
| Potentiometer (measuring) | Leeds-Northrup | 8695 (0-600°F) | 1 |
| Counter (Electronics) | Hewlett-Packard | 523-B | 1 |
| Signal Generator | Hewlett-Packard | 200CD | 1 |
| Slipring Assembly (Input Shaft) | Wendon | W-24-6-100 (24-Ring, Flange Mount) | 1 |
| Slipring Assembly (Main Rotor Shaft) | Wendon | W-24-6-100 (24-Ring, Flange Mount) | 1 |

TABLE 4 (Continued)

| Item | Manufacturer | Model No. | No. Reqd |
|---|---|---|---|
| Calibrated Sound Source (Pistonphone) | Bruel & Kjaer | 4220 | 1 |
| Filter & Amplifier Power Supply | Systron Donner | TP2C15D-1.8(OVS-2) Dual Output 15 VDC at 1.8 Amp | 2 |
| Strain Gage Junction Box | B & F | 18-200 (18 channel) | 1 |
| High Pass Filter | Burr-Brown | UAF-31 | 14 |
| Signal Amplifier | Burr-Brown | 3621-L | 14 |
| Tape Recorder | Honeywell | 5600-C (FM Record & Playback) | 1 |
| Oscilloscope | Hewlett-Packard | 120-A | 1 |
| Magnetic Pickup | Electro Products | 3030 | 2 |
| Digital Voltmeter | Fluke | 8000-A | 1 |
| Load Cell (Lift Load) | Baldwin | U-1 | 1 |
| Load Cell (Torque) | Baldwin | U-1 | 2 |

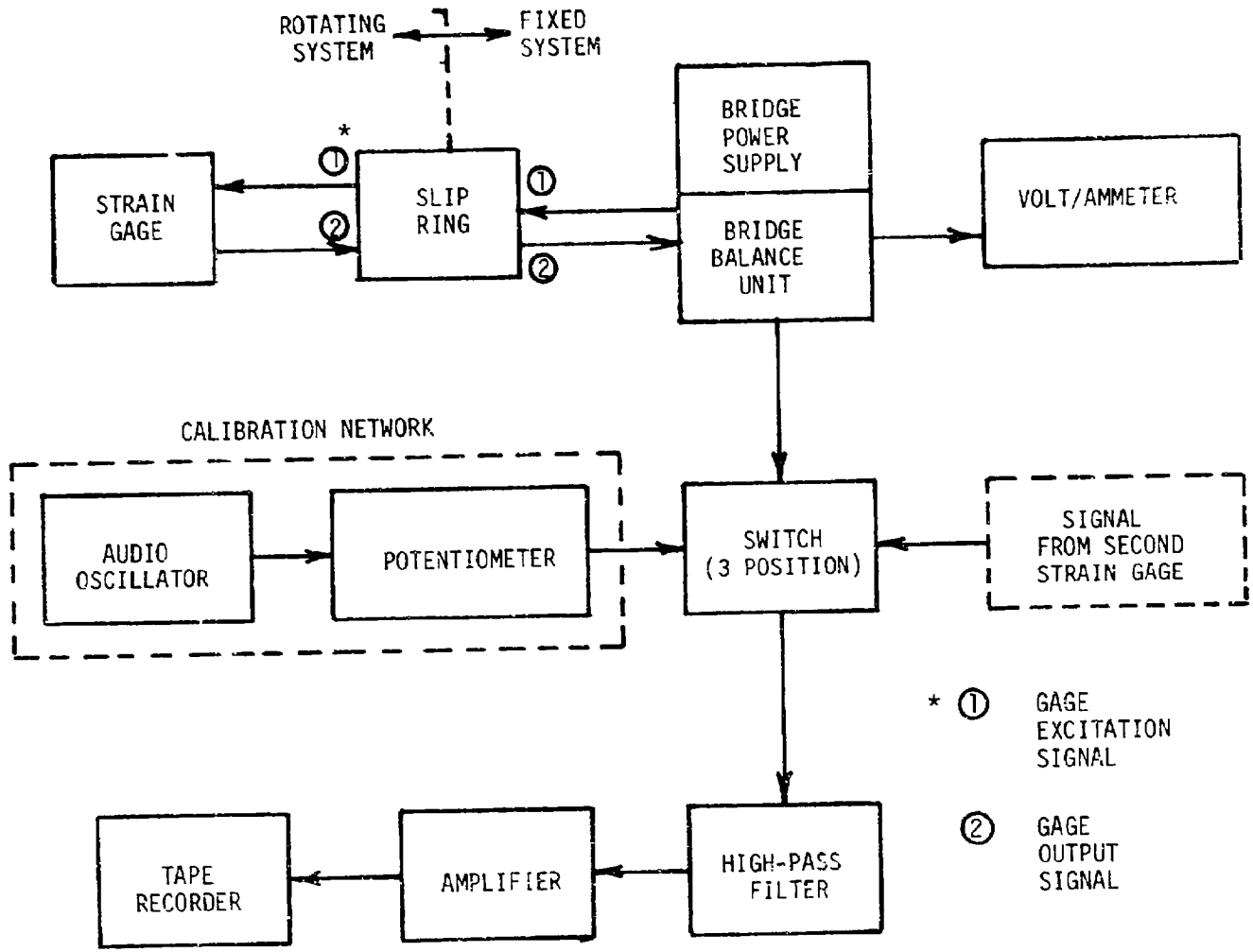


Figure 13. Shaft Strain Measurement Network

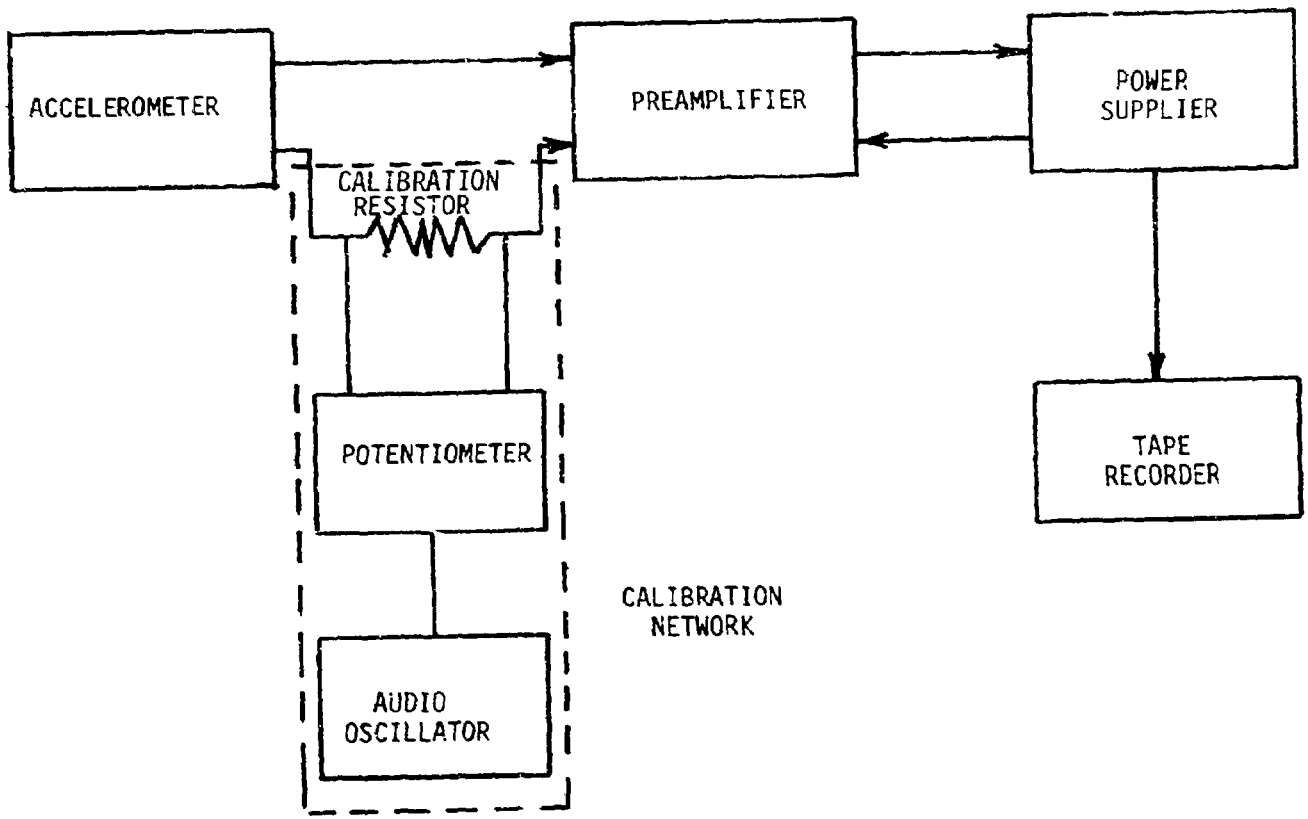


Figure 14. Acceleration Measurement Network

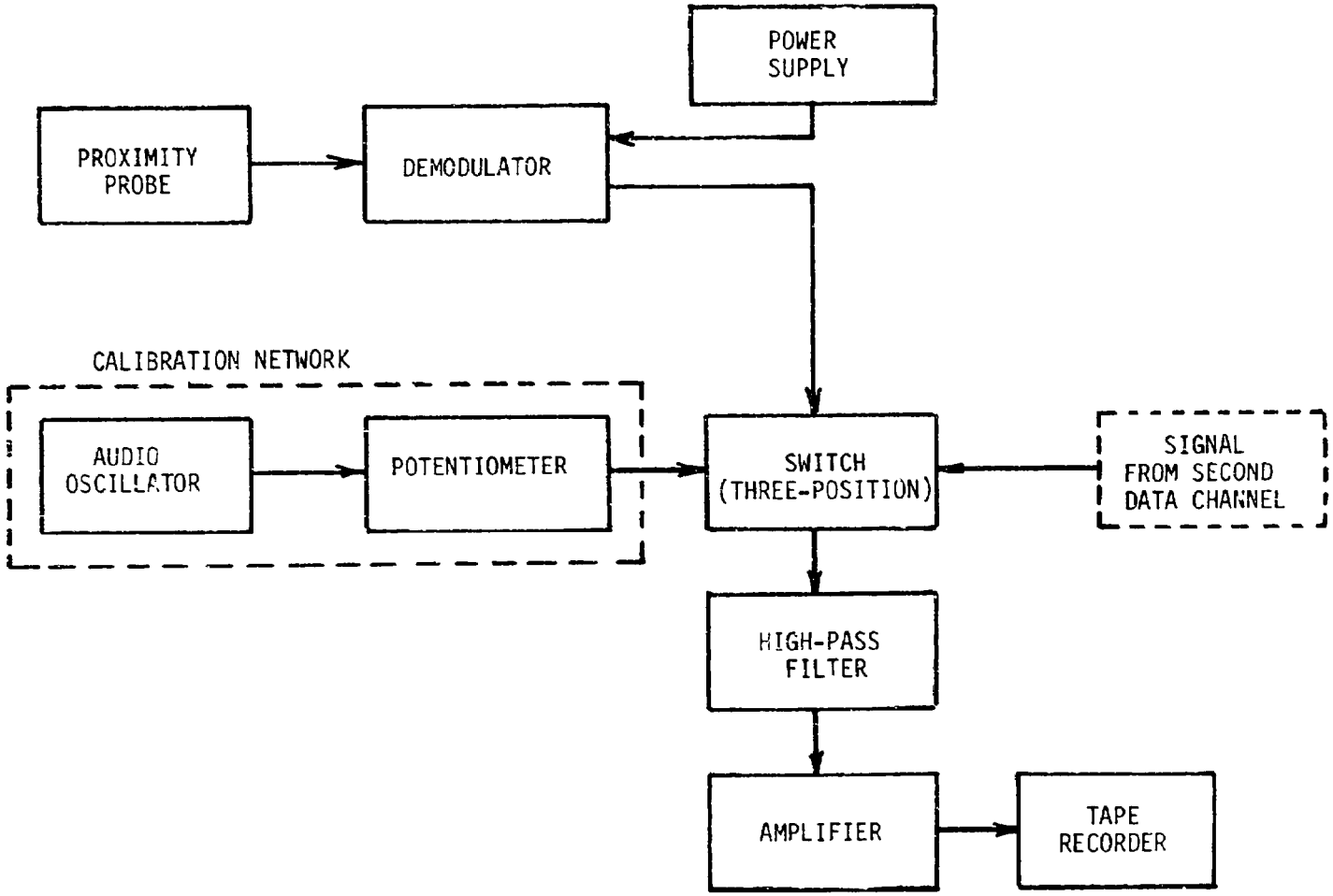


Figure 15. Shaft Displacement Measuring Network

Bench calibration of the displacement measurement system was accomplished statically, using the actual gearshafts as probe targets. Transducer system output voltage was measured as a function of probe/shaft spacing and sensitivity, calculated in terms of voltage output per inch of displacement. System calibration was accomplished using an insert voltage technique.

Radiated noise measurements were made with the instrumentation arrangement of Figure 16. High-impedance condenser microphones were used as acoustic pressure transducers. Transducer signals were conditioned with a preamplifier/power supply unit. The amplified data signal was recorded with the tape recorder in the FM mode.

The sound measurement system was calibrated with a known sound source.

Operational data were acquired using the instrumentation arrangement of Figure 17. The rotation speed of the input shaft was sensed using both a single-tooth wheel and a 60-tooth wheel with magnetic pickups. The signal generated by the single-tooth-wheel transducer was applied to the tape recorder input (edge track). The 60-tooth-wheel signal was read out on the counter. A thermocouple was used to sense transmission oil output temperature. The signal from this transducer was read out on a balancing potentiometer. Applied lift load and torque were measured with load cells (strain gage type). An integrated bridge balance/power supply and readout system was used to monitor these loads.

## TEST STAND

The transmission test stand used in the subject test effort is shown schematically in Figure 18. This stand is regenerative, with two gearboxes mounted output-to-output. The input torque loop is closed by test rig gearboxes and shafting. The speed, torque, rotor lift load, and rotor pitch moment are fully adjustable while the system is stationary or operating.

The test rig is operated from a control console where the following parameters are monitored and varied as required:

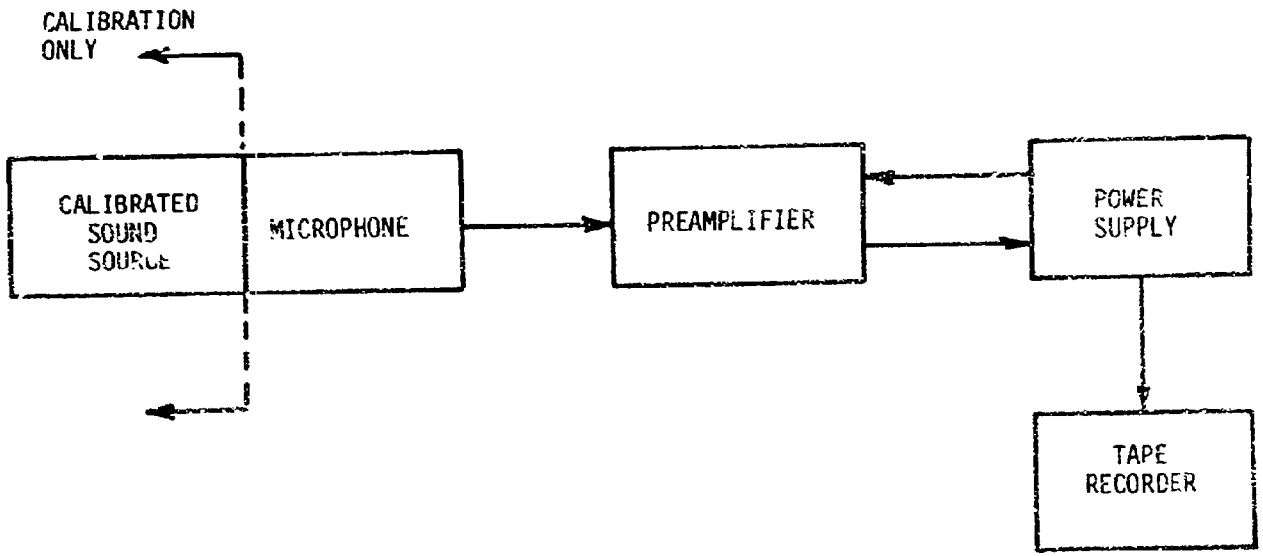


Figure 16. Sound Measurement Network

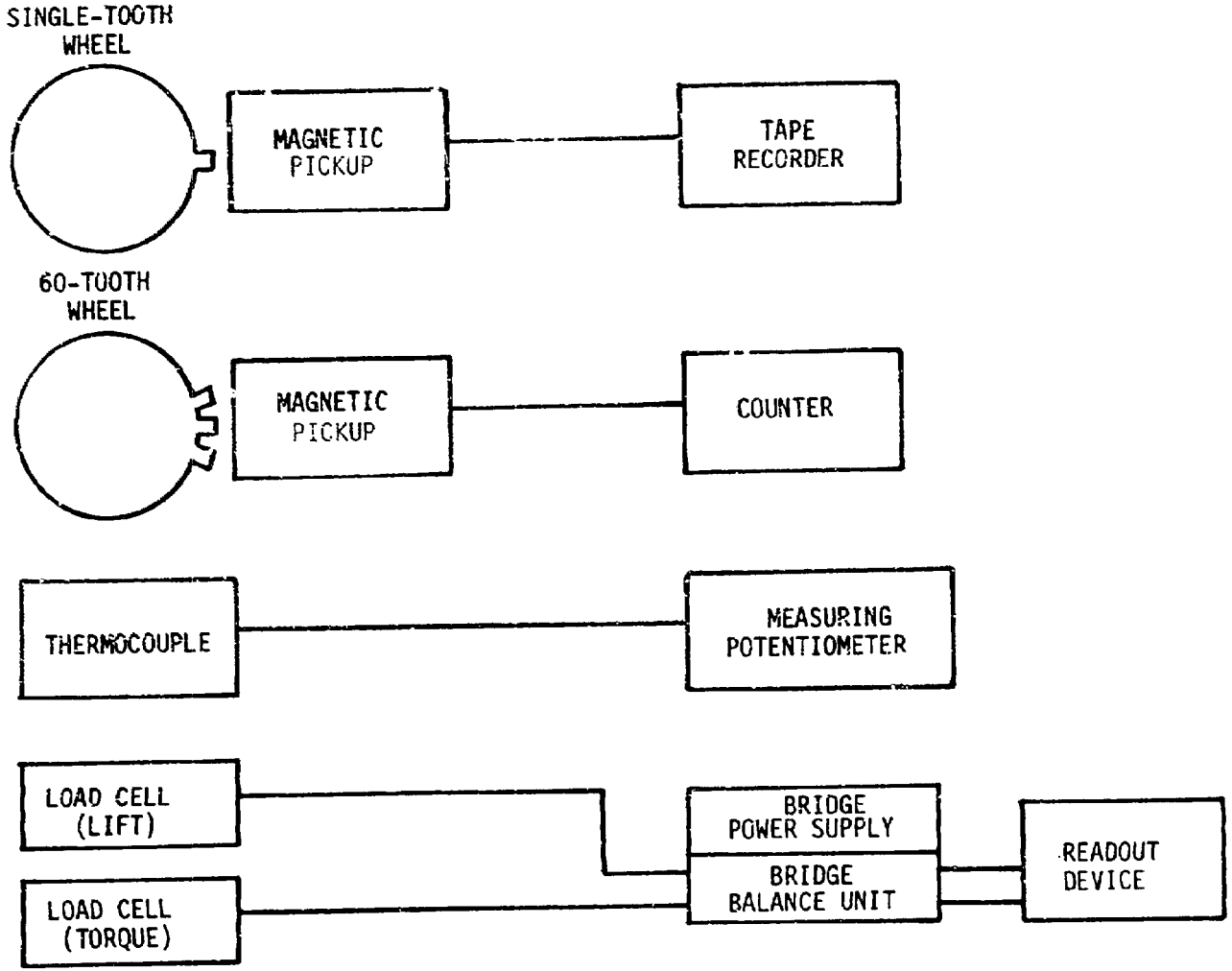


Figure 17. Operational Condition Monitoring Network

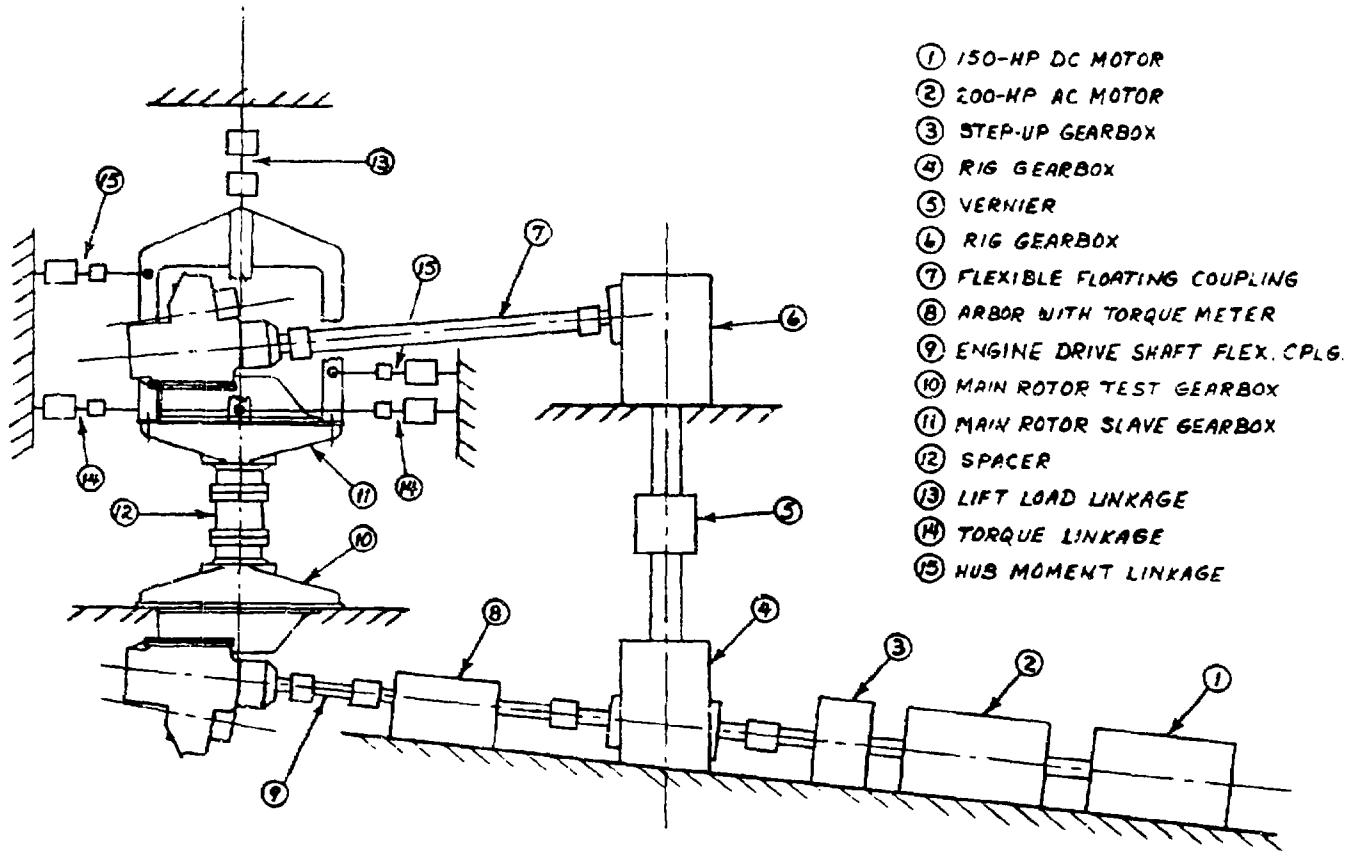


Figure 18. Main Gearbox Test Rig

1. Input speed in rpm.
2. Input torque in pound-inches.
3. Oil-in temperature of two SH-2 transmissions in °F.
4. Oil-out temperature of two SH-2 transmissions in °F.
5. Oil pressure of two SH-2 transmissions in psi.
6. Oil-in temperature of test rig gearboxes in °F.
7. Oil pressure of test rig gearboxes in psi.
8. Rotor lift cylinder pressure in psi.
9. Rotor lift load in pounds.
10. Rotor torque cylinder pressure in psi.
11. Rotor torque cylinder load in pounds.
12. Rotor torque in pound-inches.
13. Rotor pitch moment cylinder pressure in psi.
14. Rotor pitch moment cylinder load in pounds.

## TEST STAND MODIFICATIONS

The basic test stand was modified to meet the requirements of the subject test program. Specific modifications were limited to installation of an acoustic enclosure surrounding the test gearbox, and a vibration-isolating coupling between the test and slave gearboxes.

The design of the acoustic enclosure is illustrated in Figure 19. Outside dimensions are approximately 54 inches high by 54 inches deep by 54 inches wide. The enclosure is constructed of 1-inch plywood and lined with an acoustically soft (highly absorptive) material incorporating a high transmission loss septum. The lining arrangement is shown in Figure 20, along with curves relating the anticipated acoustic characteristics of the enclosure.

The vibration-isolating coupling used to connect the slave and test gearboxes is shown in Figure 21. The working element of this coupling is a 48 inch diameter, 4 inch thick neoprene disk of 50 durometer hardness, which reacts torque loads in shear and thrust (lift) loads in tension/compression. The top and bottom surfaces of the neoprene disk are bonded to circular steel plates, 48 inches in diameter and 1.25

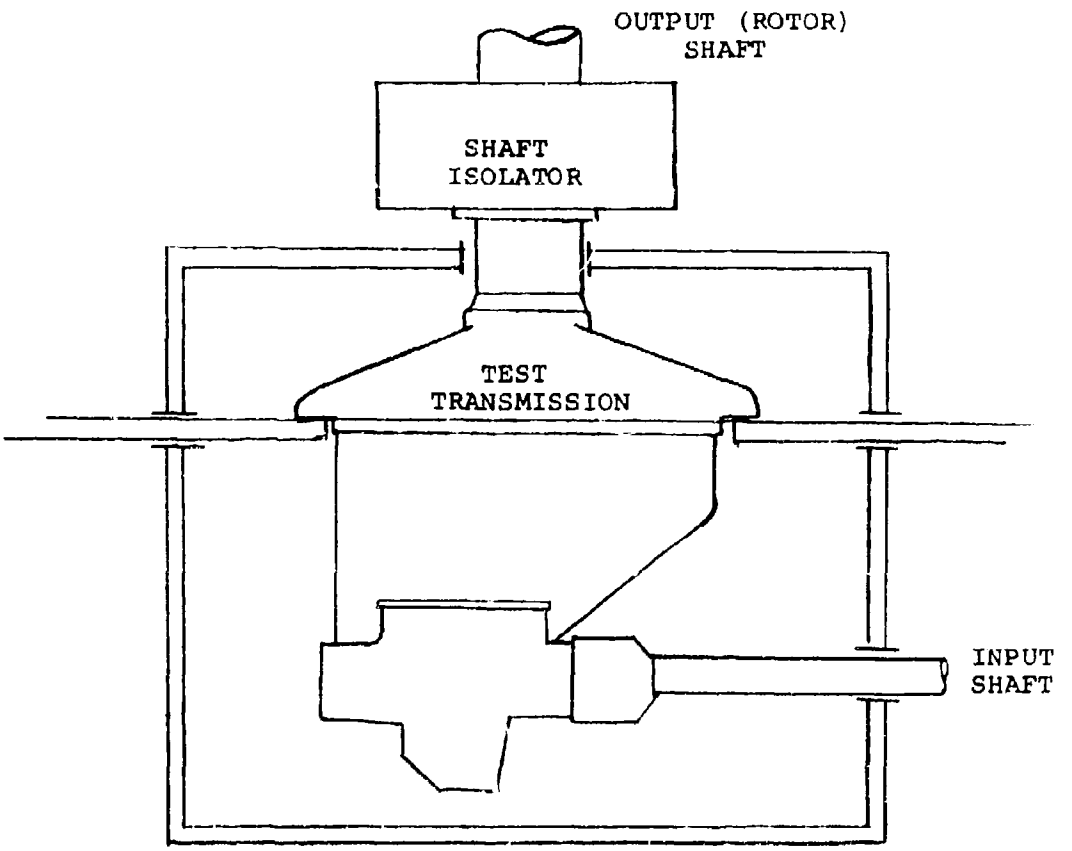


Figure 19. Acoustic Enclosure Schematic

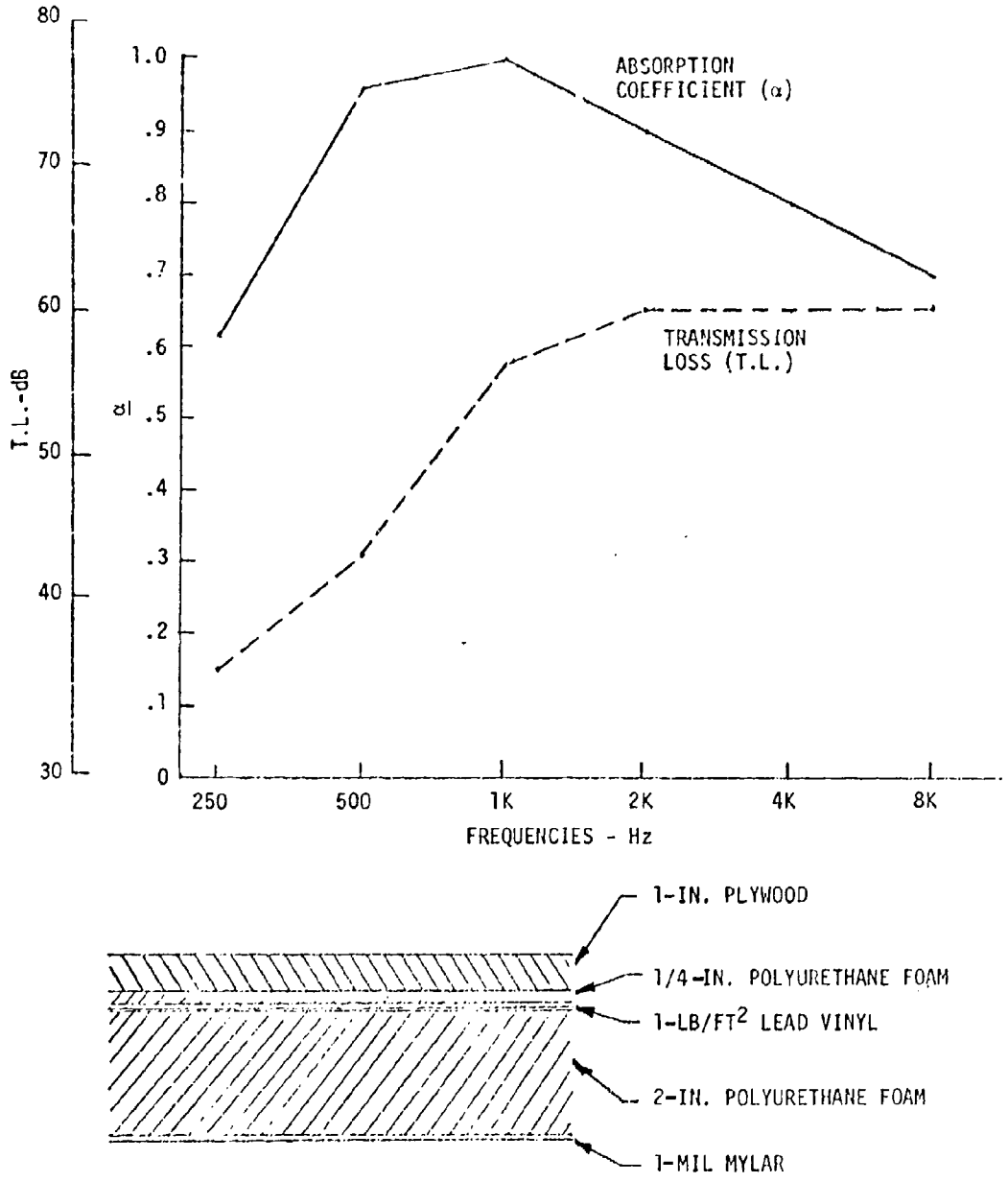


Figure 20. Acoustic Enclosure Lining Arrangement and Expected Characteristics

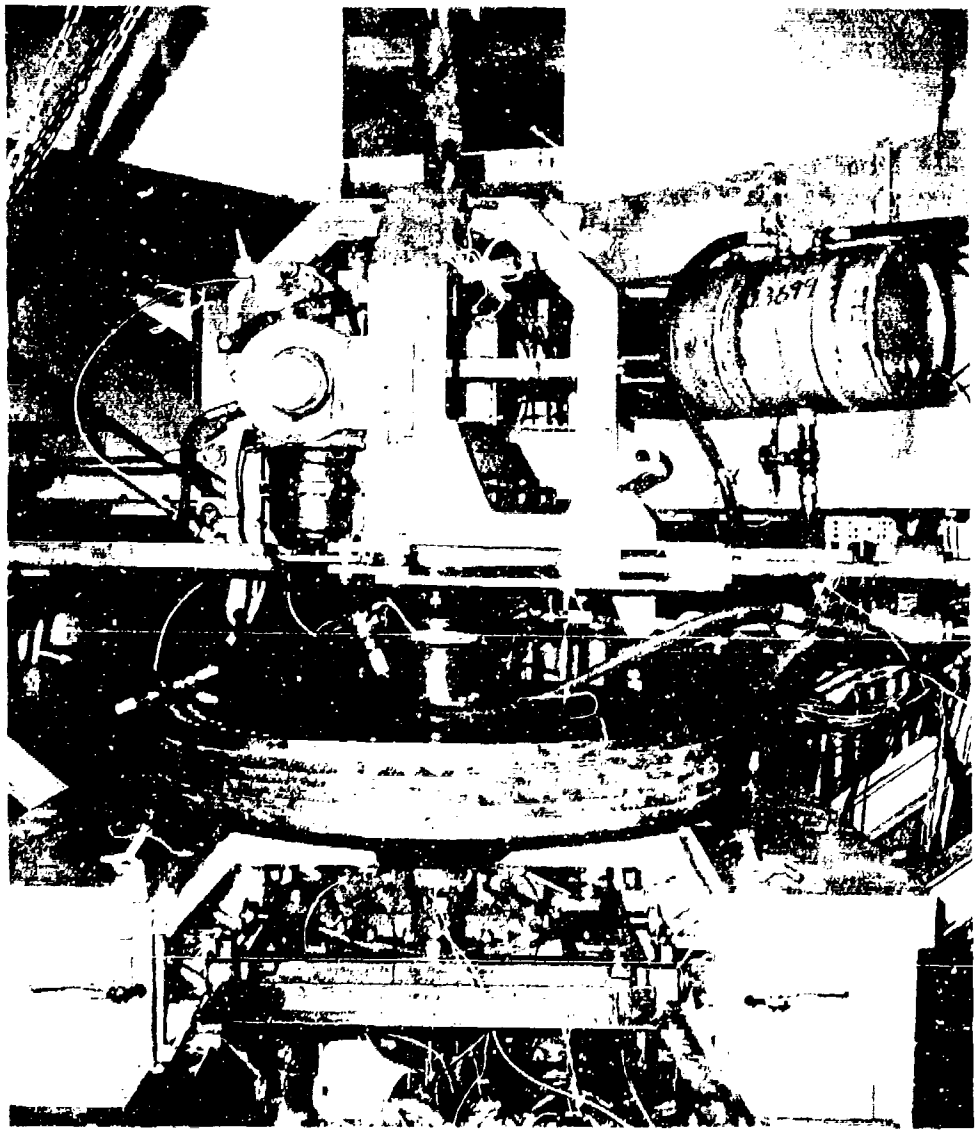

Figure 21. Slave/Test Gearbox Vibration-Isolating Coupling

inches thick, which include provisions for mounting to the slave and test gearbox output shafts. This isolator was designed to provide greater than 98-percent attenuation of structure-borne sound. Decoupling of slave and test gearbox dynamics was also anticipated. The coupling was designed to accommodate the rotor shaft torque of 320,000 in.-lb as well as the lift load of 12,000 lb.

## TEST PROCEDURE

Testing consisted of recording data signals corresponding to each of the dynamic parameters of the section on Test Parameters at discrete points over a range of transmission torque and rpm settings. Specific conditions tested are shown in Table 5. In addition to the points shown, data was obtained while transmission speed was swept over the range of 80 percent (4896 rpm) to 100 percent (6120 rpm) of full rpm, with the torque set at 80 percent (12,160 in.-lb).

TABLE 5. MATRIX OF TEST CONDITIONS FOR TRANSMISSION DYNAMICS TESTING

| Input Shaft Speed - rpm (%) | Torque - In.-Lb (%) | |
|---|---|---|
| 4896 (80%) | 9120 (60%) | 12160 (80%) |
| 6120 (100%) | 9120 (60%) | 12160 (80%) |

Because of the large number of parameters observed and the limited data acquisition capability imposed by the use of a single 14-channel data recorder, all parameters were not recorded simultaneously. Instead, parameters were grouped into data sets, each set consisting of no more than 14 parameters, and data from each set recorded sequentially. The use of this approach to data acquisition required that the test matrix of Table 5 be repeated for each data set.

Data sets were selected which retain the required interparameter phasing information, minimize instrumentation requirements, and limit exposure time for the anticipated low survival lifetime rotating-shaft strain-gage installations. The contents of the four data sets used are given in Table 6.

TABLE 6. BREAKDOWN OF PARAMETERS BY DATA SET

| Data Set | Parameter Descriptions* | No. of Parameters* |
|---|---|---|
| A | • Bending Responses - Input Shaft<br>• Torsional Responses - Input Shaft<br>• Displacement Responses - Input Shaft<br>• Bearing Accelerations (Lateral & Axial) - Spiral Bevel Gear/Spur Pinion Shaft | 12 |
| B | • Bending Responses - Rotor Shaft<br>• Torsional Responses - Rotor Shaft<br>• Displacement Responses - Rotor Shaft<br>• Displacement Responses of Spur Gear Web (Axial) - Spur Gear Shaft | 12 |
| C | • Case Accelerations | 15 |
| D | • Radiated Noise | 13 |

* All data sets include an rpm signal which will be recorded on edge track.

Data sets A and B include all rotating-shaft strain measurements, with set A covering the strains in the input shaft and set B in the rotor shaft. Bending, torsion, and displacement responses for a single shaft must be recorded simultaneously in order to recover phasing information needed to define shaft mode shapes. The data of sets A and B have been included in a single wiring hookup, shown in Figure 22, using, for the most part, common signal conditioning equipment with a switching capability between the transducers used for the two data sets. This arrangement permits sequential acquisition of data from these two data sets within a single test run, since a wiring hookup change is not required to convert from recording of "A" data to "B" data. Use of this approach minimizes both equipment requirements and running time necessary to acquire rotating-shaft strain data. Switching between A and B data sets was accomplished at the control console.

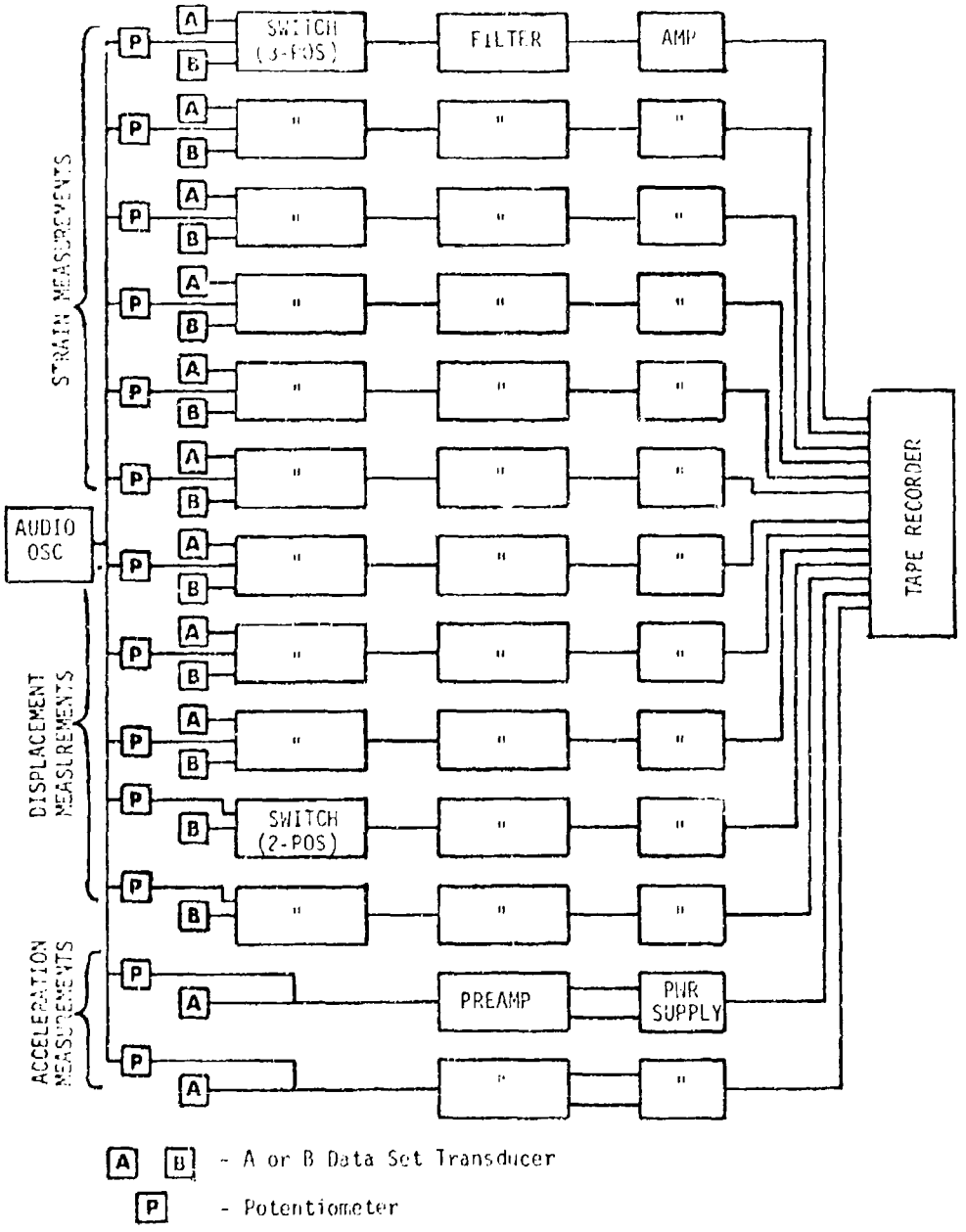


Figure 22. Wiring Schematic for Shaft Response Two-Part Test - Data Sets A and B

The wiring hookups used for acquisition of data sets C and D are shown in Figure 23. Data sets C and D include, respectively, all case surface accelerations and radiated noise measurements. Signal conditioning equipment is common to the acceleration and noise measurements; however, switching between data sets C and D during testing is not feasible, since switching would have to be effected at the transducer/preamplifier connection, which is physically located in the immediate area of the test transmission. Consequently, the full test matrix of Table 5 was satisfied for data set C, after which testing was suspended, the wiring hookup for data set D made, and the test matrix repeated. Three replications of the test matrix were required, with data sets A and B acquired during the first run, data set C during the second run, and data set D during the last run.

The sequence of events followed for each test run was as follows:

1. The instrumentation hookup was made and checked for continuity, and signal conditioner gains were adjusted to appropriate values based on predicted transducer signal outputs.

2. The data acquisition system was energized and system calibration signals were applied to all data channels.

3. Transmission orientation was adjusted to account for shaft misalignment under torque and lift load.

4. The test stand was run up to the rpm required by the given test condition, and torque and lift load applied (test data was not acquired during run-up).

5. The given torque and rpm condition was maintained until stable operation was attained, as indicated by a stable oil output temperature.

6. Recorder input signals were monitored and system gains changed, if necessary, to optimize the signal level. If gains were adjusted, calibration signals were reapplied.

7. Data were recorded for a minimum of 30 seconds.

8. For test run A/B only, data signals were switched and data recording was repeated.

9. Steps 4 through 8 were repeated for the full test matrix of Table 5, thereby completing testing of preselected steady-state test points.

10. Data recording was recommenced and rpm was swept slowly from maximum to minimum. When minimum rpm was reached, recording was stopped and the test stand shut down.

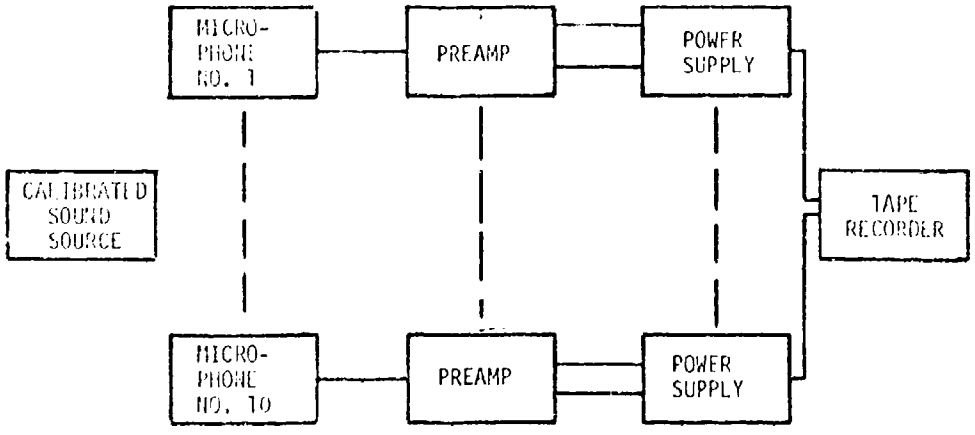


A. Sound Measurement Schematic (Data Set D)

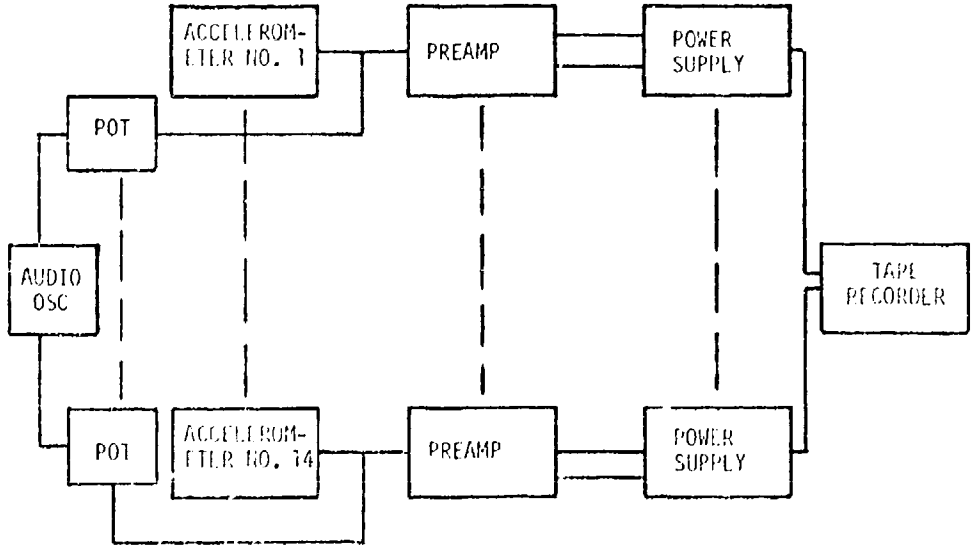


B. Acceleration Measurement Schematic (Data Set C)

Figure 23. Wiring Schematics for Data Sets C and D

## DATA REDUCTION

The data recorded during the data acquisition phase of the subject test effort contained information reflecting transmission response (shaft deflections, case accelerations, and radiated noise) to all sources of excitations present. These were expected to include shaft unbalance and misalignment, bearings, oil impingement, air pumping, etc., as well as the gear-clash-induced forces of interest. The objective of the data reduction effort was to extract the meaningful gear-clash-related components from the raw data signals and present the information obtained in physically interpretable form. To accomplish this, the data reduction system of Figure 24, which uses the instrumentation of Table 4, was used.

The key elements in the data reduction system of Figure 24 are the real-time analyzer and the digital computer. Data stored on tape, in analog form, were played back into the real-time analyzer, which transformed the recorded analog time domain data into a digital frequency domain representation. The output of the real-time analyzer, which is available both for immediate oscilloscope display and for further analysis, is a time history of the spectral content of the input signal. Within the present program, the oscilloscope display of the analyzed data was used only for visual inspection of data quality, while the parallel analyzer output was subjected to more extensive analysis.

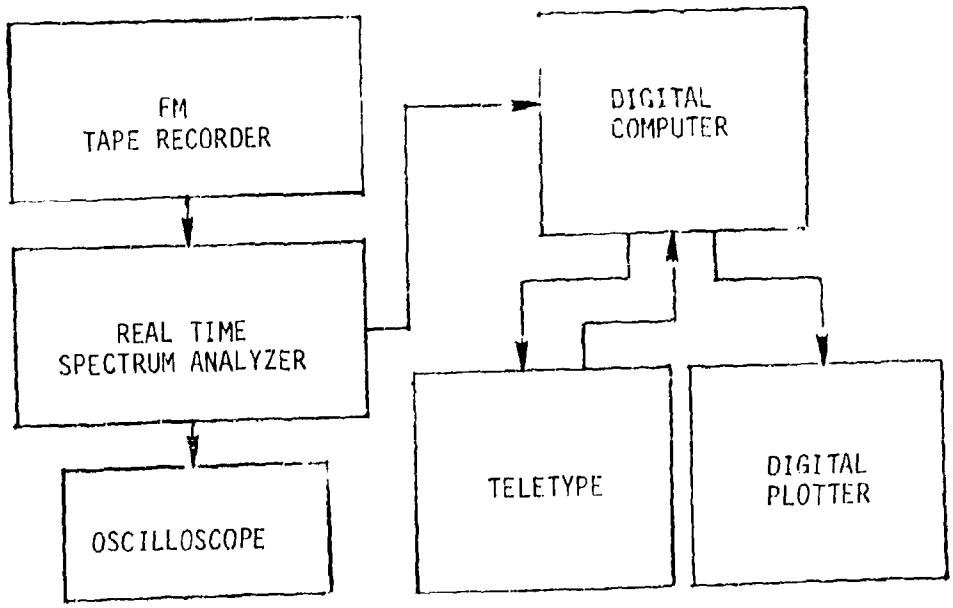


Figure 24. Data Reduction System

The output of the real-time analyzer is a measure of the instantaneous spectral content of the raw test data. The amplitudes of the various frequency components within these spectra generally fluctuate in a random manner due to small perturbations inherent in the operation of the test article. Because of this, the spectrum generated at any instant will be in error by an unknown amount. To overcome this inherent error, the spectral data from the real-time analyzer were subjected to ensemble averaging, with the final averaged spectra accepted as a true representation of the spectral content of the measured data.

The instantaneous frequency spectra generated by the real-time analyzer are not produced continuously, but rather at small, but finite, intervals. The process of ensemble averaging takes a number of these instantaneous spectra, computes the sum of the amplitudes of all frequency components within each spectrum, then divides the summed amplitudes by the number of instantaneous spectra considered. Averaging removes the effects of random fluctuations in the test data, resulting in averaged spectra that accurately reflect the steady-state amplitudes of the measured responses.

### Computer Data Processing

Each averaged spectrum generated by the ensemble averager contains the amplitudes of responses (strain, displacement, acceleration, or noise) to each gear-mesh excitation within the gearbox, generally including the amplitudes of a number of harmonics of each mesh frequency. Since data were obtained for a large number of parameters and test conditions, the quantity of the resulting data was substantial. Consequently, a computer processing method was developed to aid in interpreting the test data.

The averaged spectra generated by the real-time analyzer/ensemble averager were directed to a small general-purpose digital computer, where they were suitably identified and permanently stored on magnetic disks. After all test data were stored in this manner, a software routine was used, which automatically retrieved and processed each stored spectrum. Processing consisted of searching each spectrum for preselected frequency components, including all gear-mesh fundamental and harmonic frequencies of interest, and of generating printed numerical data tables containing all pertinent response amplitudes. Concurrently, the processing routine generates a plot of the entire averaged frequency spectrum.

## TEST DATA

The test program resulted in the generation of a substantial amount of raw test data, all of which has been reduced into meaningful form. Because of the quantity of data involved, it is not considered appropriate to include all reduced test data within this report. Selected examples of these data are, however, presented and discussed in the following paragraphs.

## Shaft Strain and Displacement

Both bending and torsion strain measurements were made at several locations on both the input and output shafts. Reduced test data corresponding to bending strain at shaft station 8.65 on the input shaft are shown in Figure 25. Output shaft bending strain data, at shaft station 20, are given in Figure 26. The data shown in these two figures refer to a test condition of 100-percent transmission speed (6120 rpm input shaft speed) and 80-percent torque (12,160 inch-pounds input torque).

The measured bending strain spectra for both the input and output shafts contain frequency components associated with each gear-mesh. Gear meshing frequencies evident in both Figures 25 and 26 include the planetary system fundamental and second harmonic, at frequencies of 435 Hz and 870 Hz, the fundamental and second harmonic of the spur gear mesh, at 1497 Hz and 2994 Hz; and the bevel gear fundamental and second harmonic, at 3060 Hz and 6120 Hz. The data of Figures 25 and 26 also show significant components at equal frequency increments above and below each of the gear-mesh fundamental and harmonic components. These upper and lower sideband components, which occur at frequency increments of 100 Hz in both the input and output shaft data, are comparable in amplitude to the responses at the gear-meshing frequencies. Because these sideband responses are not predicted by the analytical model, their existence in the test data complicates data interpretation to the extent that these data could not be used to correlate model predictions.

The importance of the sideband frequency components of Figures 25 and 26 is limited only to their detrimental impact on data interpretation. They do not impact transmission noise and vibration because they are a result of the measurement process and are not caused by physical bending of the shafts at the sideband frequencies. This conclusion is supported by the fact that sideband frequency components do not appear in any of the fixed-system-measured data, including shaft displacement, case acceleration, and sound pressure data. These sideband frequency components can be directly attributed to amplitude modulation of the gear mesh frequency strain signals caused by a 100 Hz torsional oscillation of the drive system, which corresponds to one-per-rev of the input shaft. The fact that a strong 100 Hz frequency component is not evident in the torsional strain data of Figures 27 and 28 is explained by the fact that the strain data were subjected to high pass filtering during the data acquisition process.

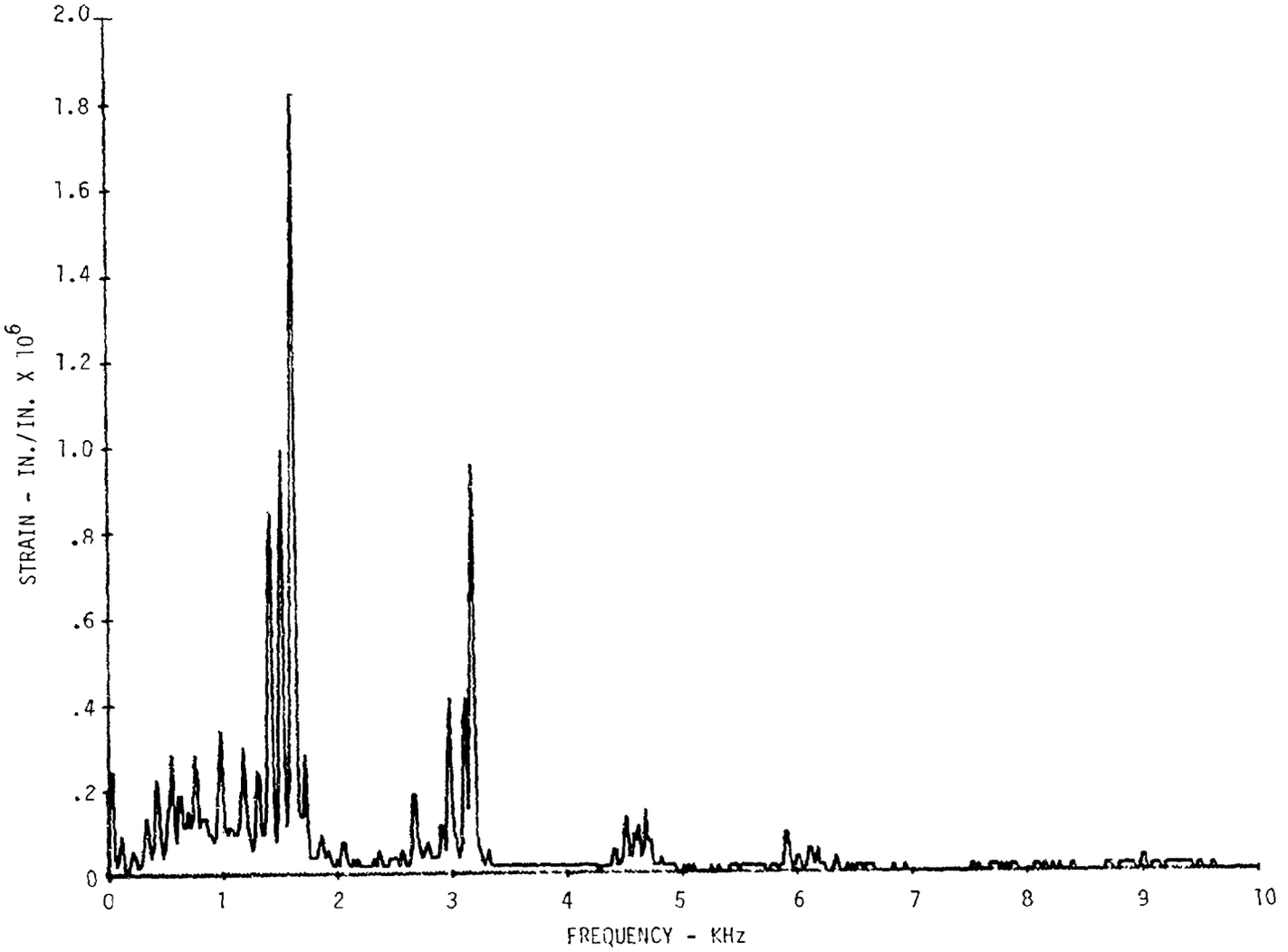


Figure 25. Input Shaft Bending Strain at Shaft Station 8.65, 100% rpm, 80% Torque

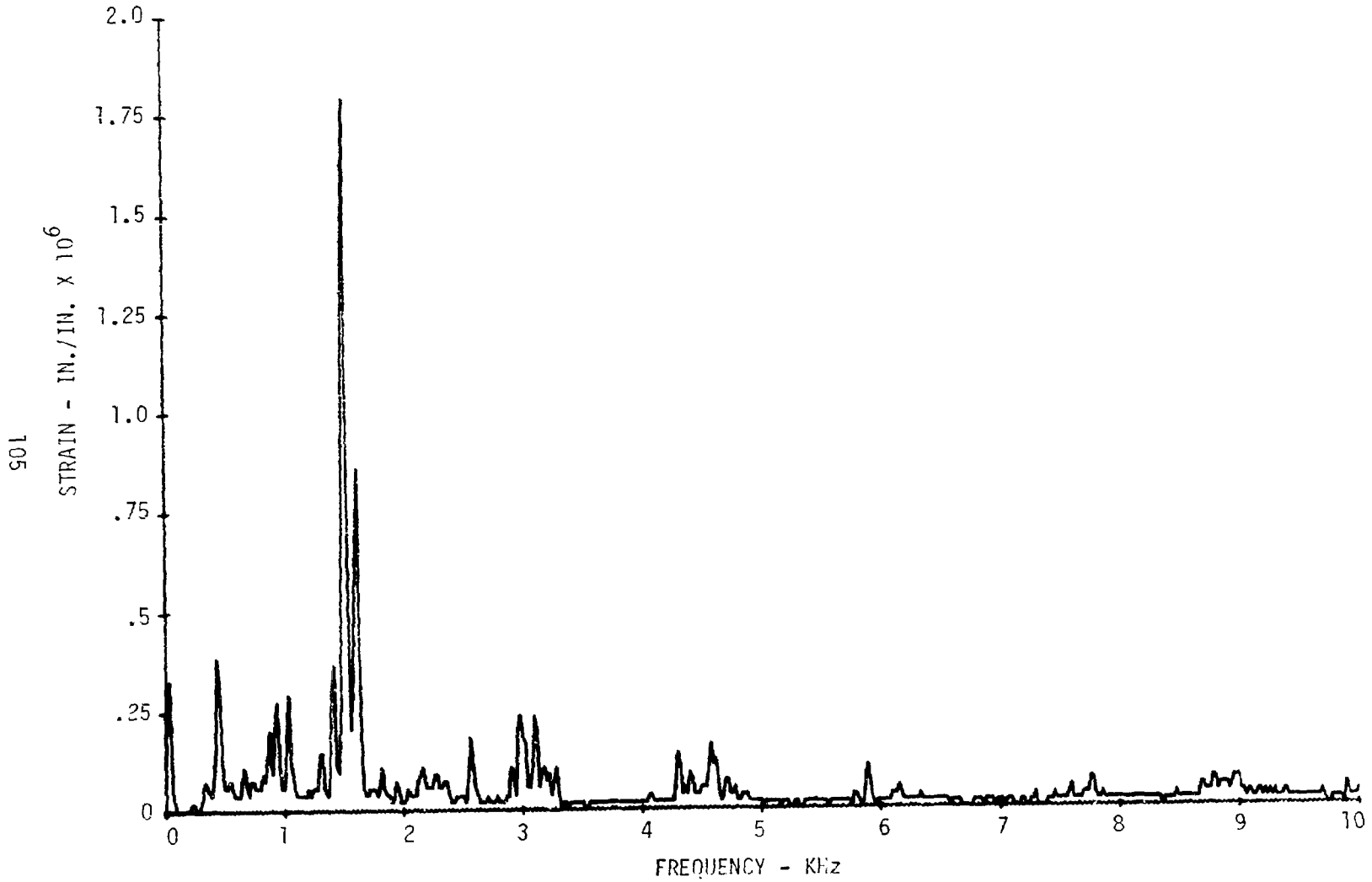


Figure 26. Output Shaft Bending Strain at Shaft Station 20, 100% rpm, 80% Torque

The measured input and output shaft torsional strain data of Figures 27 and 28 are similar to the bending strain data except that multiple upper and lower sideband responses are shown. These data refer to the same 100-percent rpm and 80-percent torque condition as the bending strain data, and the shaft measurement stations used are also the same. As for the bending strain sidebands, the sideband torsional strain responses occur at a frequency differential of one-per-rev of the input shaft speed, although in this case, sidebands also are shown at multiples of this frequency differential. The source of these sideband responses is the same as for the bending sideband responses. With respect to the torsional strains, however, both amplitude and frequency modulation occur.

The fact that sideband strain responses are not transmitted to the fixed system is illustrated in the lateral shaft displacement data of Figures 29 and 30, which refer to the same test conditions as previous data. Only gear-mesh-related frequency components are evident in these data, although the measurement locations shown are in close physical proximity to the previously described shaft bending strain measurement locations. Even though sideband responses were not measured in the fixed-system shaft displacements, these data proved to be equally difficult to interpret and use for correlating the shaft response prediction capability of the analytical method. These displacements are, in fact, not absolute shaft motions but rather, relative deflections between the shaft and the transmission housing which was used to support the displacement probes. To be meaningful approximations of absolute shaft motions, these measured displacements must be, therefore, significantly greater than housing displacements. The displacement magnitudes evident in Figures 29 and 30 correspond to lateral shaft accelerations on the order of a few g's to approximately 100 g. As will be shown in the following paragraphs, accelerations of this magnitude, and greater, were measured at many points on the housing surface, in close proximity to the displacement probe support locations. Because of this, it was assumed that the shaft deflections measured in the present program do not accurately reflect absolute shaft deflections and these data were not used in model correlation efforts.

## Housing Acceleration

Examples of reduced transmission acceleration data are given in Figures 31 through 34. These data refer to the same 100-percent rpm, 80-percent torque condition of previous data. Measured responses are shown for each of the housing sections, including the upper housing (Figure 31), the middle housing (Figure 32), the lower housing (Figure 33), and the input shaft housing (Figure 34). Specific housing coordinates included in Figures 31-34 are, respectively, coordinates 5, 11, 18, and 20, indicated in Figure 12.

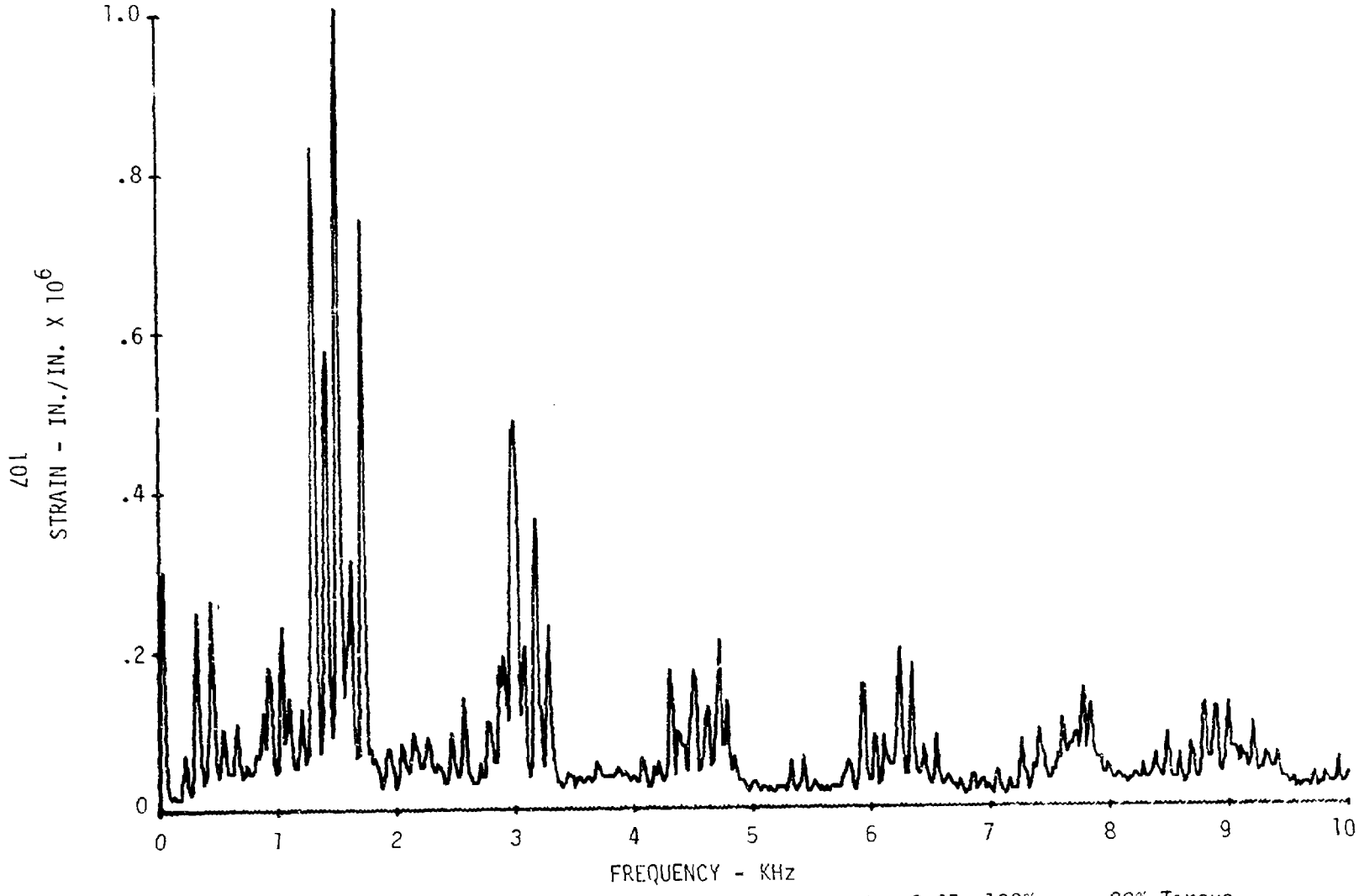


Figure 27. Input Shaft Torsional Strain at Shaft Station 8.65, 100% rpm, 80% Torque

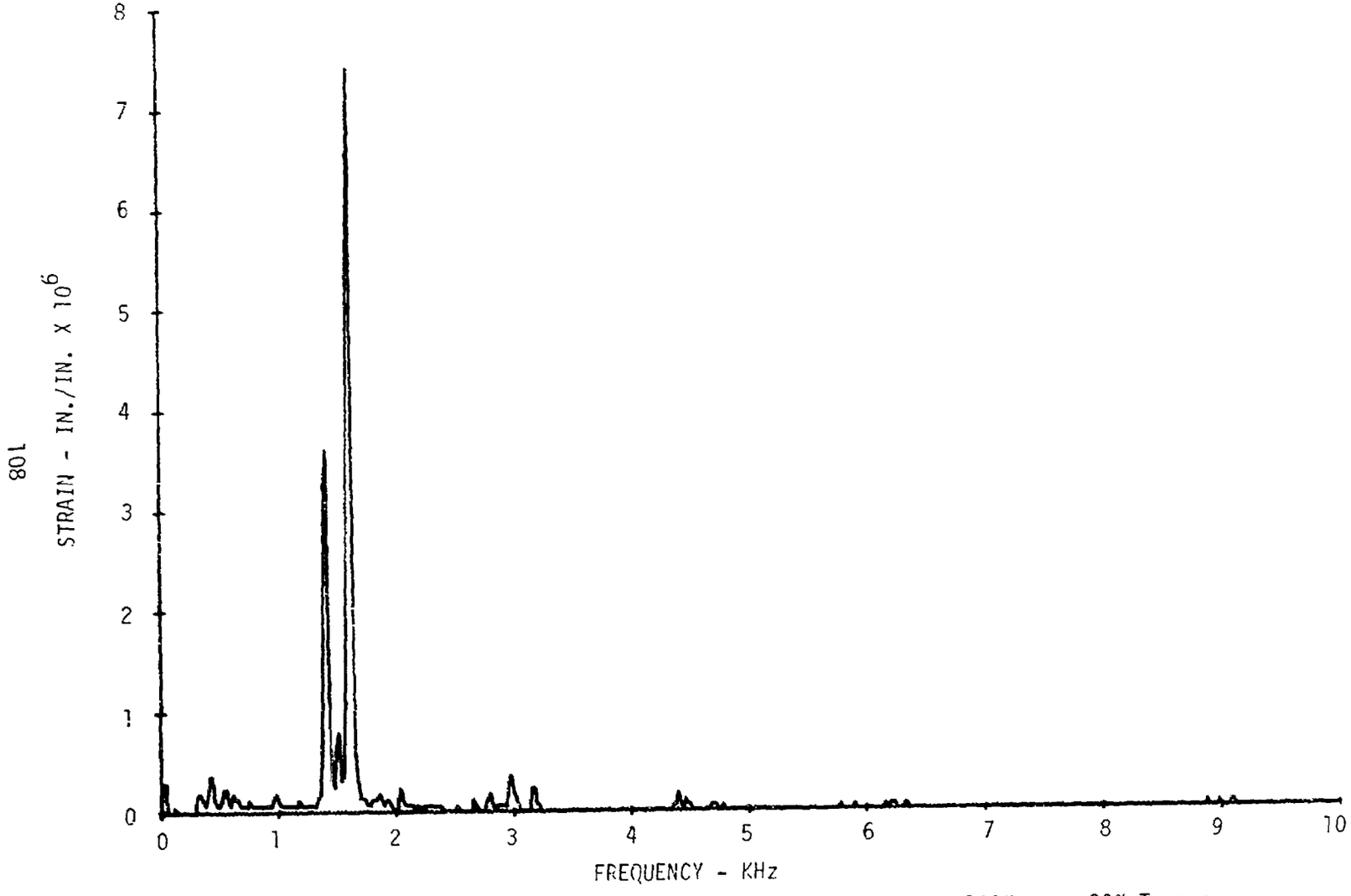


Figure 28. Output Shaft Torsional Strain at Shaft Station 20, 100% rpm, 80% Torque

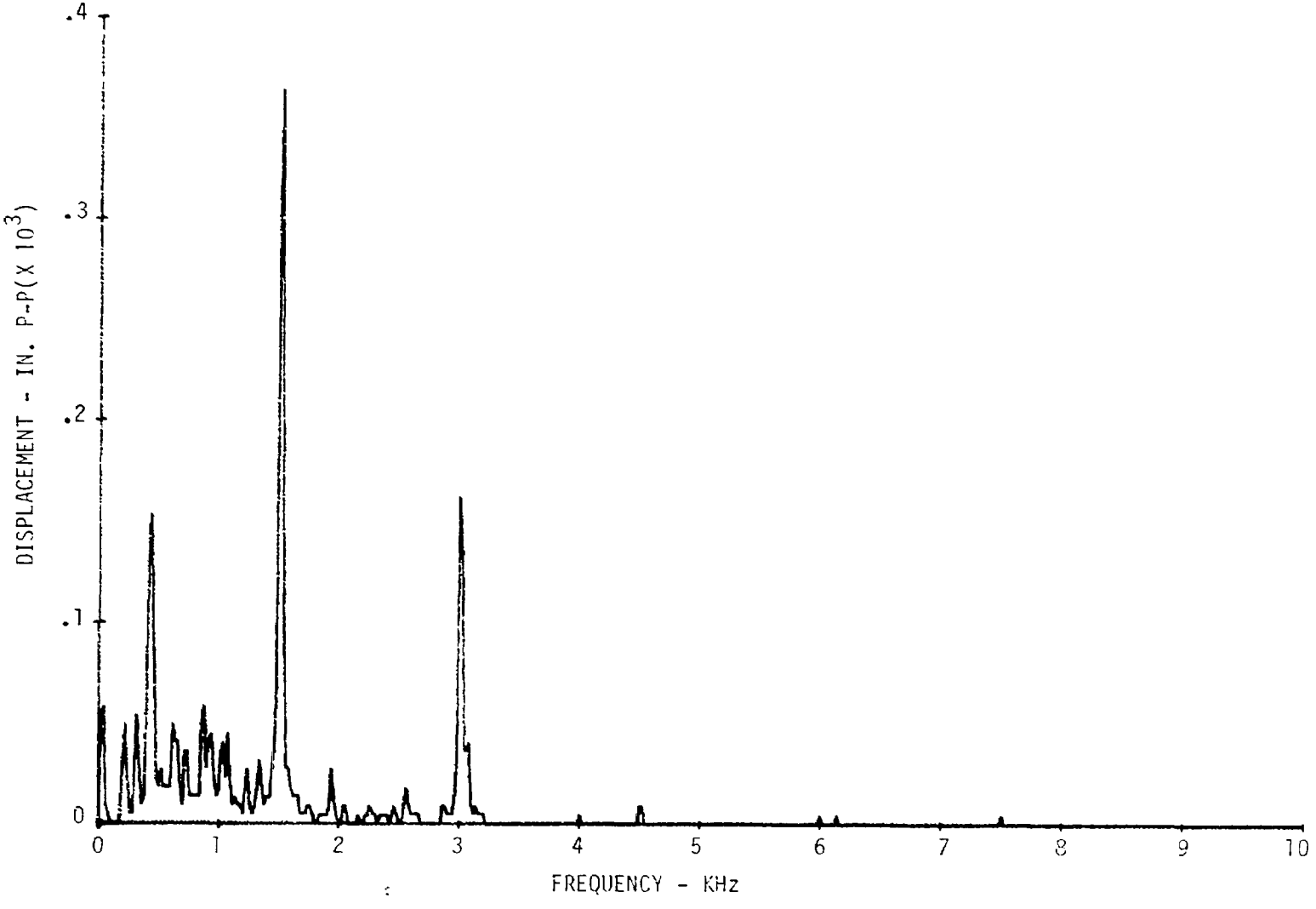


Figure 29. Input Shaft Displacement at Shaft Station 8.27, 100% rpm, 80% Torque

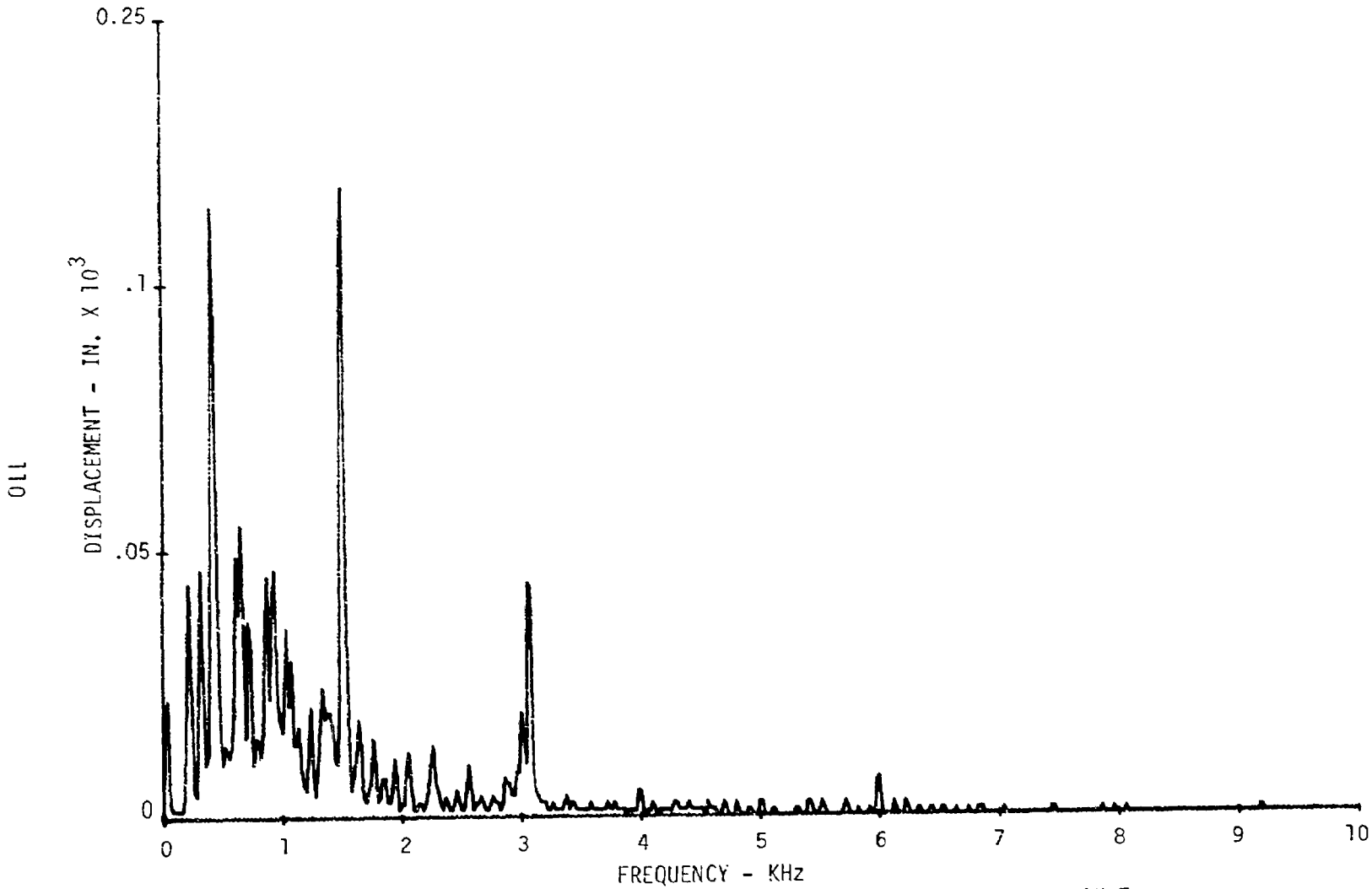


Figure 30. Output Shaft Displacement at Shaft Station 17, 100% rpm, 80% Torque

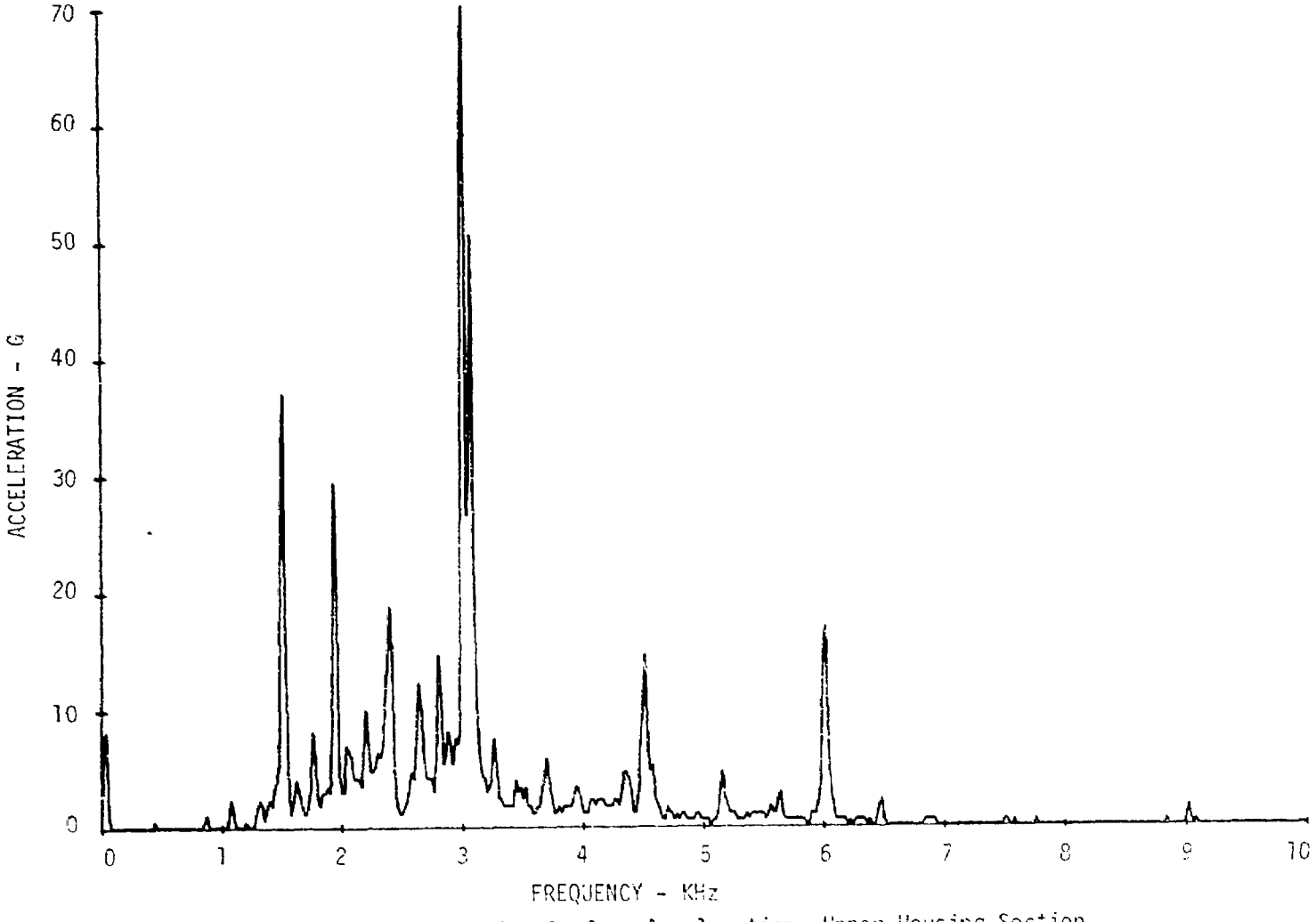


Figure 31. Transmission Housing Surface Acceleration, Upper Housing Section, 100% rpm, 80% Torque

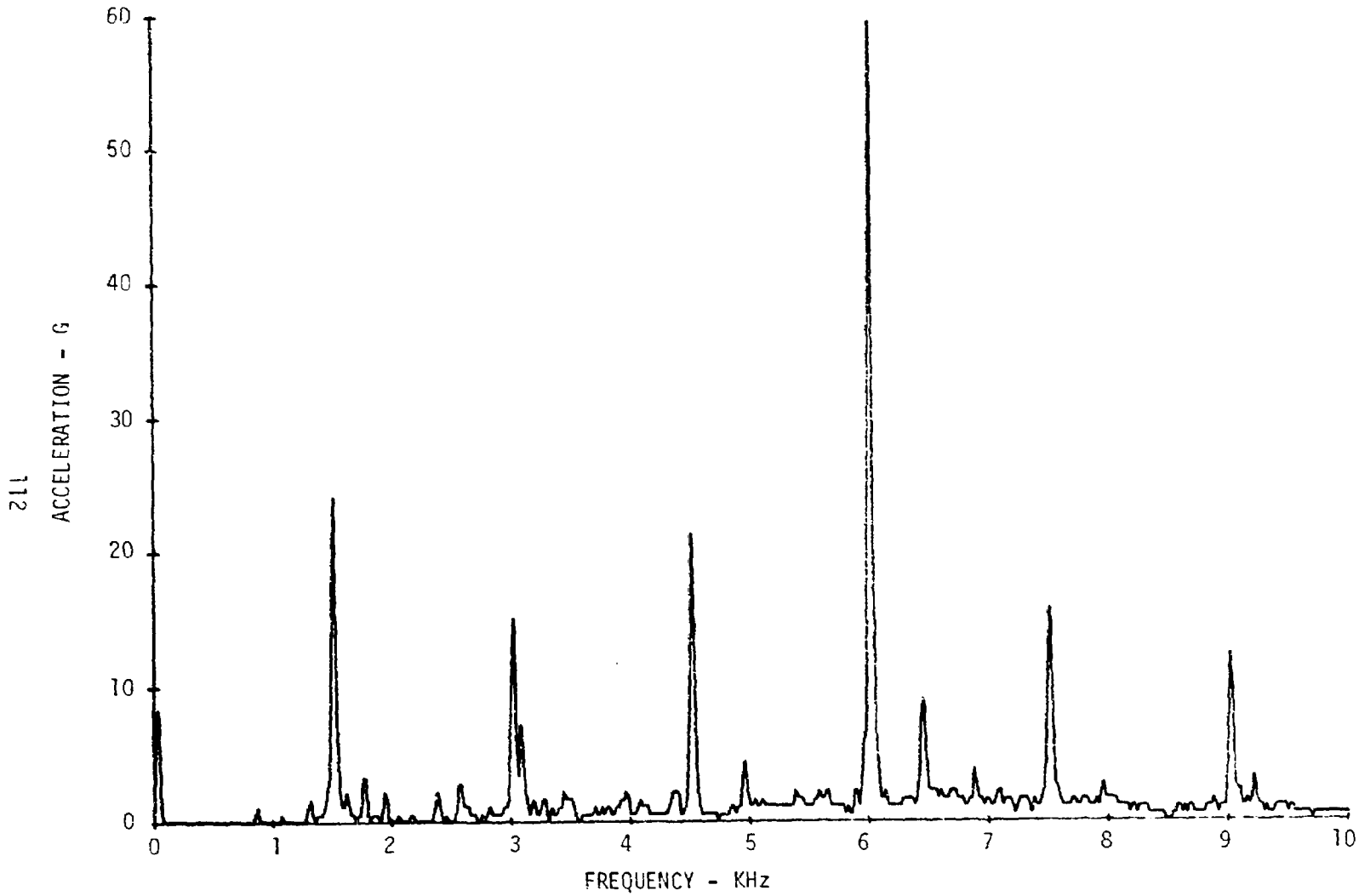


Figure 32. Transmission Housing Surface Acceleration, Middle Housing Section, 100% rpm, 80% Torque

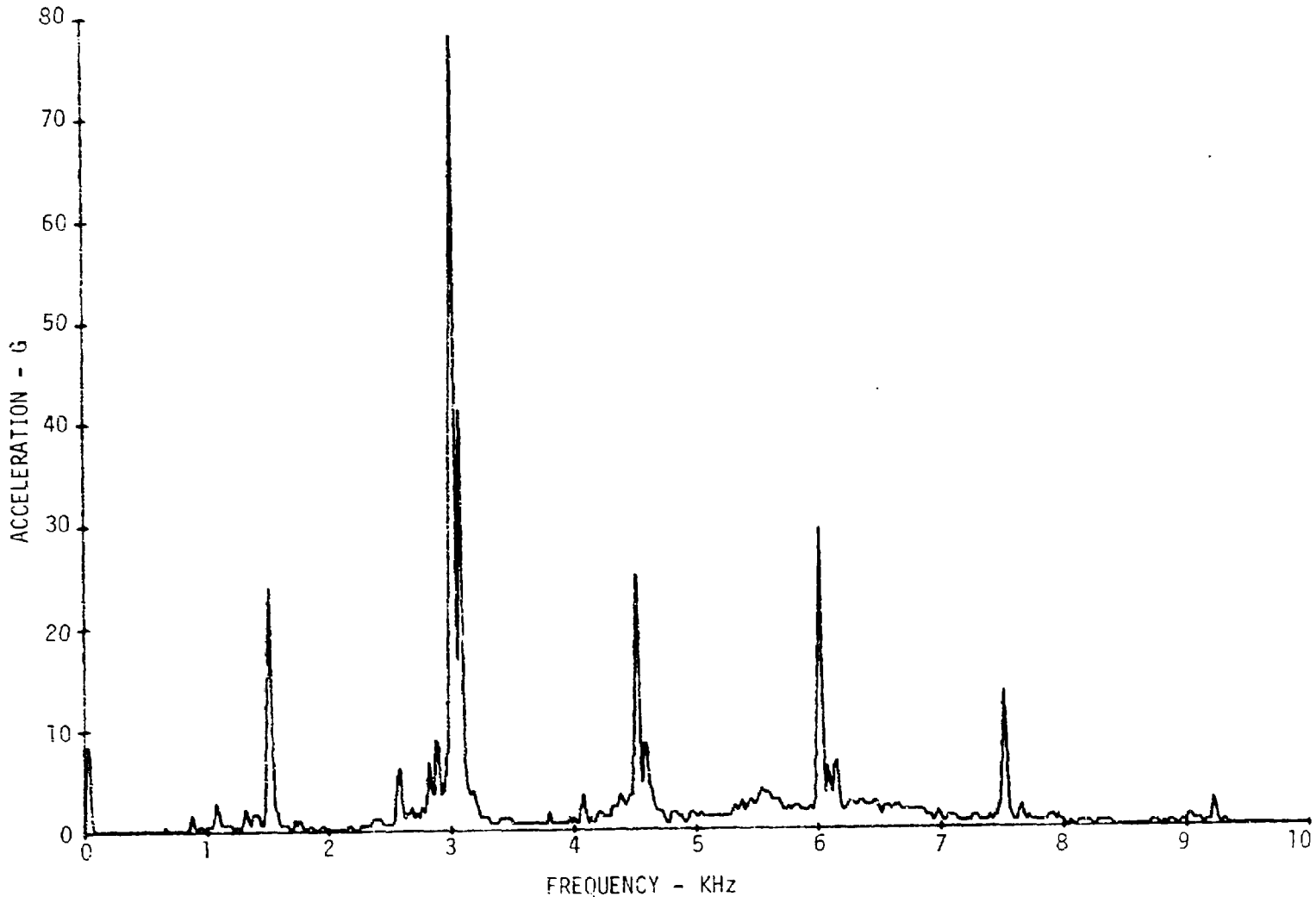


Figure 33. Transmission Housing Surface Acceleration, Lower Housing Section, 100% rpm, 80% Torque

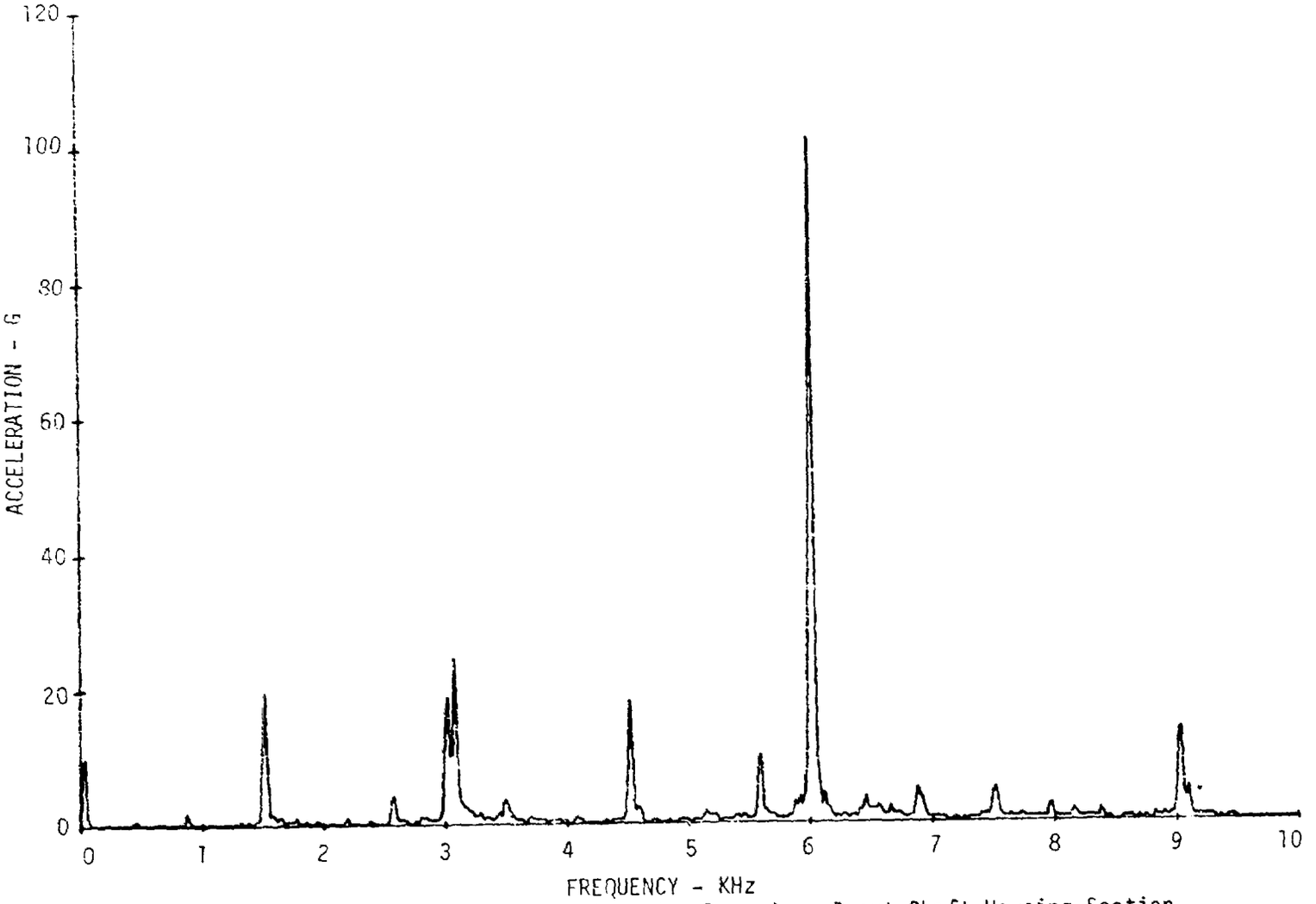


Figure 34. Transmission Housing Surface Acceleration, Input Shaft Housing Section, 100% rpm, 80% Torque

The frequency content of all of the measured housing accelerations of Figures 31-34 is similar. All of the gear-mesh frequencies of interest are evident in these data, with the exception of the planetary system fundamental and second harmonic. Although these components were discernable in the raw data, and their amplitudes were, in fact, extracted for use, these components are not shown because of their (relatively) low magnitude.

No sideband responses are evident in the measured acceleration data, lending further credence to the supposition that these rotating-system responses are experimental artifacts.

Radiated Noise

Examples of reduced measured sound pressure level data are shown in Figures 35-38. As for previous data, these figures correspond to a 100-percent rpm, 80-percent torque test condition. Figure 35 refers to a measurement station on the upper, aft, port side of the transmission, while the data of Figure 36 were obtained diagonally opposite this point, on the lower, forward, starboard side. The measurements of Figures 37 and 38 were obtained on the upper, aft, starboard side and lower, forward, port side, respectively. All measurements were made approximately 2 feet from the surface of the transmission housing. The frequency content and general characteristics of the sound pressure level data are similar to the acceleration data presented previously.

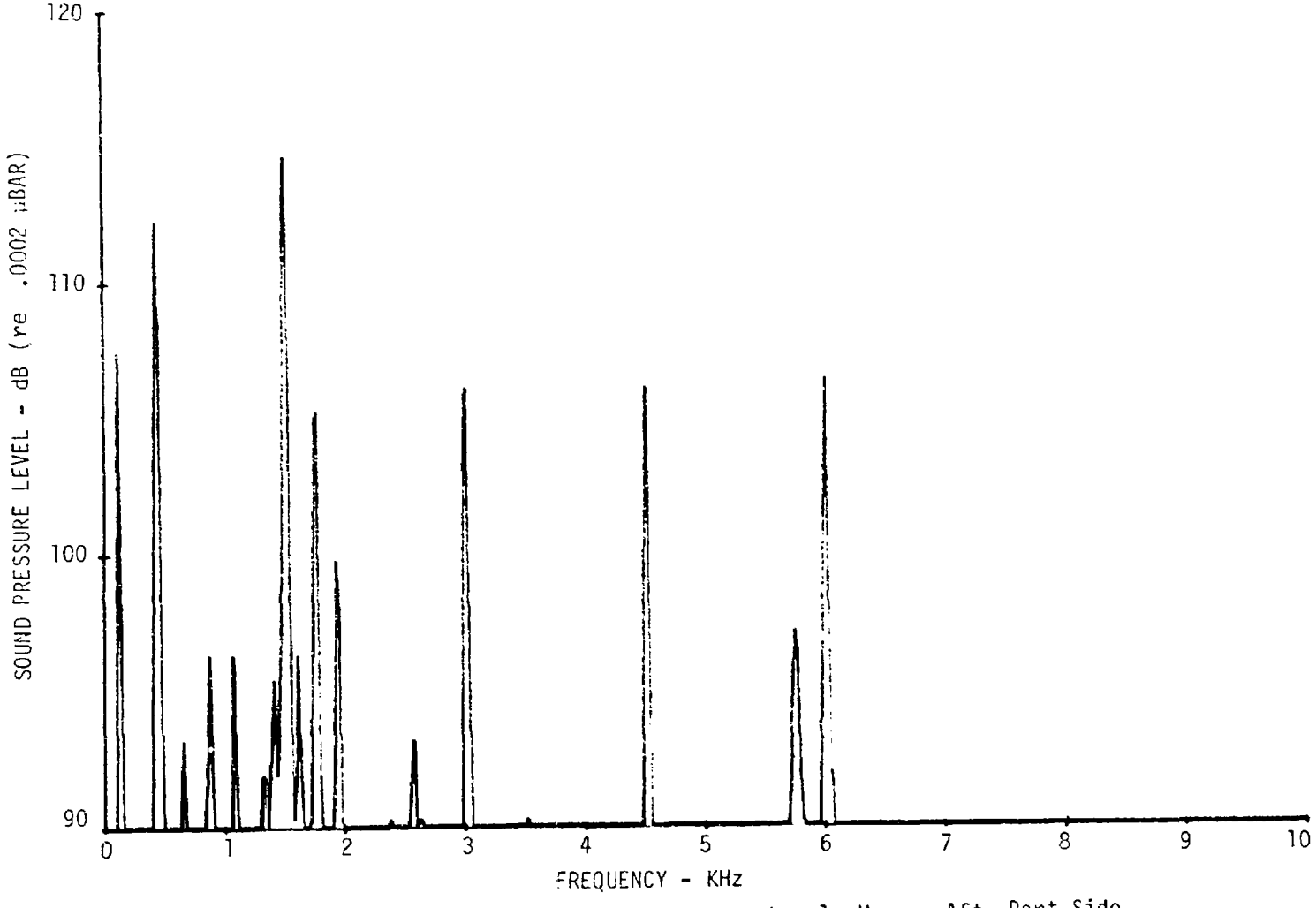


Figure 35. Transmission-Radiated Sound Pressure Level, Upper, Aft, Port Side, 100% rpm, 80% Torque

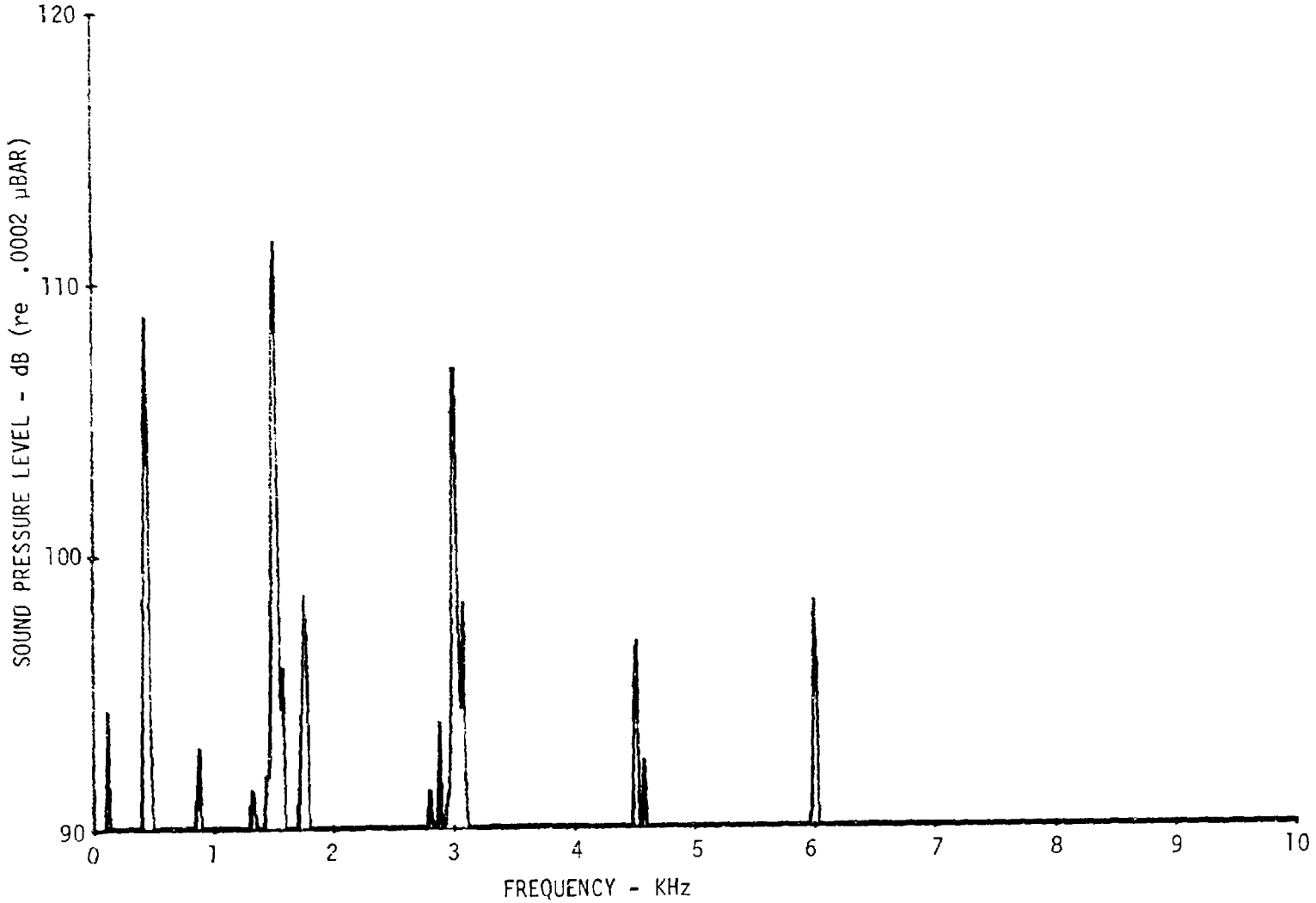


Figure 36. Transmission-Radiated Sound Pressure Level, Lower, Forward Starboard Side, 100% rpm, 80% Torque

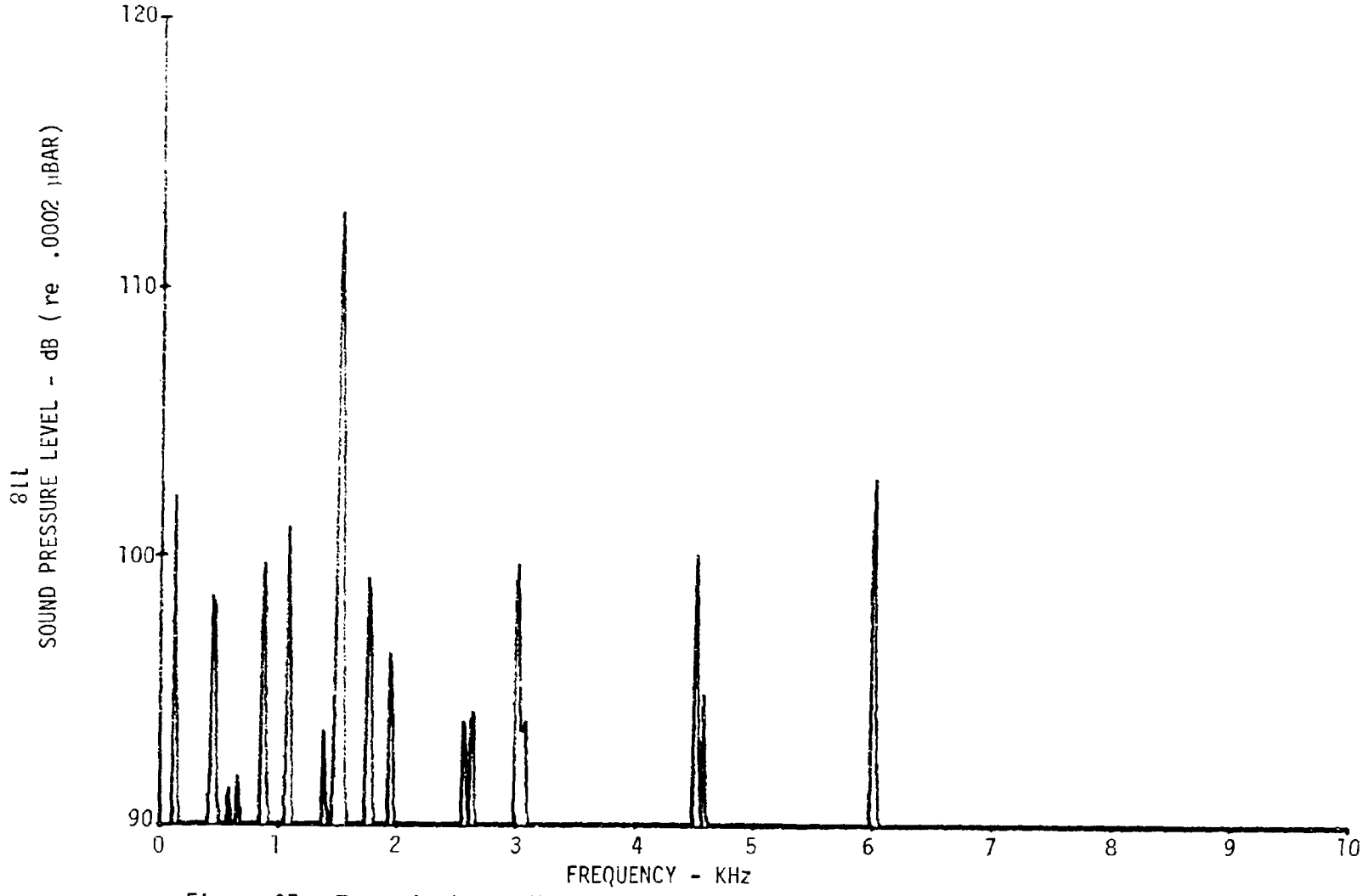


Figure 37. Transmission-Radiated Sound Pressure Level, Upper, Aft, Starboard Side, 100% rpm, 80% Torque

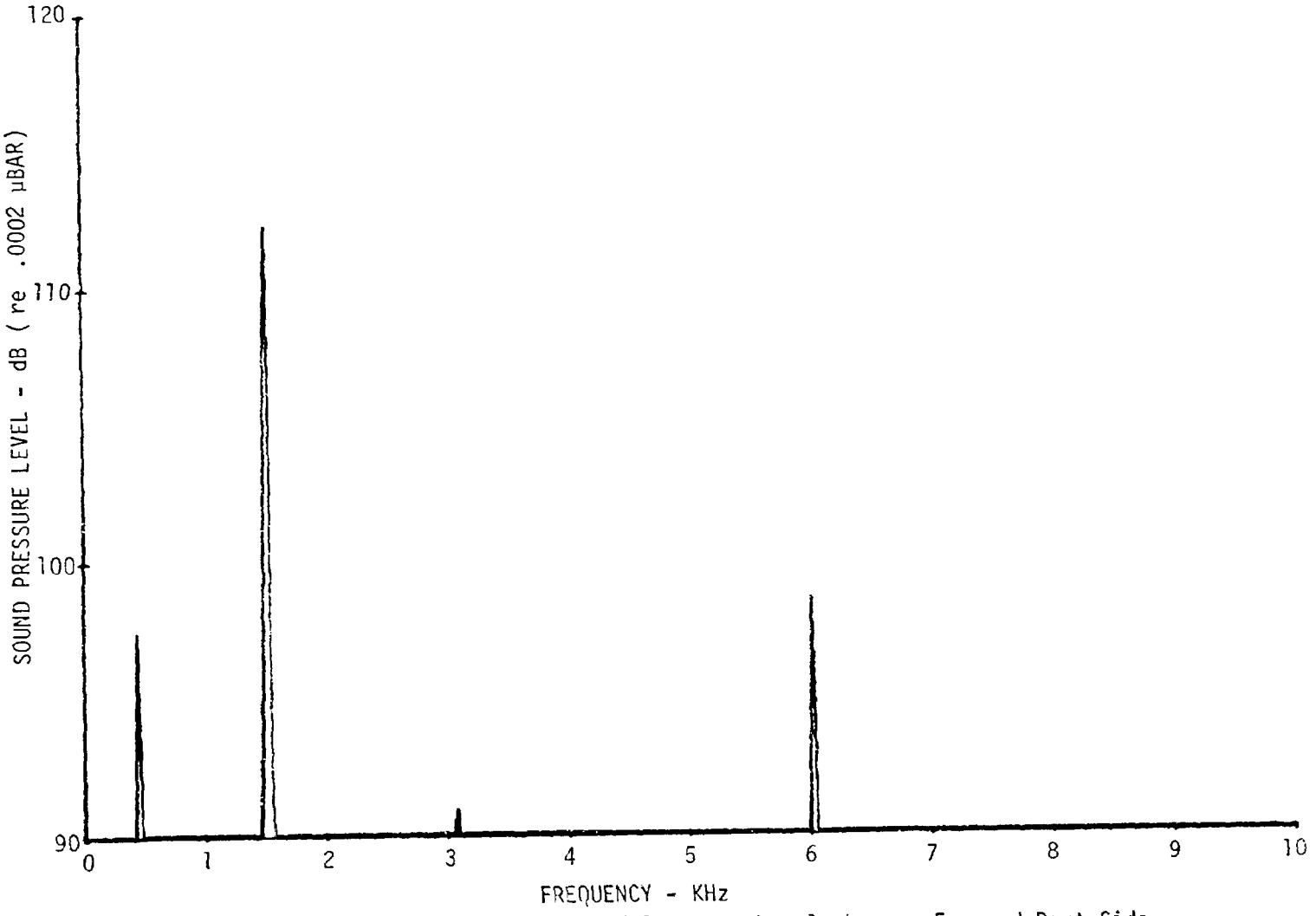


Figure 38. Transmission-Radiated Sound Pressure Level, Lower, Forward Port Side, 100% rpm, 80% Torque

## METHOD CORRELATION

Analytical predictions of the dynamic responses of the SH-2D main transmission were made, for comparison with the measured test data. Predictions were made for the specific conditions of transmission speed and torque loading for which data were available, including:

- 4896 rpm input shaft speed (80-percent rpm) and 9120 in.-lb input shaft torque (60-percent torque)
- 6120 rpm input shaft speed (100-percent rpm) and 9120-in.-lb shaft torque (60-percent torque)
- 4896 rpm input shaft speed (80-percent rpm) and 12,160 in.-lb input shaft torque (80-percent torque)
- 6120 rpm input shaft speed (100-percent rpm) and 12,160 in.-lb shaft torque (80-percent torque)

While predictions of all relevant transmission responses were made, only case acceleration and radiated noise proved to be of value in correlating the analytical method. As mentioned previously, the measured shaft dynamic responses, including bending and torsion strain and shaft lateral displacement, were found to be difficult to interpret, and therefore were not used in the correlation efforts. Shaft bending and torsion strain and lateral displacement are intermediate responses which give rise to the ultimate housing accelerations and radiated noise which are of primary interest. As such, these intermediate responses must be accurately predicted to obtain accurate predictions of housing acceleration and noise. Conversely, good correlation between measured and predicted housing acceleration and radiated noise implies that the intermediate shaft responses are also predicted accurately. For this reason, failure to specifically validate the shaft response prediction methods was not considered to be an essential element in the overall analytical method validation effort.

### CASE ACCELERATION

Predictions of case surface acceleration at 14 locations were made and compared to accelerations measured at these same points. Comparisons were made at each gear-mesh related frequency of interest, including:

- Planetary system fundamental and second harmonic
- Spur gear mesh fundamental and second harmonic
- Spiral bevel gear mesh fundamental

Since two transmission speeds were considered in both the analytical and test efforts, a total of 10 discrete frequency acceleration components were available for comparison, covering the frequency range of 342 Hz to 3060 Hz. Table 7 defines the discrete frequency excitation/response components which were used in this correlation effort.

Figures 39-43 compare measured and predicted transmission housing accelerations for each gear-mesh excitation listed in Table 7, at the 80-percent rpm test condition. Data for both the 60-percent and 80-percent torque conditions are shown and the housing coordinates used in Figures 39-43 correspond to those identified in Figure 12. Similar comparative data are given in Figures 44-48 for the 100-percent rpm test condition.

The predicted housing accelerations of Figures 39-48 show reasonable agreement with the measured data shown, over the full range of gear-mesh excitation frequencies and torque levels. Although coordinate-by-coordinate agreement is by no means exact, the average acceleration over the entire housing surface, in most cases, shows very good correlation. The maximum acceleration is also generally well correlated, which is of more significance, given the impact of housing acceleration on radiated noise.

The transmission noise and vibration prediction method developed in the present program represents an attempt to strike a balance between prediction accuracy and application cost. Because of this, some inaccuracy in the model predictions is to be expected because of simplifying assumptions and approximations which have been included in the analytical method to obtain a reasonable application cost. These approximations and assumptions lead directly to the lack of perfect agreement evident in the housing acceleration data of Figures 39-48. It is important to note, however, that the level of agreement in these data is sufficient to demonstrate the ultimate validity of the modeling methods.

The degree of correlation is evident when the magnitude of accelerations associated with the various excitation sources are compared. At the planetary system fundamental, for example, at the 60-percent torque condition, measured acceleration ranges from a minimum of .2 g to a maximum of 1.4 g. Predicted accelerations range from .14 g to 1.3 g. At the higher 80-percent torque condition, measured accelerations cover a higher range, extending from .16 g to 2.3 g, while the predicted accelerations range from .18 g to 1.54 g. The higher disparity at the high torque level is due to changes in the measured accelerations, which show variations in both "mode shape" and absolute magnitude relative to their low torque values. The predicted accelerations, on the other hand, show no difference in "mode shape" and only a small increase in magnitude, which is consistent with the mathematical modeling formulation. This difference in the effect of torque indicates a shortcoming in the model formulation, but this was not investigated further since the generally good agreement was considered to be adequate.

TABLE 7. DISCRETE FREQUENCY EXCITATION/RESPONSE COMPONENTS USED TO CORRELATE ACCELERATION PREDICTION METHOD

| Excitation Source | Excitation/Response Frequency (Hz) | |
|---|---|---|
| | 80% rpm | 100% rpm |
| Planetary System Fundamental | 348 | 435 |
| Planetary System Second Harmonic | 696 | 870 |
| Spur Gear Fundamental | 1198 | 1497 |
| Spur Gear Second Harmonic | 2396 | 2994 |
| Spiral Bevel Gear Fundamental | 2448 | 3060 |

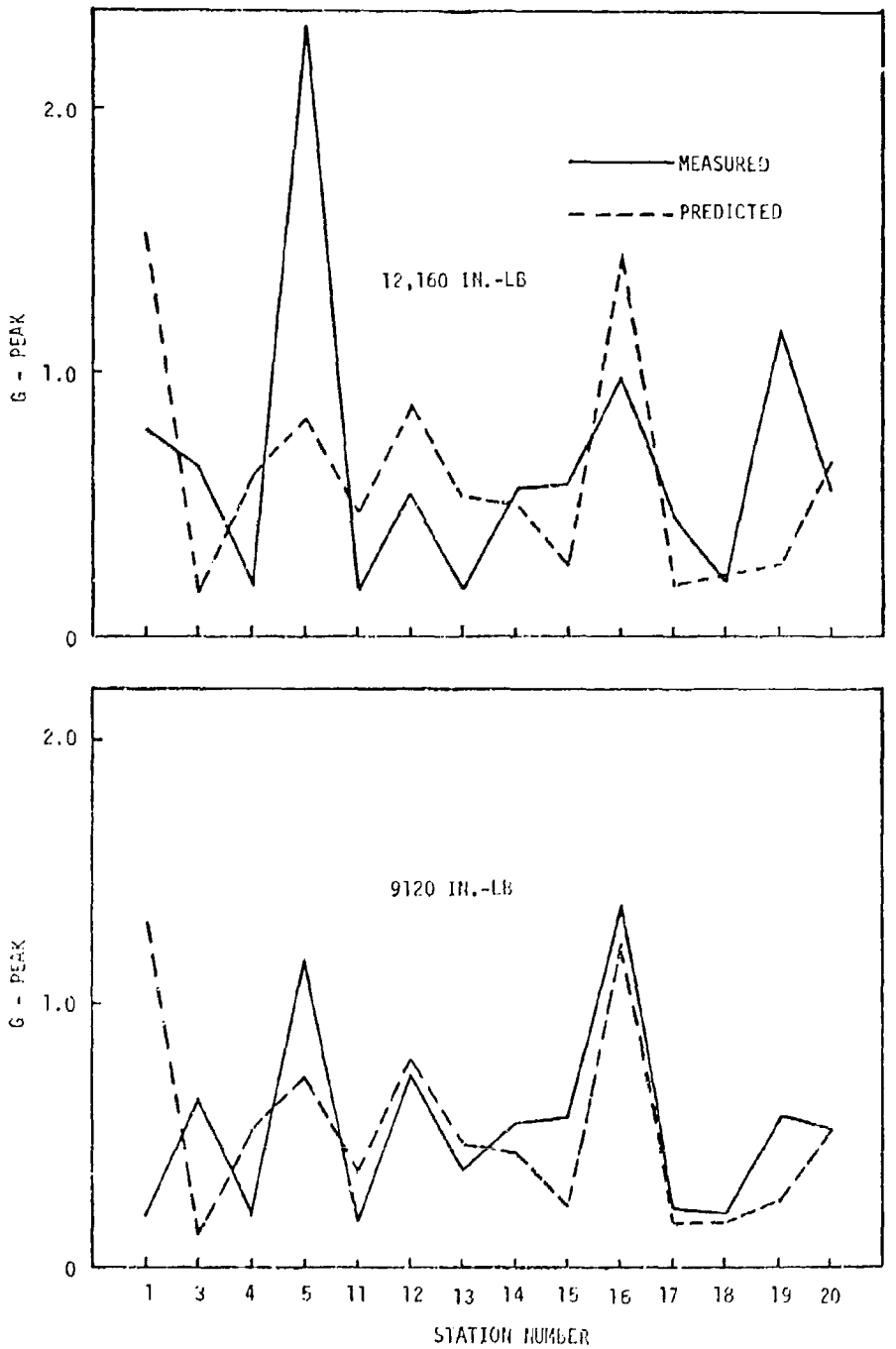


Figure 39. Measured vs. Predicted Case Acceleration for 348 Hz Excitation

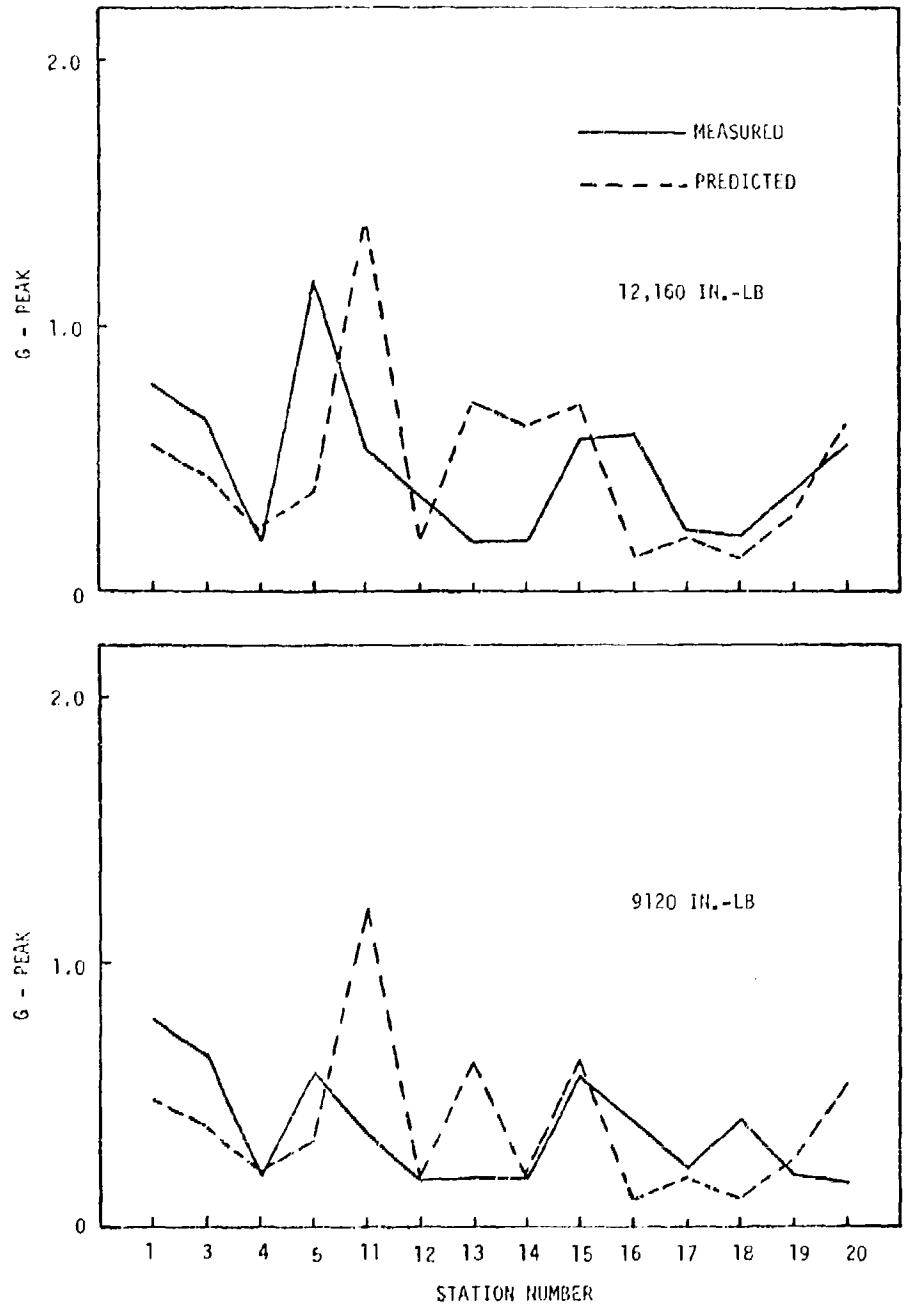


Figure 40. Measured vs. Predicted Case Acceleration for 696 Hz Excitation

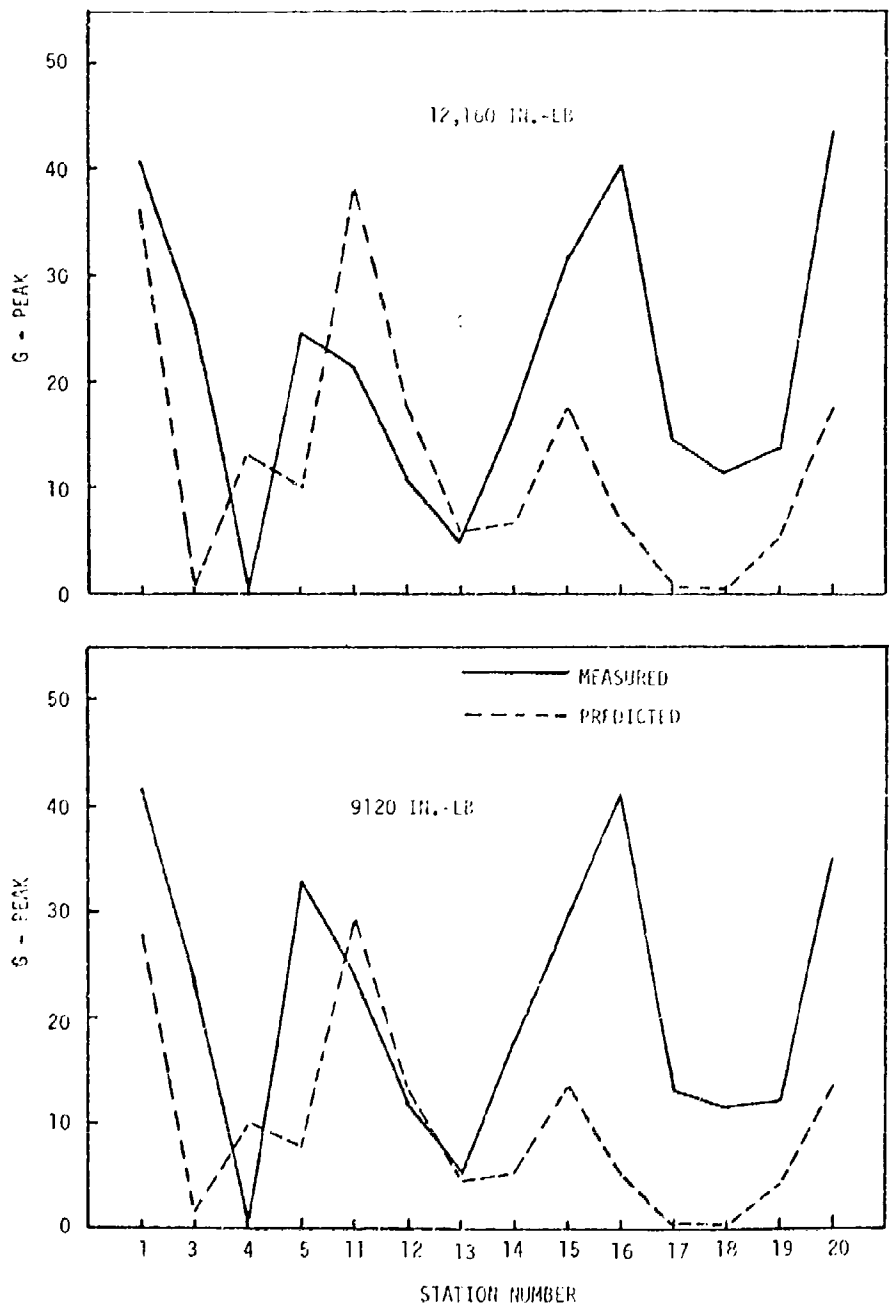


Figure 41. Measured vs. Predicted Case Acceleration for 1198 Hz Excitation

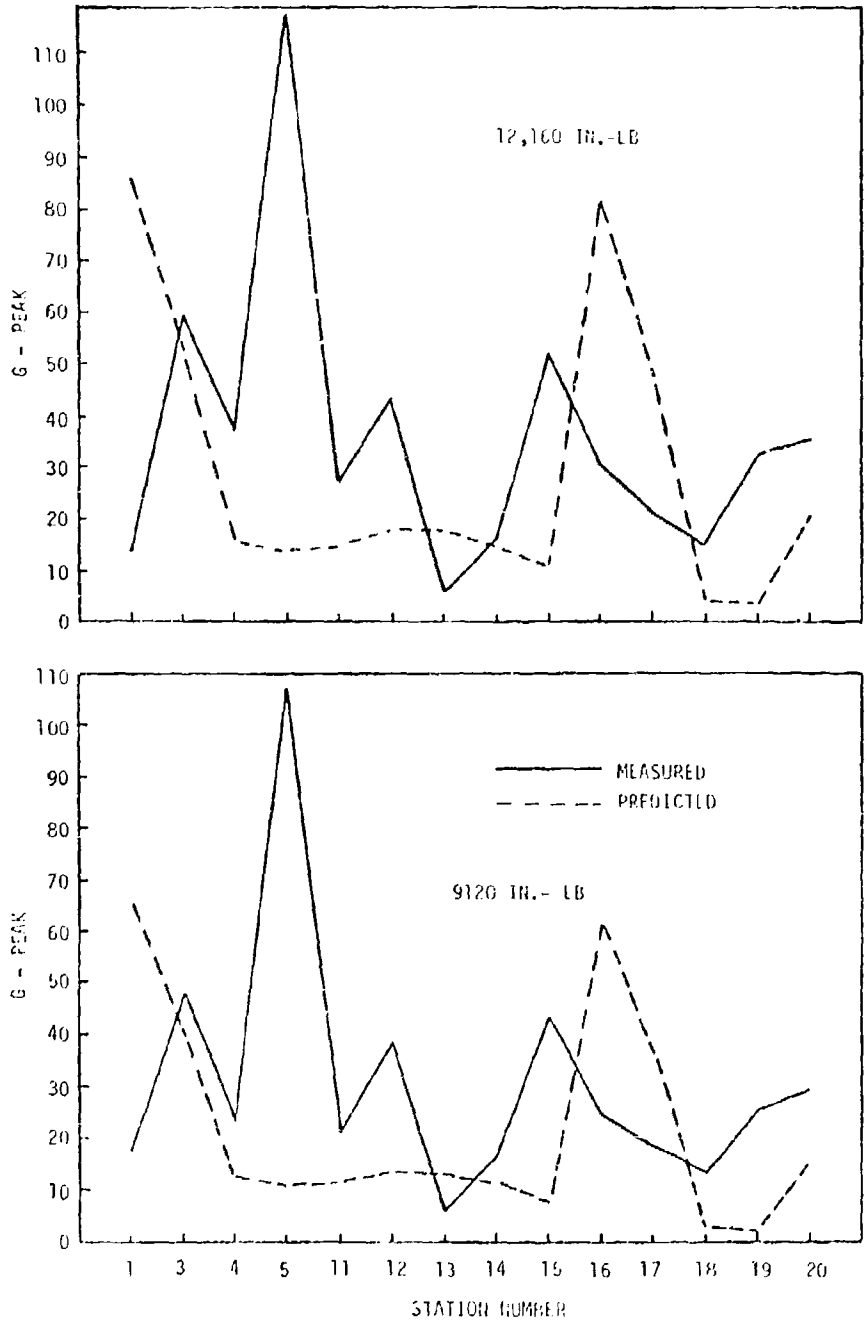


Figure 42. Measured vs. Predicted Case Acceleration for 2396 Hz Excitation

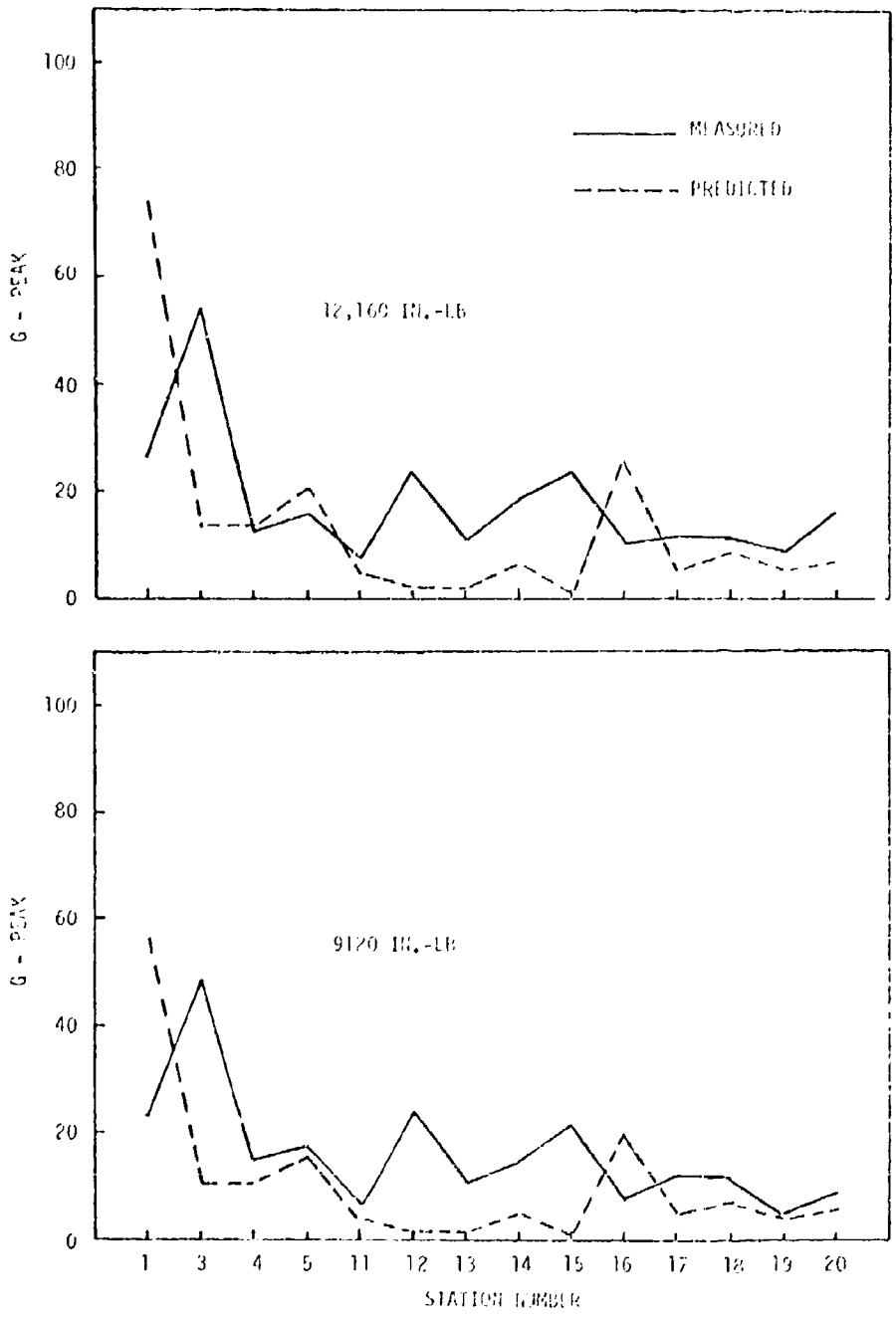


Figure 43. Measured vs. Predicted Case Acceleration for 2448 Hz Excitation

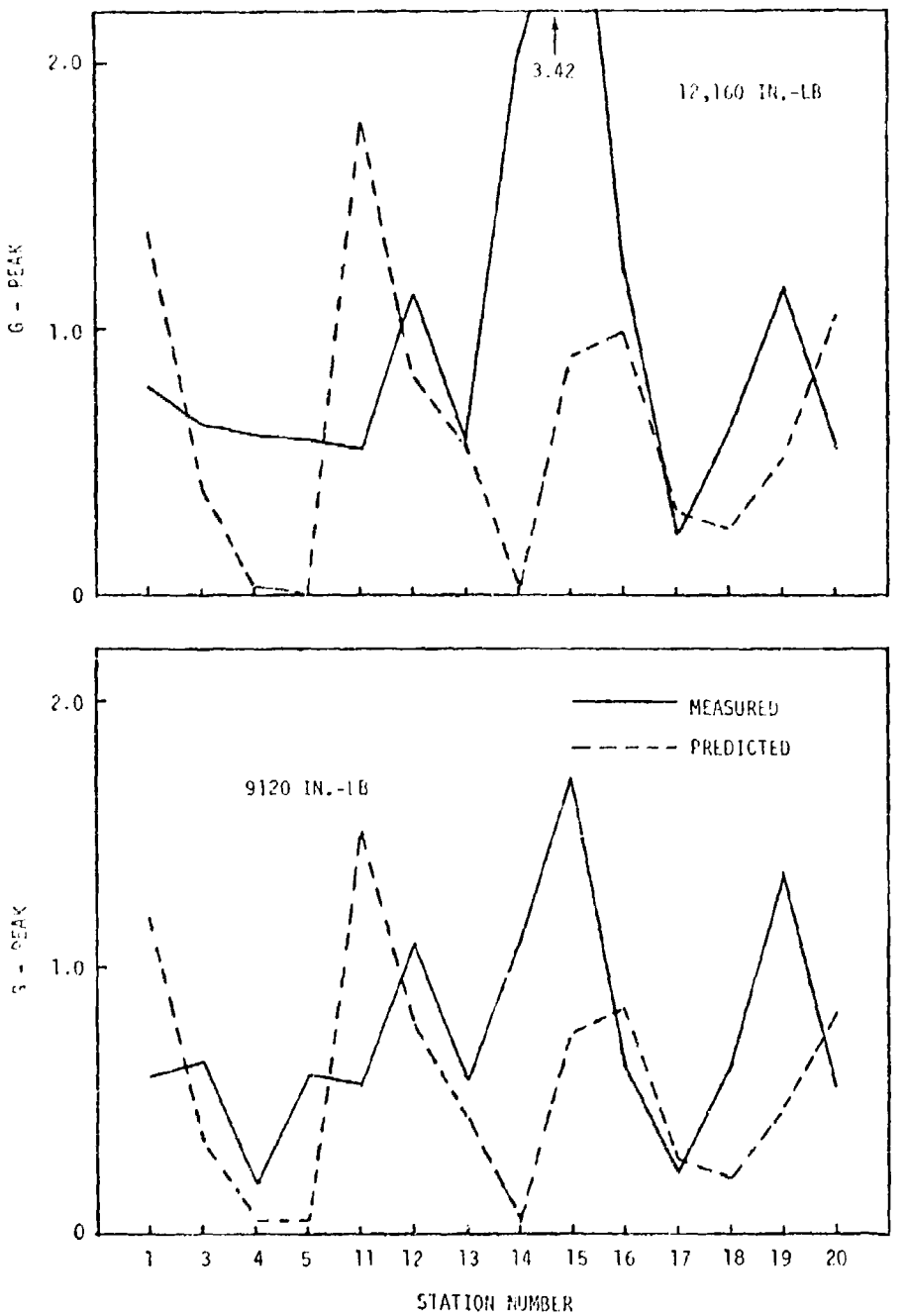


Figure 44. Measured vs. Predicted Case Acceleration for 435 Hz Excitation

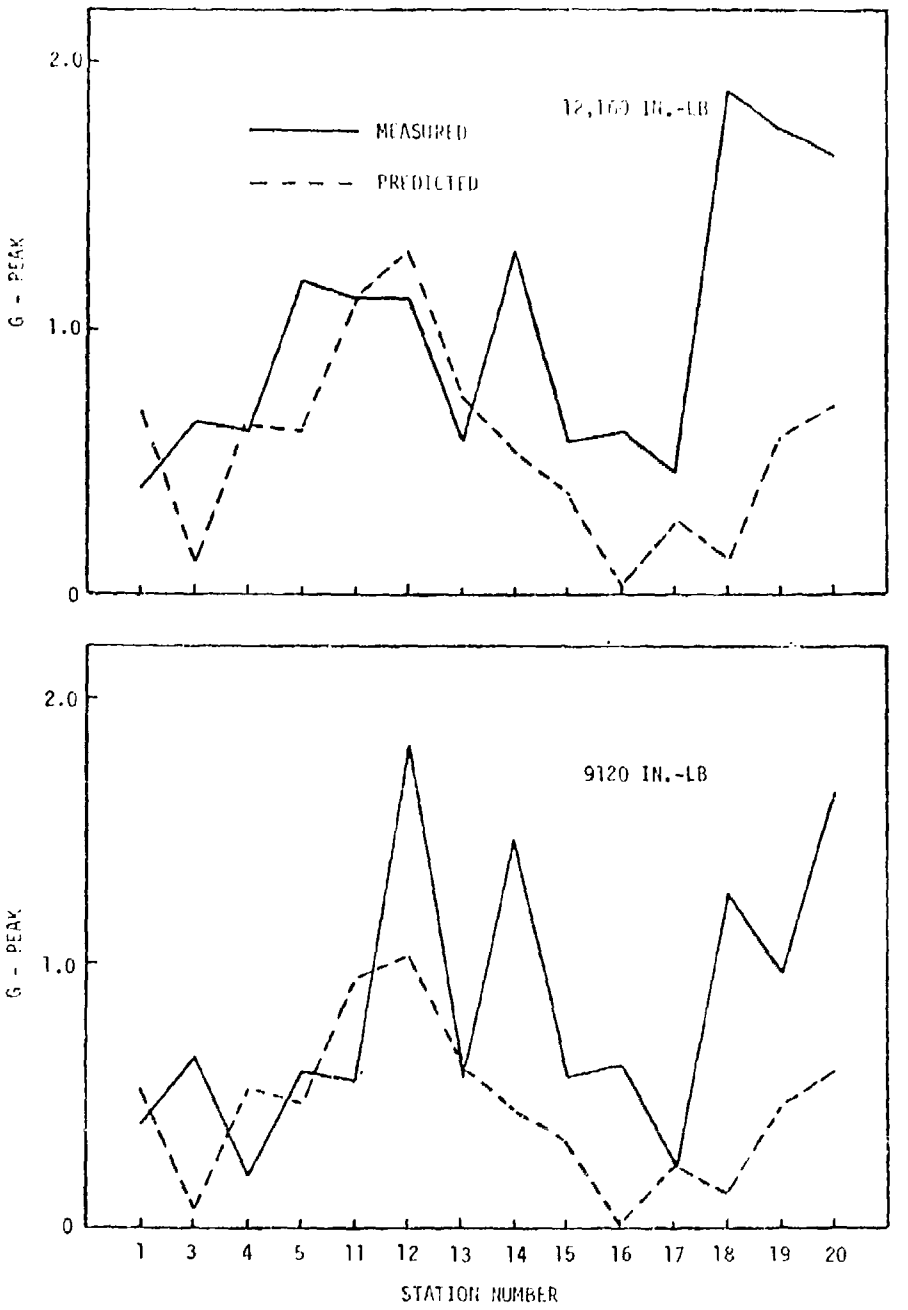


Figure 45. Measured vs. Predicted Case Acceleration for 870 Hz Excitation

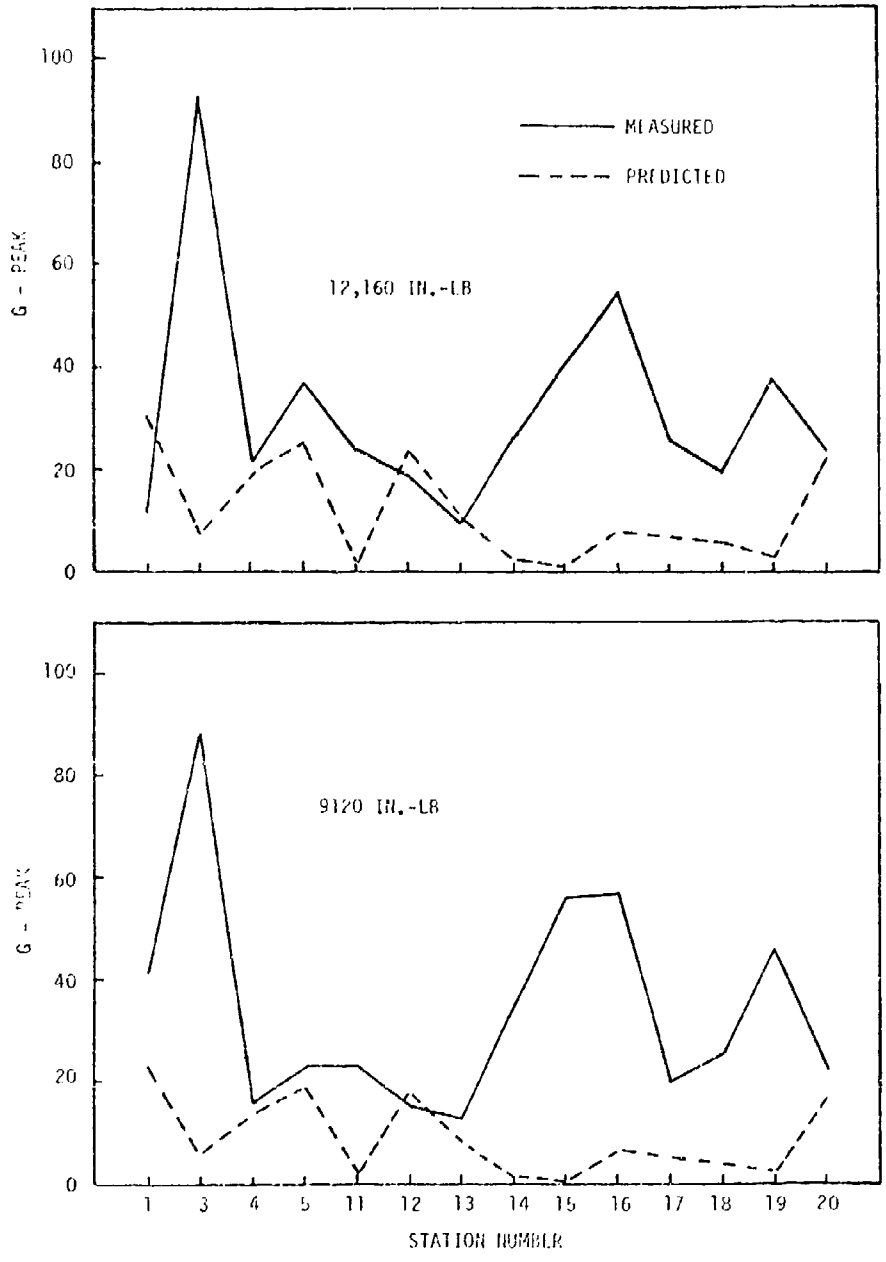


Figure 46. Measured vs. Predicted Case Acceleration for 1497 Hz Excitation

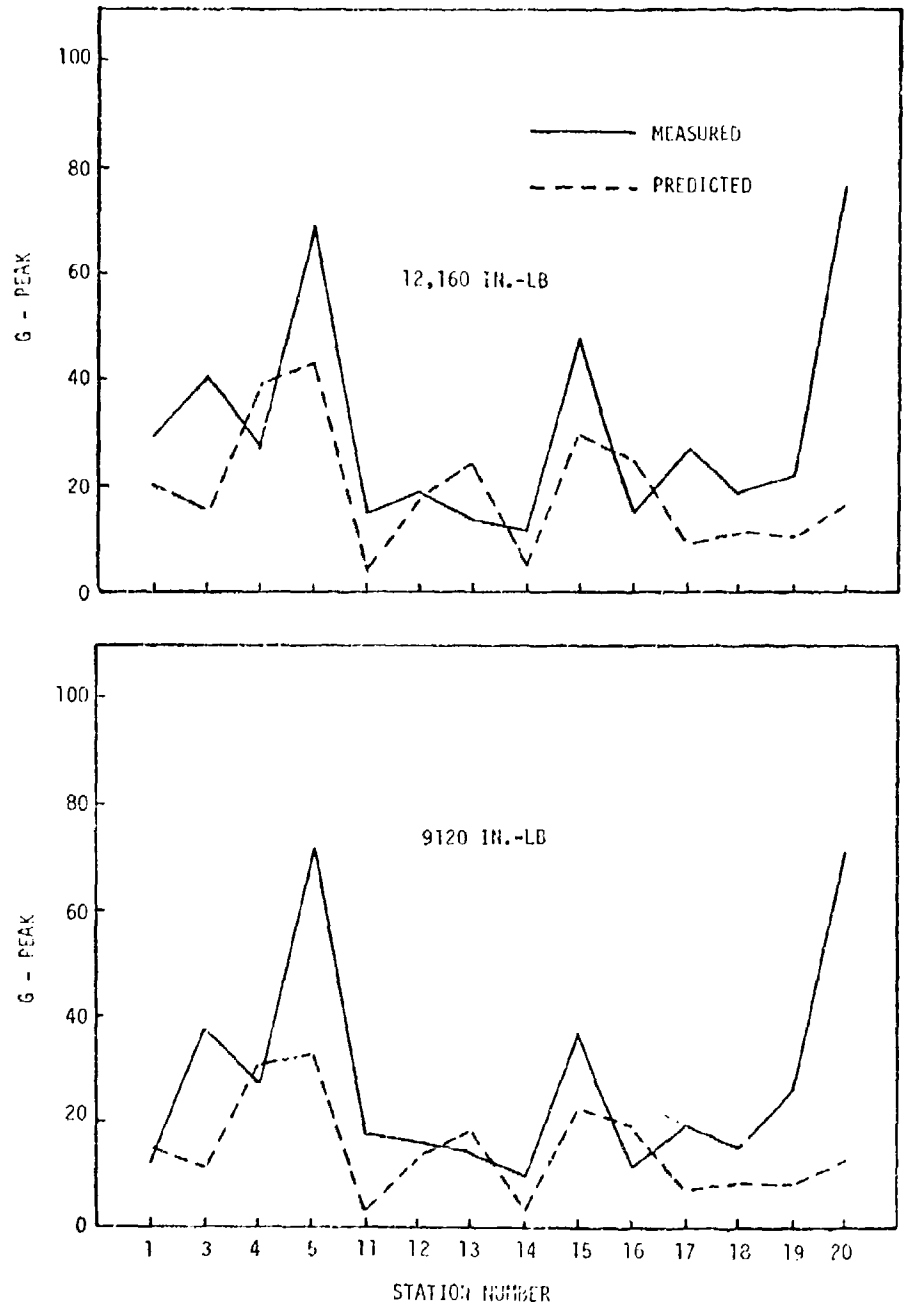


Figure 47. Measured vs. Predicted Case Acceleration for 2994 Hz Excitation

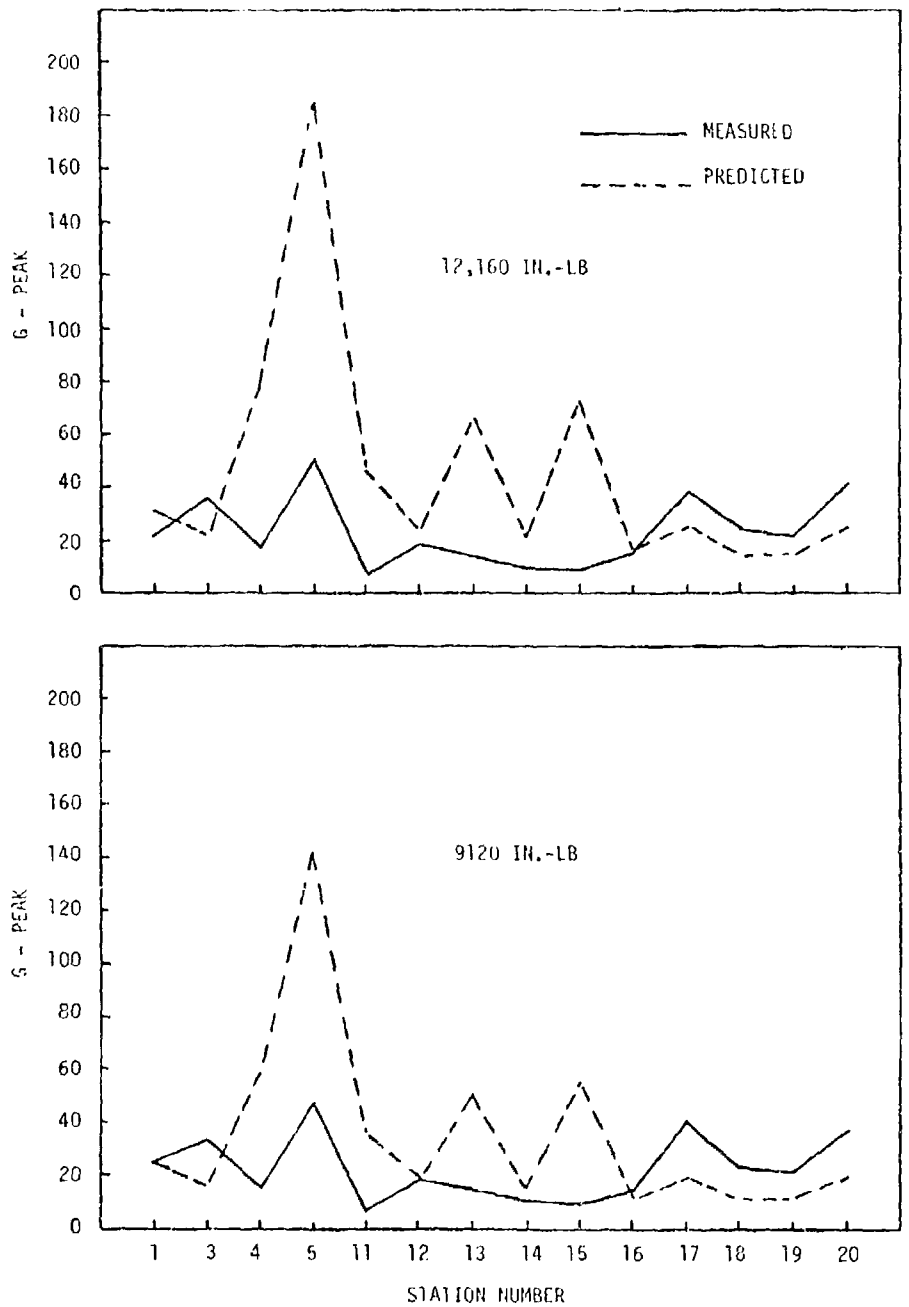


Figure 48. Measured vs. Predicted Case Acceleration for 3060 Hz Excitation

In Figure 41, the housing accelerations at the spur gear-mesh fundamental frequency of 1198 Hz are seen to be substantially higher than those at the planetary system fundamental. In this case, the measured accelerations range from 1.0 g to 41 g, at the same 60-percent torque condition discussed previously. Calculated accelerations for this case run from a minimum of .5 g to a maximum of 30 g. Again, a disparity is shown between the measured and predicted acceleration with regard to the effect of torque.

RADIATED NOISE

Analytical predictions were made for the housing radiated sound power levels associated with each of the gear-mesh excitation frequencies of Table 7, for both conditions of torque. Sound power levels were also calculated from the measured sound pressure levels.* In subsequent discussions, sound power levels derived entirely from the analytical method are referred to as predicted values, while those derived from measured sound pressure level data are referred to as measured values.

Comparisons of measured and predicted sound power levels are shown in Figures 49 and 50. The data of Figure 49 refer to the 80-percent rpm test condition, while Figure 50 shows similar data for the 100-percent rpm test condition. Excellent correlation is shown in the 80-percent rpm data of Figure 49, with the average deviation between measured and predicted sound power levels less than two dB. The 100-percent rpm data of Figure 50 do not agree, as well, however, with an average deviation of almost 8 dB. The source of much of this error can be traced to overprediction at the spiral bevel gear mesh frequency of 3060 Hz, and underprediction at the spur gear mesh frequency of 1497 Hz. Similar prediction errors are evident in the housing accelerations of Figures 46 and 48, and based on similarity of these errors it can be concluded that the source of the prediction errors is the system dynamic response model and not the housing noise radiation model.

It is believed that the above errors resulted from miscalculation of system resonance frequencies near the two mesh frequencies of 1497 Hz and 3060 Hz. System responses are very sensitive to excitation frequency at or near resonance and, in this case, even small errors in resonance frequency calculation can lead to large errors in predicted responses. In an actual application, however, system responses would not be calculated only at the actual excitation frequency, but rather for a frequency band encompassing this frequency. In this way the presence of resonances near the actual excitation frequency would be established and these resonances could then be shifted to avoid possible excitation.

* Sound power is not a directly measurable parameter, but must be calculated from sound pressure.

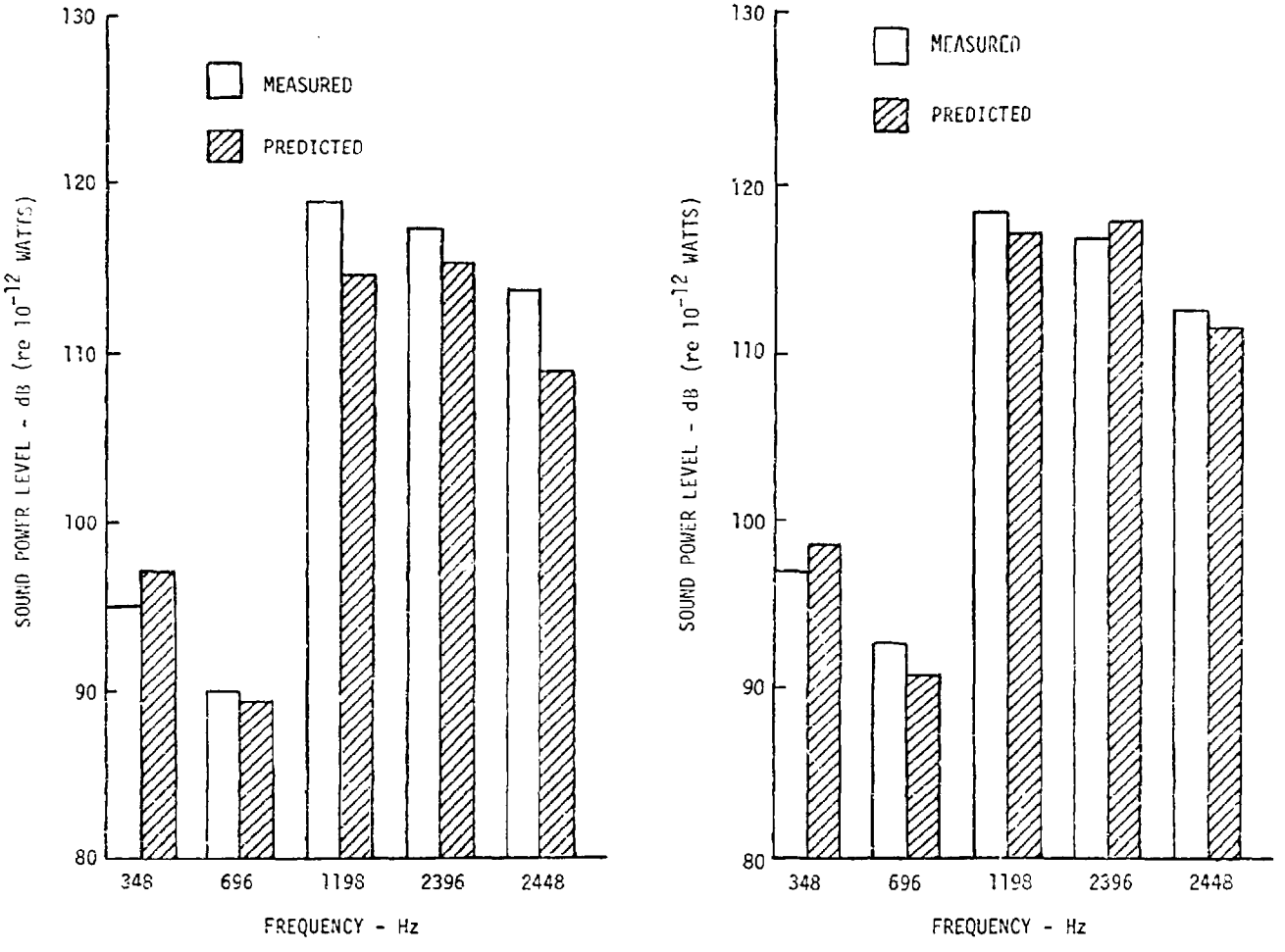


Figure 49. Comparison of Measured and Predicted Sound Power Level, 80% rpm

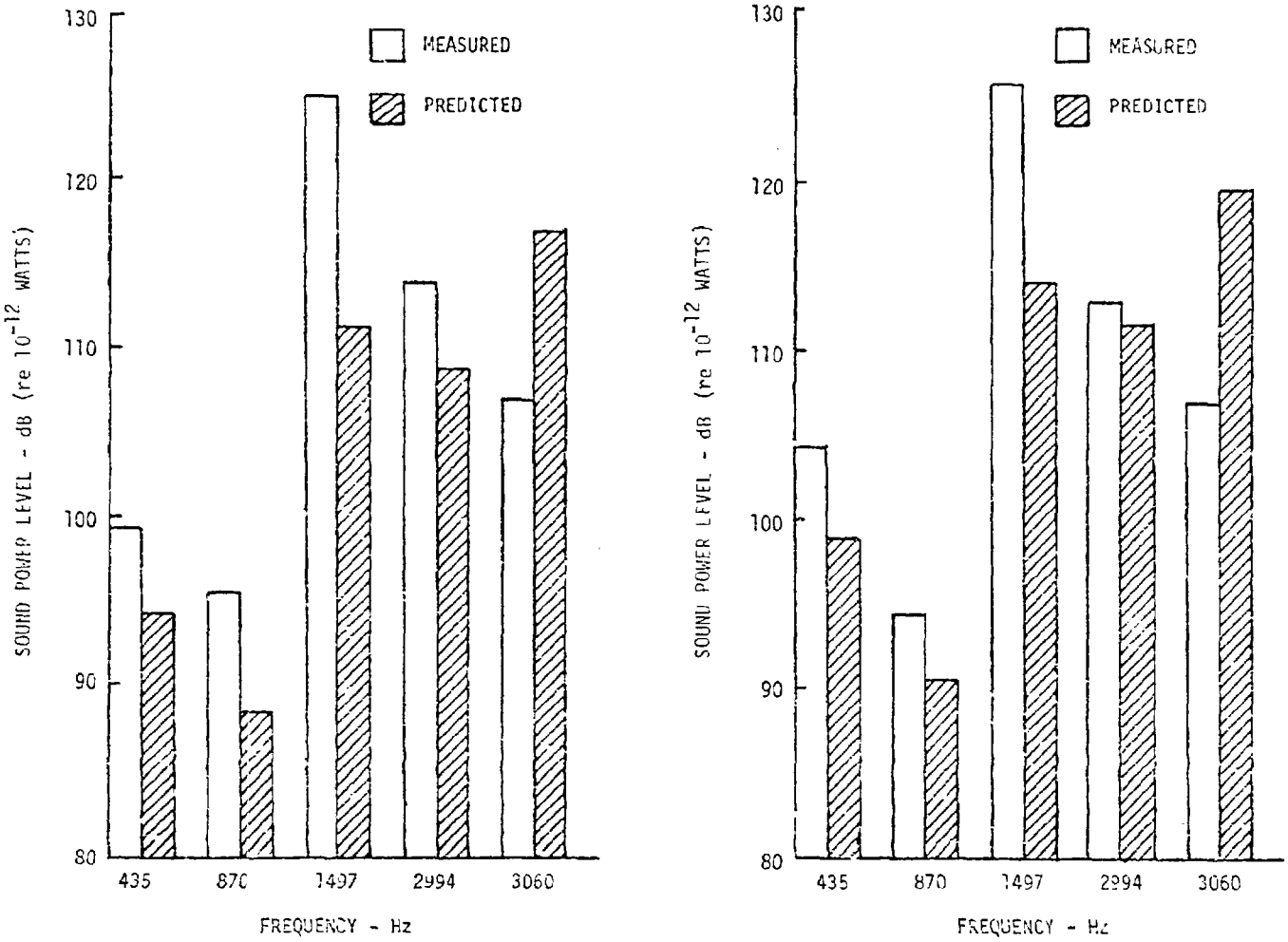


Figure 50. Comparison of Measured and Predicted Sound Power Level, 100% rpm

## METHOD APPLICATION

The transmission dynamic modeling technique developed in the present program permits the rapid and economical evaluation of transmission design changes. Once the individual mechanical element models have been derived, they can be manipulated in various ways without the need for rederivation. This is accomplished through the use of a computer routine, which is an inherent part of the system modeling method and which can be used to perform the following functions:

- Add (or subtract) structural damping to any element or any part of an element.
- Add vibration absorbers at any location of an element.
- Add (or delete) lumped masses at any location.
- Add spring/damper systems between any two elements or from an element to the ground.
- Change system geometry.

The performance of system design studies is further promoted by the fact that changes in individual elements may be made separately. For example, if a change in shaft stiffness or mass distribution is desired, only the shaft model in question need be changed. The remaining shaft and housing models are left alone, and a new system model is synthesized using the new shaft model with these unchanged models.

An applications study has been performed using the analytical method. The purpose of this study is to demonstrate the range of transmission design changes which may be investigated with the method. Design changes which have been considered in this study effort include:

- Reduced bearing stiffness
  - All shafts
- Planet carrier stiffness change
- Increased shaft stiffness
  - Input shaft
  - Output shaft
  - Spur/bevel shaft
- Increased shaft mass
  - Input shaft
  - Spur/sun shaft

- Increased case damping

- Increased case mass

- Bearing relocation

While a considerable range of design changes was investigated, none of these individual changes was studied in sufficient depth to establish their ultimate practical value or noise-reduction potential. The study results do, however, serve as an indication of the relative sensitivity of transmission response to the various design changes which were considered, at least with regard to the particular transmission studied.

## SHAFT MASS AND STIFFNESS DISTRIBUTION

Redistribution of the bending and torsion stiffnesses of the input, spur/bevel, and output shafts was analytically simulated by changing the cross-sectional area distributions of these shafts in their respective analytical models. In each case, the shaft cross-sectional area was increased by increasing shaft [illegible]ness radius approximately 10 percent. This change in shaft radius extended over only one-third of the total shaft length, with the modified radius shaft segment centered at the midpoint of shaft length. The mass distribution was not changed by this modification.

The effect of increasing input shaft stiffness is shown in Figure 51, in terms of changes in radiated sound power level for each mesh excitation frequency. The changes given are relative to sound power levels calculated for the baseline transmission. Only data for the 80-percent torque condition are presented, since the changes in sound power level calculated for the 60-percent torque condition are identical to those shown.

As indicated in Figure 51, increasing the input shaft stiffness caused significant changes in the radiated sound power level at several mesh frequencies, and not merely at the spiral bevel gear-mesh frequencies of 2346 Hz and 3060 Hz, which are most directly associated with the input shaft. Although the greatest change, an 11-dB reduction, did occur at the 100-percent rpm spiral bevel gear-mesh frequency of 3060 Hz, a comparable magnitude change, in this case a 10-dB increase, is shown for the 80-percent rpm, spur gear-mesh second-harmonic frequency, at 2396 Hz. Furthermore, no change in sound power level was obtained at the 80-percent rpm spiral bevel gear-mesh frequency of 2448 Hz.

The data of Figure 51 provide a graphic illustration of the fact that the analytical model considers the transmission as a coupled dynamic system, with responses determined by all the mechanical elements acting as a unit. This fact must always be considered in applying this method, particularly when it is used to evaluate potentially beneficial design changes. Such changes, although usually predicated on the basis of

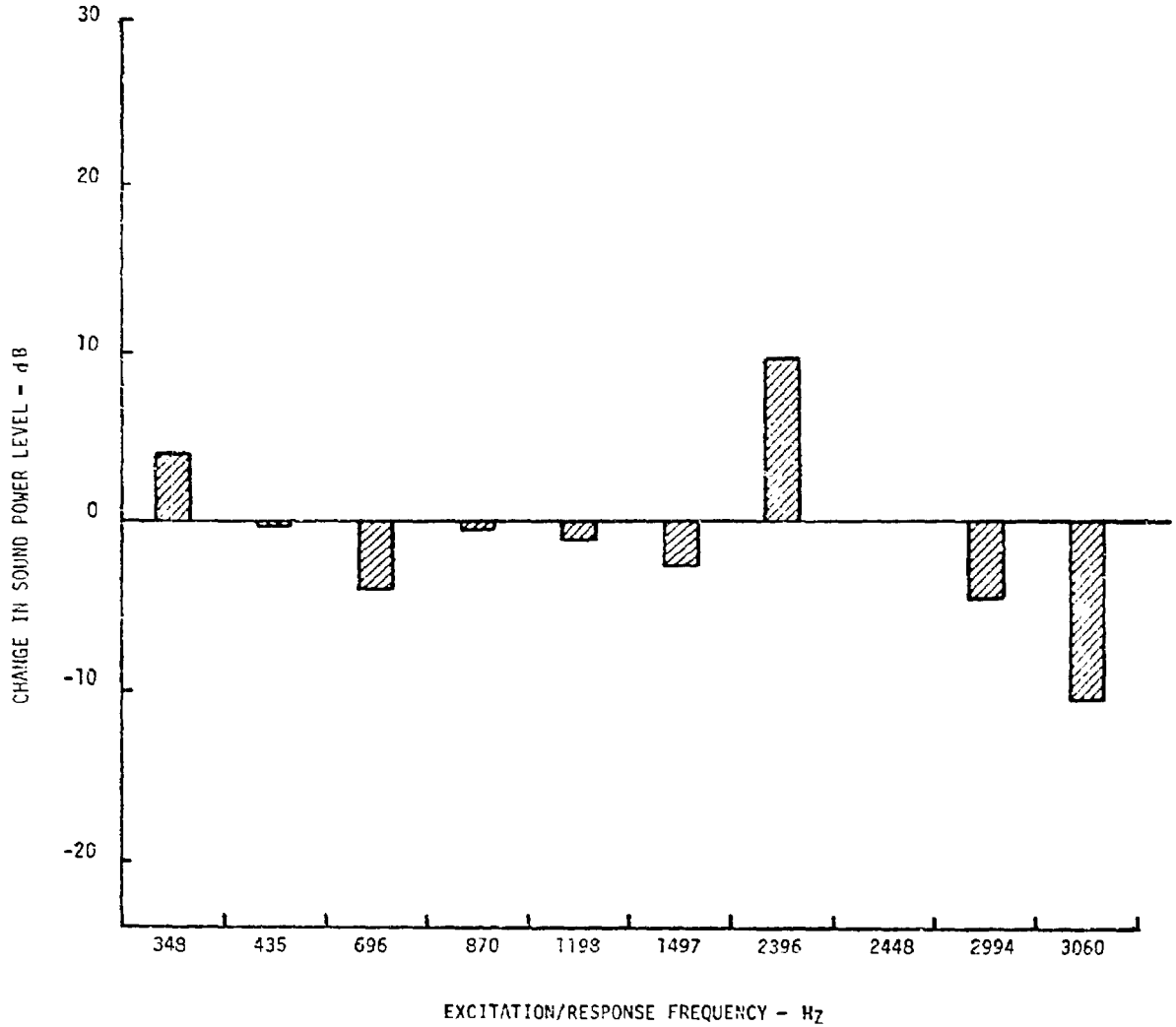


Figure 51. Effect of Increased Input Shaft Stiffness

reducing the response to only one gear-mesh excitation, will normally have an effect on all mesh-induced responses; furthermore, these effects will be a function of transmission speed. While a given design change may produce a reduction in response at the principal mesh frequency of interest, this same change may very well raise the response at other mesh frequencies, thus curing one problem and creating others. A reduction obtained at one transmission speed may not prevail at another speed, even if these two speeds are reasonably close. Because of these considerations, transmission design changes should always be evaluated with regard to their effect on all gear-mesh-induced responses and for pertinent transmission speeds. Although this approach does require extensive evaluation of each design change, the analytical method has been set up to perform the required analyses in an economical, efficient manner, requiring a minimum effort on the part of the analyst.

While the interrelated nature of the transmission dynamic system is somewhat disadvantageous in terms of the effort required to evaluate the effectiveness of a given design change, this same characteristic also extends the range of potentially beneficial design changes to include any mechanical element. If, for example, a reduction were required in the responses to a given gear-mesh excitation, it would not be necessary to consider only design changes of components directly associated with that mesh; for example, the shafts supporting those specific meshing gears. In fact, a change in some other element might be more effective in reducing response, and more practical to introduce. This approach is illustrated in Figure 52, which shows the changes in sound power levels due to stiffening of the SH-2D output shaft.

The major effects of stiffening the output shaft were substantial reductions in both the 100-percent rpm spur gear second harmonic and spiral bevel fundamental responses, at 2994 Hz and 3060 Hz, respectively, and an equally substantial increase in the response to the 100-percent rpm spur gear fundamental at 1497 Hz. Physically, these two gear meshes occur at points distant from the output shaft, as shown in Figure 1, but as demonstrated in Figure 52, responses to excitations introduced at these meshes are highly influenced by changes in output shaft characteristics. Furthermore, this design change produced no significant variation in planetary system mesh-induced responses, and the planet system mesh is, physically, the closest source of excitation to the output shaft.

Similar observations to those discussed above pertain to the data of Figure 53, which relates the effects of a change in spiral bevel/spur gear shaft stiffness. Again, substantial changes in sound power level are indicated, and taking these data with the data of Figures 51 and 52, it can be concluded that transmission responses are, in fact, sensitive to shaft stiffness distributions.

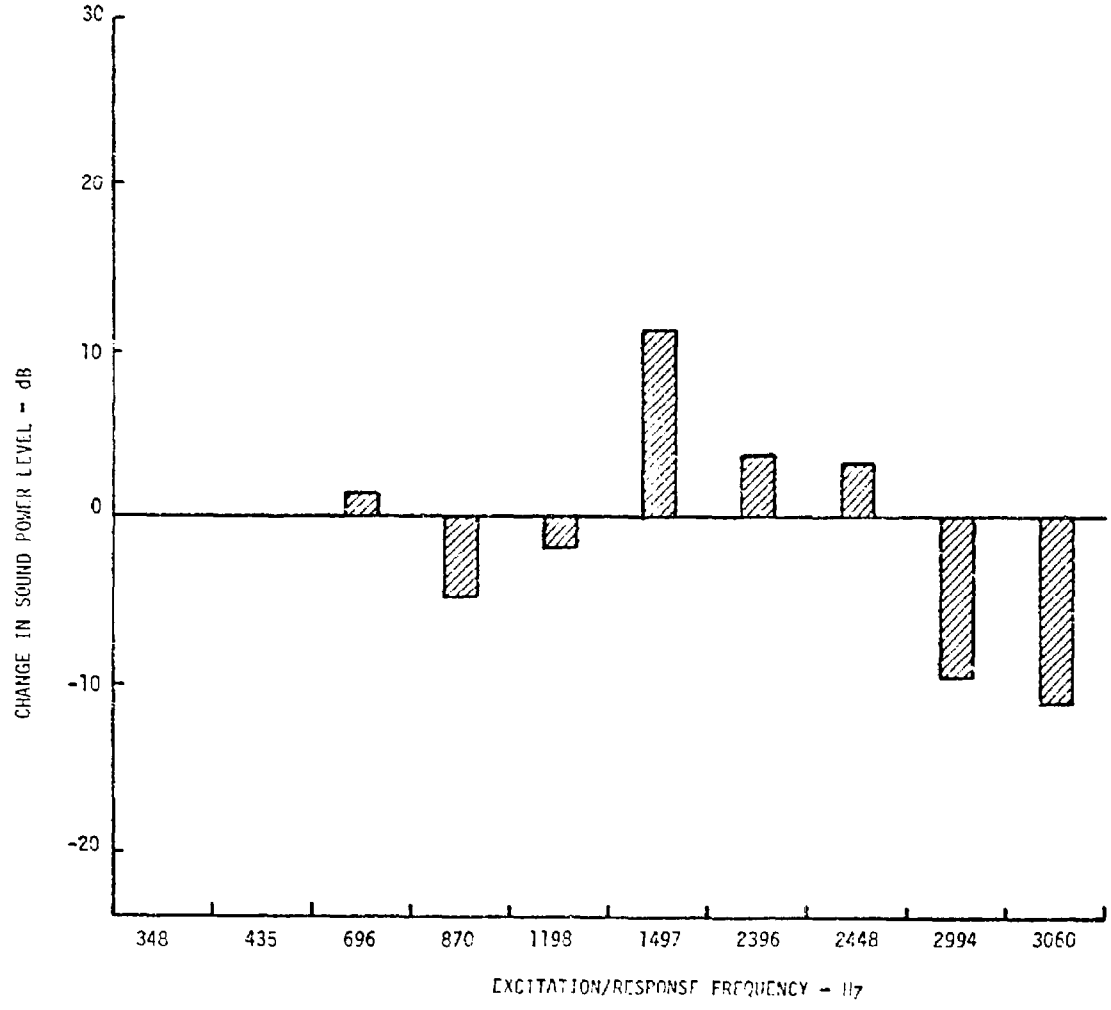


Figure 52. Effect of Increased Output Shaft Stiffness

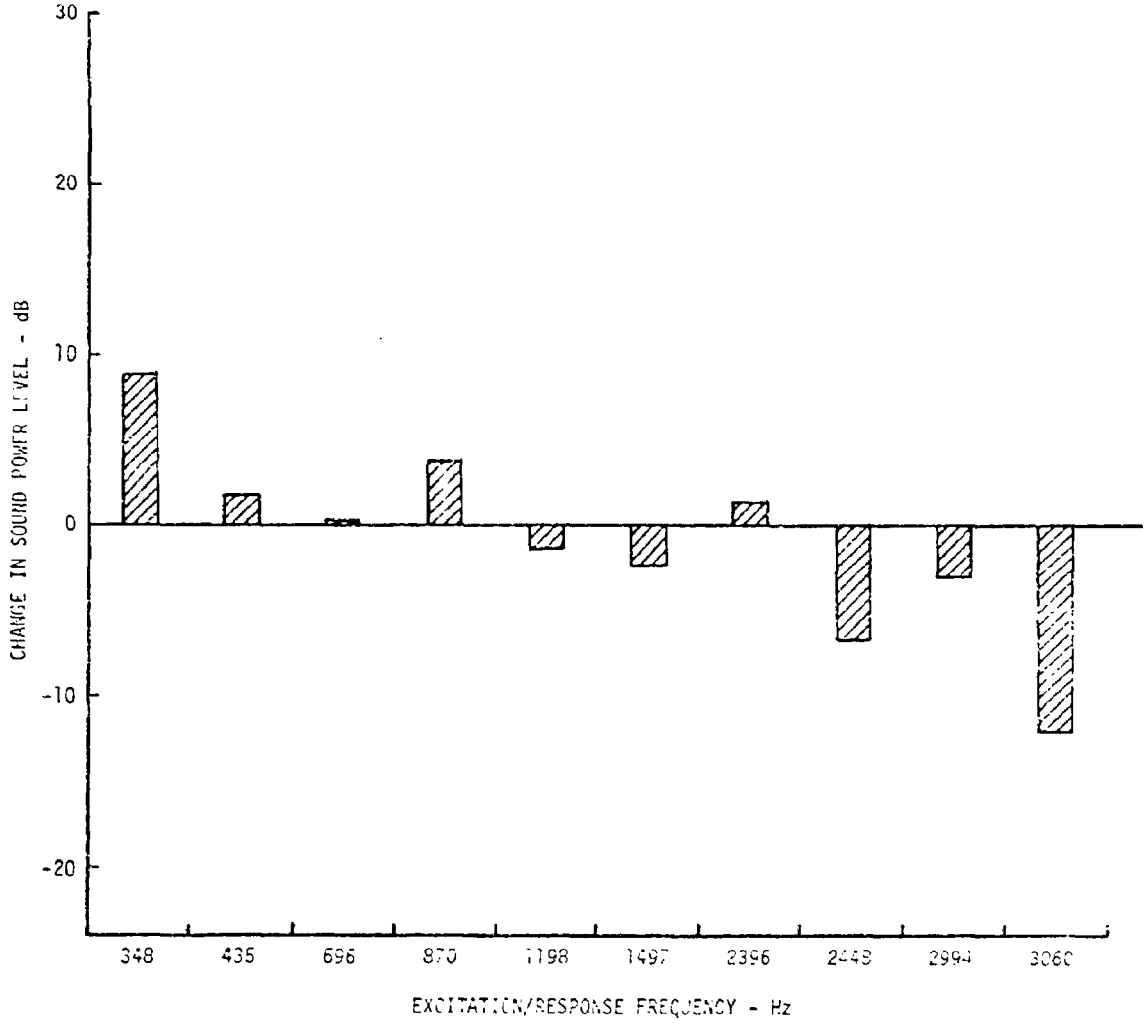


Figure 53. Effect of Increased Spiral Bevel/Spur Shaft Stiffness

The effects of changing shaft mass distribution were evaluated by determining the changes in sound power level which resulted from increasing the mass of both the input and the spur/sun gear shafts. As was done for the stiffness changes discussed above, shaft mass was changed only over the central one-third of shaft length, and also by 10 percent. Net changes in the total shaft mass were small, since most of the shaft mass is concentrated at the gears, with the shaft mass itself very low by comparison. Figures 54 and 55 show the changes in sound power levels due to changing the input and spur/sun gear shaft mass distributions.

The mass distribution of the input shaft is very influential in determining system responses and radiated noise. This sensitivity is illustrated in Figure 54, which indicates almost a 30-dB sound power level increase for the 80-percent-rpm planet system second-harmonic mesh-induced sound power level at 696 Hz and a nearly 13-dB increase at the 100-percent rpm spiral bevel mesh frequency of 3060 Hz. The fact that the changes shown are positive, with increasing sound power level, is not significant, but only the fact that sound power level is sensitive to this parameter. This sensitivity indicates that in an actual application, a suitable mass distribution could be found which would produce reductions of comparable magnitude to the increases shown.

Similar conclusions could readily be drawn with regard to the spur/sun gear shaft mass redistribution data of Figure 55.

BEARING STIFFNESS AND LOCATION

The sensitivity of transmission dynamic response to shaft support characteristics was evaluated by analytically simulating changes in both bearing stiffness and location. These changes are readily accomplished with the present analytical method, merely by respecifying either the location or nature of the interface coordinates joining the elemental shaft and housing models. The elemental models themselves need not be rederived and are, in fact, retained in their original form.

The effect of shaft support bearing stiffness reduction is illustrated in Figure 56. For the case shown, the stiffnesses of all bearings within the transmission were reduced by 50 percent. The original values of these spring rates ranged from approximately $1 \times 10^6$ lb/in. to $1 \times 10^7$ lb/in. and, consequently, while large in percentage terms, this 50-percent stiffness reduction was not considered unreasonable in absolute terms.

As shown in Figure 56, the effects of bearing stiffness reduction were significant only in the high-frequency range. Based on these and similar results, it is concluded that bearing stiffness alone is not a significant determinant of transmission response. This lack of significance is most probably due to the very high bearing spring rates, which can, for practical purposes, be considered rigid relative to the dynamic stiffness of either the shafts or housing.

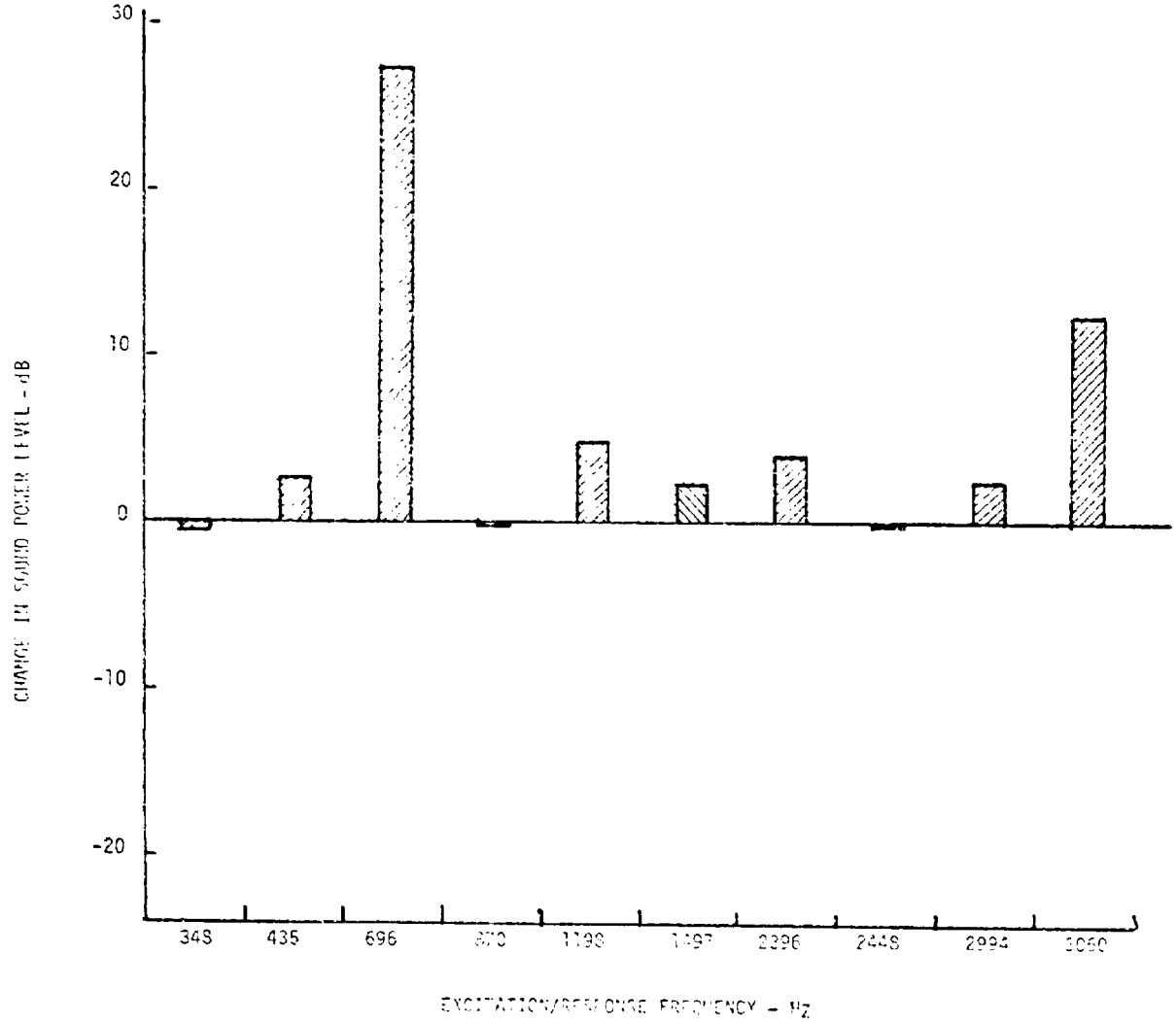


Figure 54. Effect of Increased Input Shaft Mass

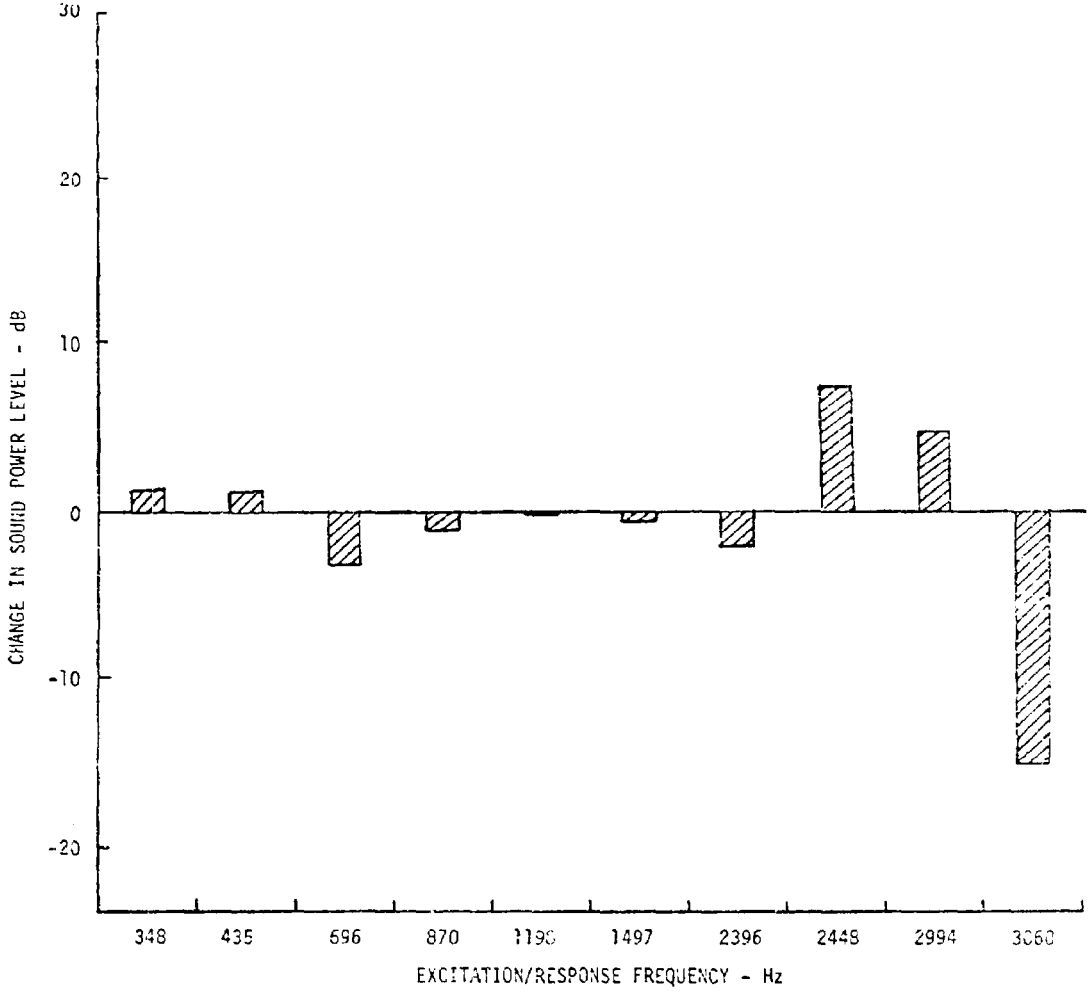


Figure 55. Effect of Increased Spur/Sun Gear Shaft

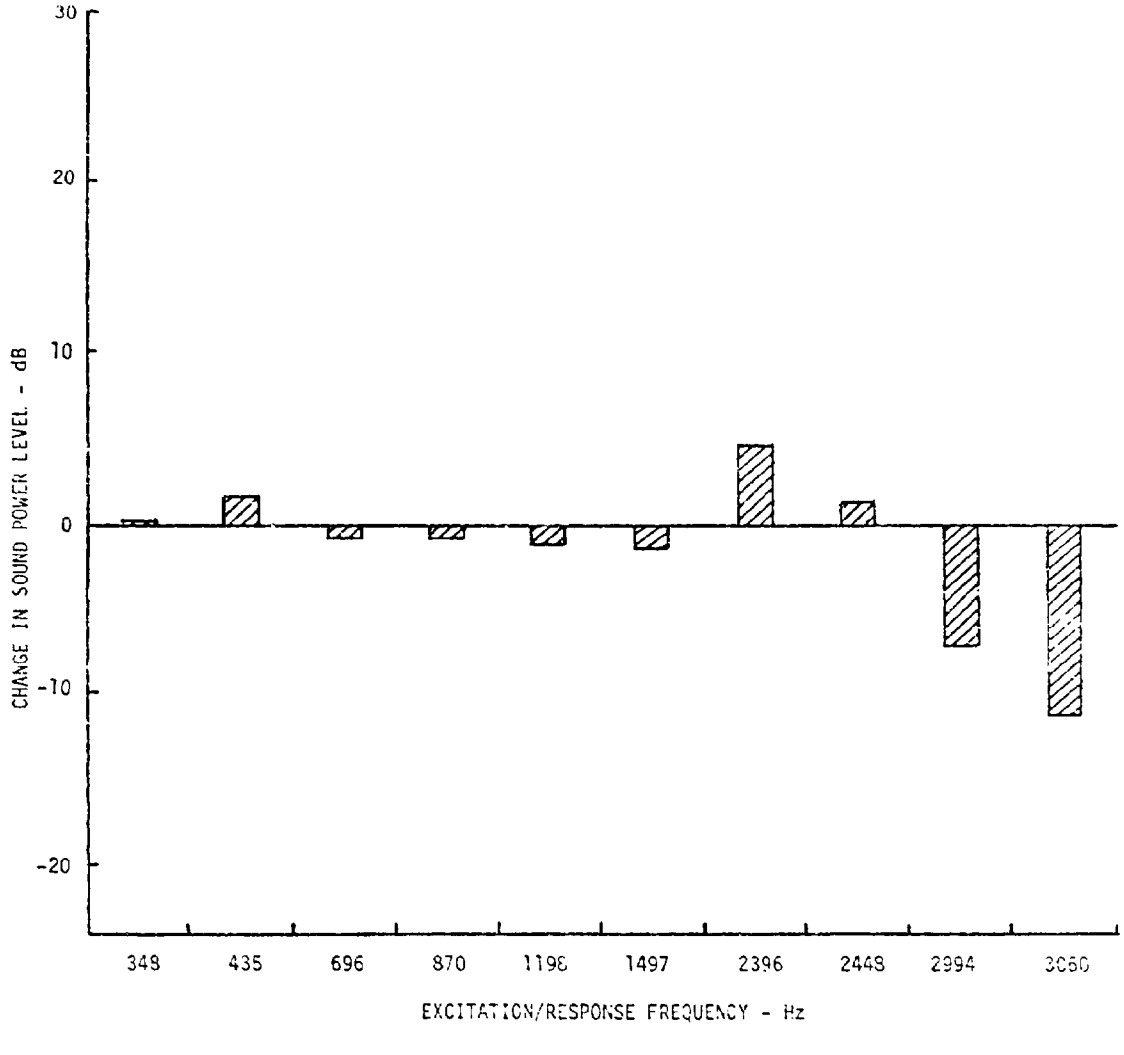


Figure 56. Reduced Shaft Support Bearing Stiffness - All Shafts

The effect of bearing relocation is shown in Figure 57. In this case, only one bearing was moved - the duplex ball bearing supporting the input shaft (Figure 10A). In the original system model, this bearing was modeled as an effective stiffness at shaft station 14.5. For the present evaluation the location of this bearing was shifted to shaft station 15.5, while the stiffness was kept constant.

## PLANETARY SYSTEM CARRIER STIFFNESS

The design changes discussed previously are not generally effective in changing planetary system responses. Since, in many cases, helicopter transmissions exhibit their highest responses due to planetary system excitations, an attempt was made to develop and evaluate a method for changing these responses. These efforts concentrated on the effects of planetary system carrier stiffness modification and, specifically, a reduction of planet carrier radial stiffness only. An example of the results of these investigations is shown in Figure 58.

The data of Figure 58 illustrate the effects of reducing the radial stiffness of the planet carrier by 50 percent. This change was considered to be practical, because only radial stiffness was changed, with torsional stiffness held constant. Since system torque is reacted by the carrier in torsion with little or no static load reacted in the radial direction, the carrier radial stiffness is not a primary static design factor, and can be changed based on dynamic requirements.

As shown in Figure 58, reducing planet carrier stiffness causes significant changes in the planetary system responses at 348 Hz, 435 Hz and 696 Hz. Further, the effects are isolated to the planetary system excitations, with little or no response change shown for the remaining gear-mesh excitations. While further analytical work is required, it is felt that the beneficial effects of this concept could be readily applied in future helicopter transmission designs.

## TRANSMISSION HOUSING MODIFICATIONS

One of the major advantages of the present analytical approach is the ability to model the transmission housing. While a prototype housing is required to develop this model, changes in the housing can be simulated by purely analytical means. In this way, changes in mass and stiffness distributions and housing damping can be considered.

Two examples of case mass redistribution are shown. In the first example, a total of 3 pounds was added to the case. This total added mass was made up of three 1 pound masses which were added at case coordinates 1, 11, and 15 (Figure 12). These coordinates were chosen based on their relatively high acceleration responses. The second example of case mass redistribution involved the addition of a total of 15 pounds. This total added mass was made up of three 5 pound masses which were added at case coordinates 1, 11, and 15 (Figure 12).

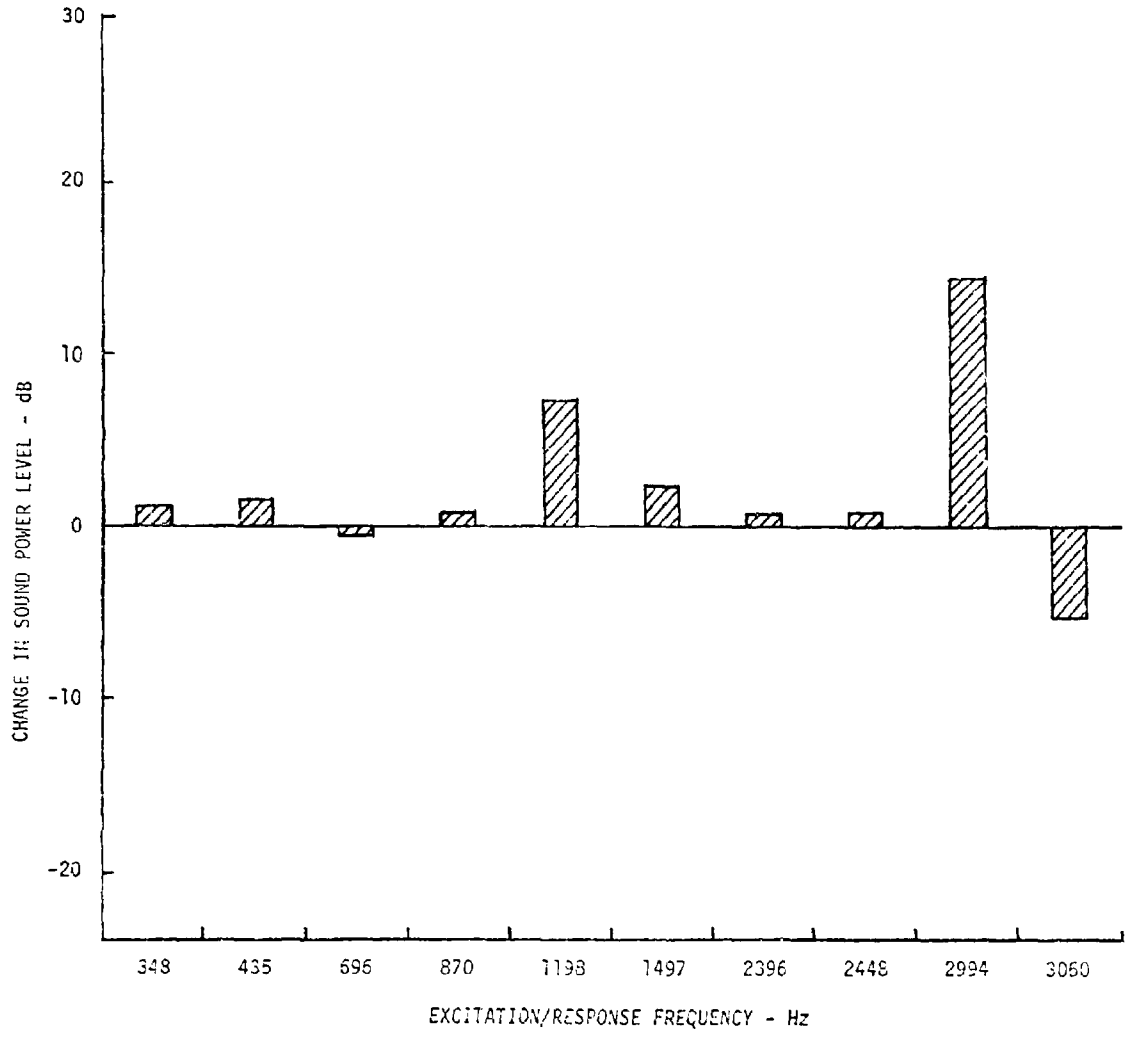


Figure 57. Relocation of Input Shaft Support Bearing

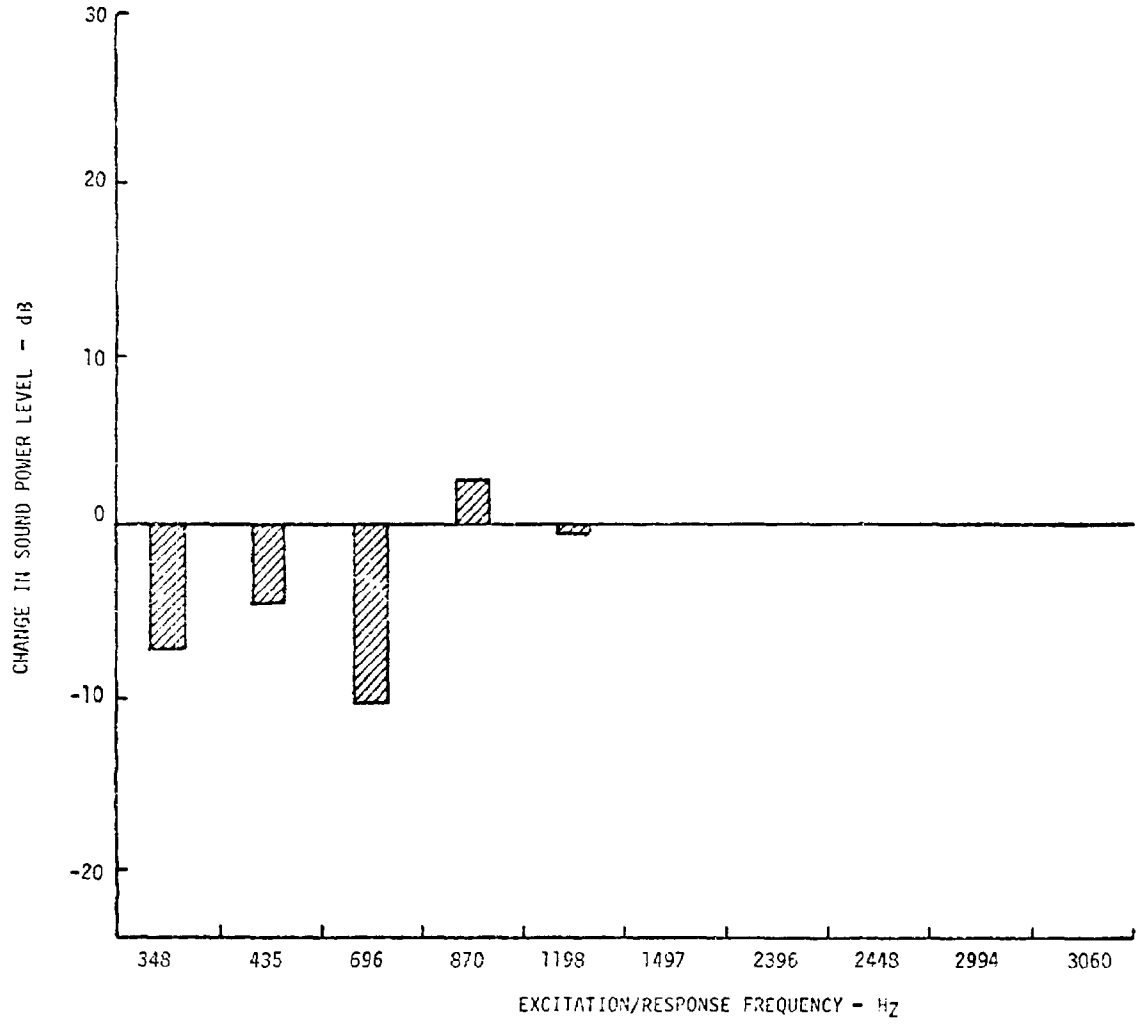


Figure 58. Effect of Reduced Planet Carrier Radial Stiffness

While significant changes in all gear-mesh responses are not shown in Figure 59, several responses were appreciably affected. This suggested that lack of general effectiveness is not considered significant because of the random approach used in applying the mass redistribution. It is further felt that systematic selection of mass redistribution, keyed to a particular desired response change, could result in optimum tuning of the transmission system. On this basis, it is believed that the use of housing mass adjustments, and presumably, stiffness adjustments, could ultimately lead to the development of helicopter transmissions having improved dynamic characteristics.

The addition of external damping treatments to transmission housings has often been suggested as a means to reduce housing response and radiated noise. Within the present program, this approach has been evaluated analytically by simulating surface damping through increasing the housing structural damping coefficient. Three levels of damping increase were considered, with structural damping coefficients (g) of .05, .1 and .2. As mentioned in a previous section, the structural damping of the housing itself was determined to be very low, with modal damping coefficients ranging from .0015 to .03. Increasing damping to the degree considered, then, represents a substantial increase, but one which can readily be obtained with commercial materials.

The effects of increased housing damping are indicated in Figure 60. As shown, appreciable sound power level reductions were obtained at several gear-mesh excitation frequencies, but the reductions were by no means universal. This is to be expected, since the effects of damping are dependent upon the proximity of excitation frequencies and system natural response frequencies. For excitations close to natural frequencies, damping can be effective, but if excitations are substantially removed from the natural frequencies, damping will have no effect. As shown in Figure 60, damping can also produce an adverse effect, since added damping may increase the response for excitations close to the system antiresonant frequencies.

Given the data of Figure 60, it is apparent that housing damping is a sensitive parameter, which can be adjusted to reduce transmission response. Proper application of this approach, however, requires knowledge of system dynamic response characteristics, most importantly the proximity of gear-mesh excitation frequencies and system resonant and antiresonant frequencies.

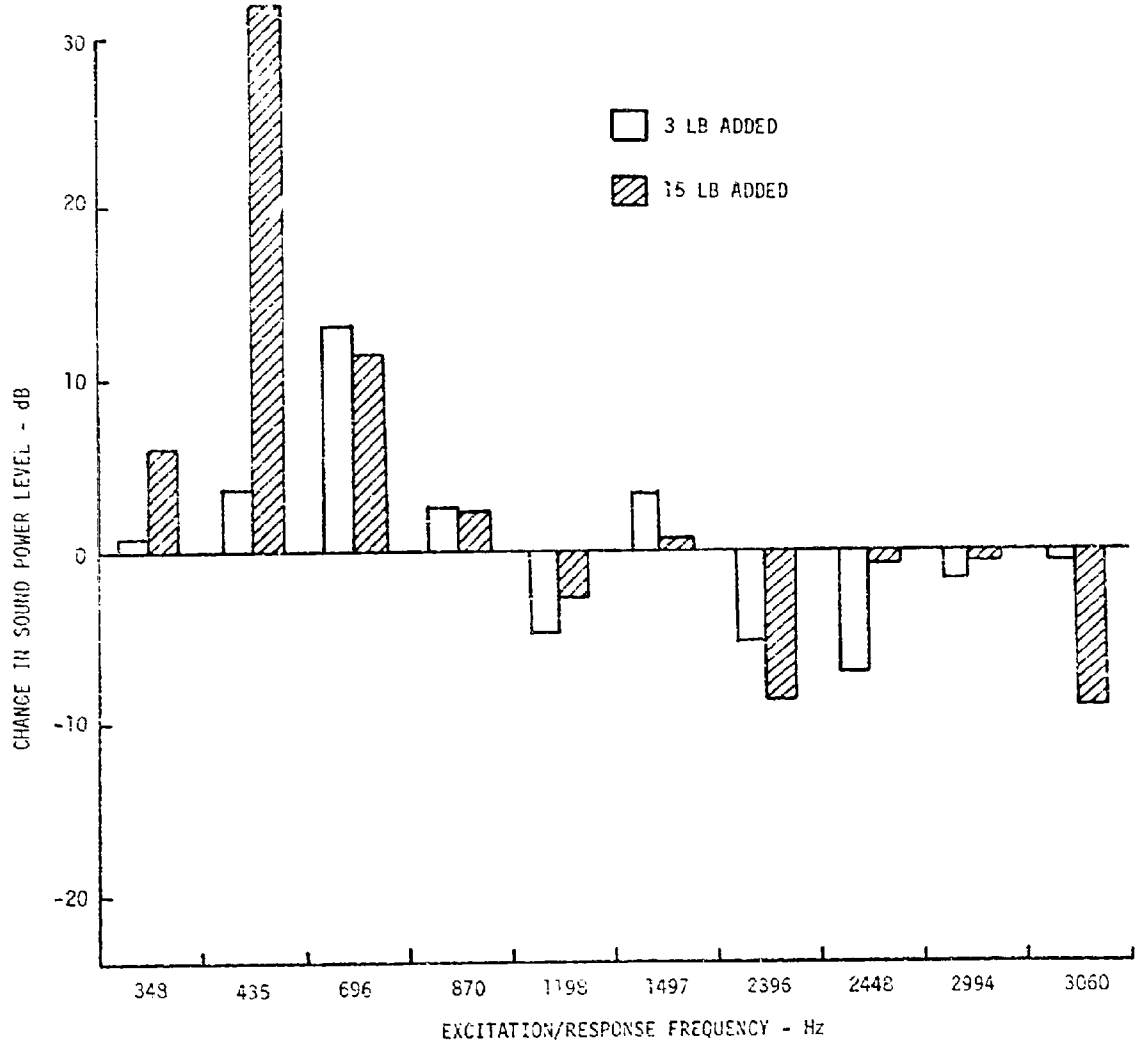


Figure 59. Effect of Housing Mass Redistribution

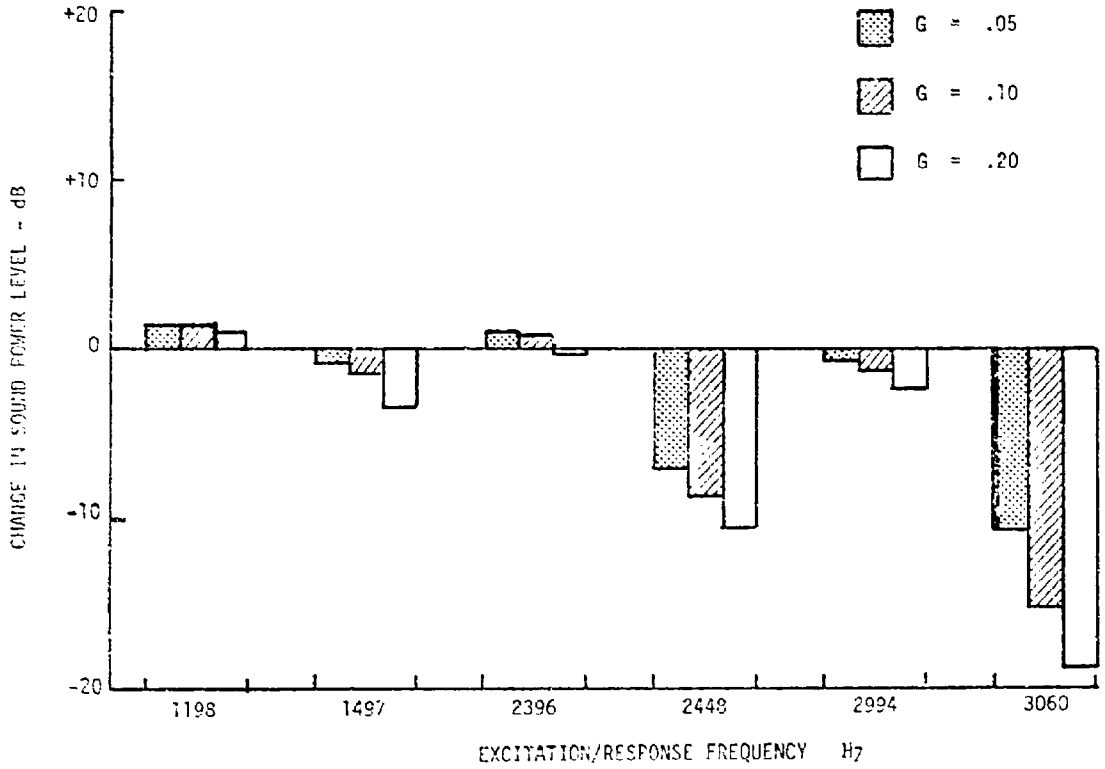


Figure 60. Effect of Case Damping

## CONCLUSIONS AND RECOMMENDATIONS

An analytical method has been developed which permits the calculation of helicopter transmission dynamic responses to gear-mesh-induced excitations. This method has been validated through direct comparison of analytical predictions with test data, and its use is recommended as an aid in the design of future helicopter transmissions having reduced vibration and noise characteristics. The method is fully computerized, and descriptions of all computer programs involved in the analysis are given in a companion document, Reference 10, along with all necessary operating instructions.

The analytical method includes the derivation of a detailed dynamic model of the transmission housing from test data. While this approach, of necessity, delays application of the full system model until a prototype transmission housing is available, it is felt that current dynamic modeling technology does not offer a viable alternative. Existing methods for modeling such a complex structure by purely analytical means are not sufficiently advanced to permit accurate estimation of the responses of complex structures at the very high gear-mesh frequencies of interest. In addition, these methods, at least in this application, appear to be too costly both to apply and to use. Since, ultimately, it is desirable to be able to generate a dynamic transmission housing model within the design, or even predesign phase of helicopter development, it is recommended that additional research efforts be conducted to develop this capability. Based on the success of the present approach, it is recommended that these efforts be directed towards the development of a generalized housing response model, using measured dynamic data obtained from a number of differing existing housing designs.

A number of potentially influential transmission design changes have been evaluated, primarily for the purpose of demonstrating the capabilities of the analytical method. Significant changes in transmission response characteristics were shown to result from modification of shaft mass and stiffness distributions, and to lesser extent, reductions of shaft support bearing spring rates and bearing relocation. Planetary system carrier radial stiffness was shown to be a significant determinant of responses to planetary system mesh excitations, and it is recommended that this approach be pursued through further research, test and development.

Since the analytical method does include a detailed housing representation, this capability was used to evaluate the effects of housing design changes, including mass redistribution and increased damping. Based on these evaluations, it is concluded that housing design is a significant parameter affecting transmission system dynamic response, and it is recommended that response modification through transmission housing tuning be pursued through a combined analytical and test effort.

While it is felt that the correlation efforts performed in the present program provide an adequate validation of the analytical method, it is also believed that acceptance and use of the method as a design aid would be greatly promoted by the performance of additional work in this area. On this basis, it is recommended that the transmission design changes which have been analytically evaluated in the present program be incorporated in the SH-2D transmission and subjected to operational testing. This effort could be performed at minimum cost because of the availability of all necessary test hardware and instrumentation.

## REFERENCES


1. Sternfeld, H., Jr., Spencer, R. H., and Schaeffer, E. G., STUDY TO ESTABLISH REALISTIC ACOUSTIC DESIGN CRITERIA FOR FUTURE ARMY AIRCRAFT, TREC Technical Report 61-72, U. S. Army Transportation Research Command, Fort Eustis, Virginia, June 1961.

2. Cox, C. R., et al, A STUDY OF THE ORIGIN AND MEANS OF REDUCING HELICOPTER NOISE, Bell Helicopter Company; TREC Technical Report 62-73, U. S. Army Transportation Research Command, Fort Eustis, Virginia, November 1962.

3. Laskin, I., Orcutt, F. K., and Shipley, E. E., ANALYSIS OF NOISE GENERATED BY UH-1 HELICOPTER TRANSMISSION, Mechanical Technology, Inc.; USAAVLABS Technical Report 68-41, U. S. Army Aviation Materiel Laboratories, Fort Eustis, Virginia, June 1968, AD 675457.

4. Badgley, R. H., and Laskin, I., PROGRAM FOR HELICOPTER GEARBOX NOISE PREDICTION AND REDUCTION, Mechanical Technology, Inc.,; USAAVLABS Technical Report 70-12, U. S. Army Aviation Materiel Laboratories, Fort Eustis, Virginia, March 1970, AD 869822.

5. Badgley, R. H., and Chiang, T., INVESTIGATION OF GEARBOX DESIGN MODIFICATIONS FOR REDUCING HELICOPTER GEARBOX NOISE, Mechanical Technology, Inc.; USAAMRDL Technical Report 72-6, Eustis Directorate, U. S. Army Air Mobility Research and Development Laboratory, Fort Eustis, Virginia, March 1972, AD 742735.

6. Badgley, R. H., RECOMMENDED DESIGN MODIFICATIONS TO THE CH-47 FORWARD ROTOR-DRIVE GEARBOX FOR REDUCTION OF HIGH-FREQUENCY VIBRATION AND NOISE, Mechanical Technology, Inc.; USAAMRDL Technical Report 73-33, Eustis Directorate, U. S. Army Air Mobility Research and Development Laboratory, Fort Eustis, Virginia, June 1973, AD 769062.

7. Sternfeld, H., Schairer, J., and Spencer, R., AN INVESTIGATION OF HELICOPTER TRANSMISSION NOISE REDUCTION BY VIBRATION ABSORBERS AND DAMPING, Vertol Division, The Boeing Company; USAAMRDL Technical Report 72-34, Eustis Directorate, U. S. Army Air Mobility Research and Development Laboratory, Fort Eustis, Virginia, August 1972, AD 752579.

8. Berman, A., VIBRATION ANALYSIS OF STRUCTURAL SYSTEMS USING VIRTUAL SUBSTRUCTURES, The Shock and Vibration Bulletin, Volume 5, No. 6, The Shock and Vibration Information Center, Naval Research Laboratories, Washington, D. C., June 1973, pp 13-22.

## REFERENCES (Continued)


9. Flannelly, W. G., Berman, A., and Barnsby, R. M., THEORY OF STRUCTURAL DYNAMIC TESTING USING IMPEDANCE TECHNIQUES, VOLUME I - THEORETICAL DEVELOPMENT, Kaman Aerospace Corporation; USAAVLABS Technical Report 70-6A, U. S. Army Aviation Materiel Laboratories, Fort Eustis, Virginia, June 1970, AD 874509.

10. Giansante, N., HELICOPTER TRANSMISSION VIBRATION/NOISE REDUCTION PROGRAM ANALYTICAL PREDICTION COMPUTER PROGRAM - USERS GUIDE, Kaman Aerospace Corporation; USAAMRDL Technical Report (To be published).

11. Berman, A., Flannelly, W. G., THEORY OF INCOMPLETE MODELS OF DYNAMIC STRUCTURES, AIAA Journal, Volume 9, No. 8, August 1971, pp 1481-1487.

12. Berman, A., SYSTEM IDENTIFICATION OF A COMPLEX STRUCTURE, AIAA Paper No. 75-809, Presented at the AIAA/ASME/SAE 16th SDC Meeting, Denver, Colorado, May 1975.

13. Jones, A. B., A GENERAL THEORY FOR ELASTICALLY CONSTRAINED BALL AND RADIAL ROLLER BEARINGS UNDER ARBITRARY LOAD AND SPEED CONDITIONS, Transactions of the American Society of Mechanical Engineers, Series D, Journal of Basic Engineering, Volume 82, June 1960, pp 309-320.